Gas Lift Valve Failure Mode Analysis and the Design of a Thermally-Actuated Positive-Locking Safety Valve

by

Eric Gilbertson

B.S., Massachusetts Institute of Technology (2008)

Submitted to the Department of Mechanical Engineering
in partial fulfillment of the requirements for the degree of

Masters of Science in Mechanical Engineering

at the

MASSACHUSETTS INSTITUTE OF TECHNOLOGY

June 2010

Author .....
Department of Mechanical Engineering
May 14, 2010

Certified by .....
Franz Hover
Doherty Assistant Professor in Ocean Utilization
Thesis Supervisor

Accepted by .....
David E. Hardt
Graduate Officer, Department of Mechanical Engineering

Gas Lift Valve Failure Mode Analysis and the Design of a Thermally-Actuated Positive-Locking Safety Valve

by

Eric Gilbertson

Submitted to the Department of Mechanical Engineering
on May 14, 2010, in partial fulfillment of the
requirements for the degree of
Masters of Science in Mechanical Engineering

Abstract

Gas-lifted oil wells are susceptible to failure through malfunction of gas lift valves. This is a growing concern as offshore wells are drilled thousands of meters below the ocean floor in extreme temperature and pressure conditions and repair and monitoring become more difficult. Gas lift valves and oil well systems have been modeled but system failure modes are not well understood. In this thesis a quasi-steady-state fluid-mechanical model and a transient thermal model are constructed to study failure modes and sensitivities of a gas-lifted well system including the reservoir, two-phase flow within the tubing, and gas lift valve geometry. A set of three differential algebraic equations of the system is solved to determine the system state. Gas lift valve, two-phase flow, and reservoir models are validated with well and experimental data. Sensitivity analysis is performed on the model and sensitive parameters are identified. Failure modes of the system and parameter values that lead to failure modes are identified using Monte Carlo simulation. In particular, we find that the failure mode of backflow through the gas lift valve with a leaky check valve is sensitive to small variations in several design parameters. To address the failure modes studied, a positive-locking, thermally-actuated safety valve is designed to shut off flow through the gas lift valve in the event of failure. A prototype of the positive-locking valve is constructed and thermal actuation is tested.

Thesis Supervisor: Franz Hover
Title: Doherty Assistant Professor in Ocean Utilization

Acknowledgments

I would first like to thank my advisor Dr. Franz Hover for all his guidance on the project. Thank you to my advisors at Chevron, Ed Colina, Bryan Freeman, and Jose Arellano for all your feedback and for answering all my gas lift questions. Thank you to my labmates Brenden, Brooks, Charlie, Josh, Kyle, Kyle, Lynn, and Rob. Thanks Angharad for an excellent job figuring out Labview and getting all the sensors working. I'm also grateful to the MIT Outing Club for getting me up in the mountains for breaks from schoolwork.

This work is supported by Chevron Corporation, through the MIT-Chevron University Partnership Program.

Contents

List of Figures

List of Tables

Chapter 1

Introduction

1.1 Background

1.1.1 Petroleum Production

Petroleum is one of the most widely-used natural resources in the world today. It is a key component of most plastics from shopping bags to polypropylene T-shirts, and provides more than half the world's supply of energy for use in heating, transportation, and industry [58]. Petroleum is extracted from the ground in the form of crude oil before being refined and converted for use in liquid fuels or plastics.

Petroleum was first used by the ancient Sumerians as early as 4000BC as a component of asphalt for construction and ornamentation [58]. The modern usage of petroleum for heating and transportation began in 1857 with the discovery of oil at Oil Creek, Pennsylvania. It was discovered that the black substance from the wells could be distilled into burning oils and lubrication, and the Pennsylvania Rock Oil Company was soon founded. By the mid 1870s the US was producing over 10 million barrels of oil per year for use as kerosene, paraffin, and lubrication, and by the early 1900s oil was used in the first internal combustion engine.

Today global oil consumption is approximately 180 quadrillion BTU (30 billion barrels) per year and still increasing [66]. As shown in figure 1-1, more oil is used annually worldwide than any other energy source, and the US Energy Information

Administration projects this trend to continue for at least the next 20 years.

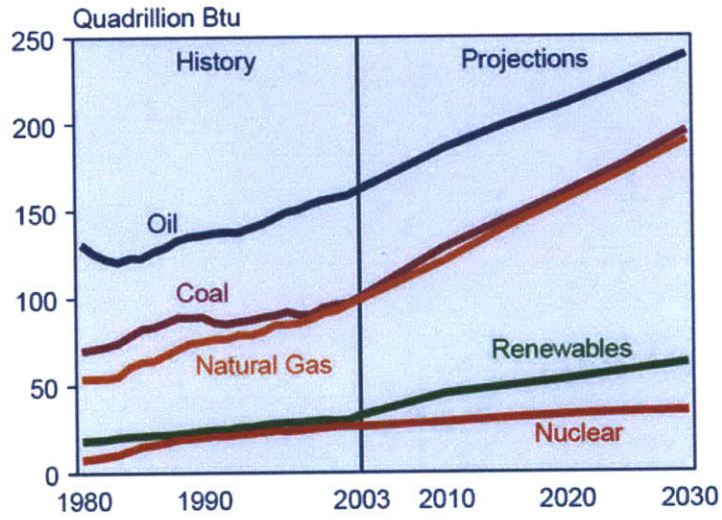

Figure 1-1: Energy Consumption [66]

Currently Saudi Arabia is the country with the highest estimated oil reserves at close to 300 billion barrels, while Canada, Venezuela, Iran, Iraq, and Russia all have estimated reserves of close to 100 billion barrels [65]. Estimated reserves for all countries are shown in figure 1-2.

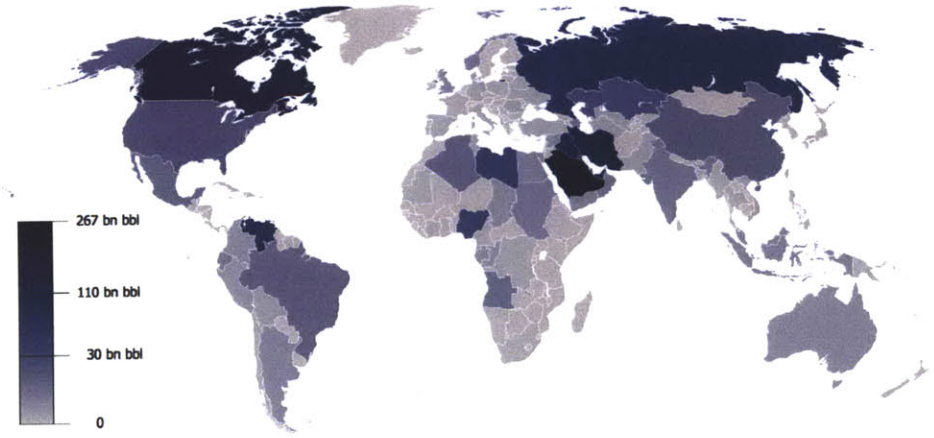

Figure 1-2: Global estimated oil reserves [65]

These estimated global oil reserve numbers can be used with the oil consumption rate to predict how much longer global oil supplies will last. According to the US Geological Survey, global oil production is projected to continue to increase, reaching

a peak value sometime between 2026 and 2047, with the most likely time being 2037 (figure 1-3). Production will then decrease sharply for the next 10 years as supplies diminish, most likely falling to year 2000 levels around 2050.

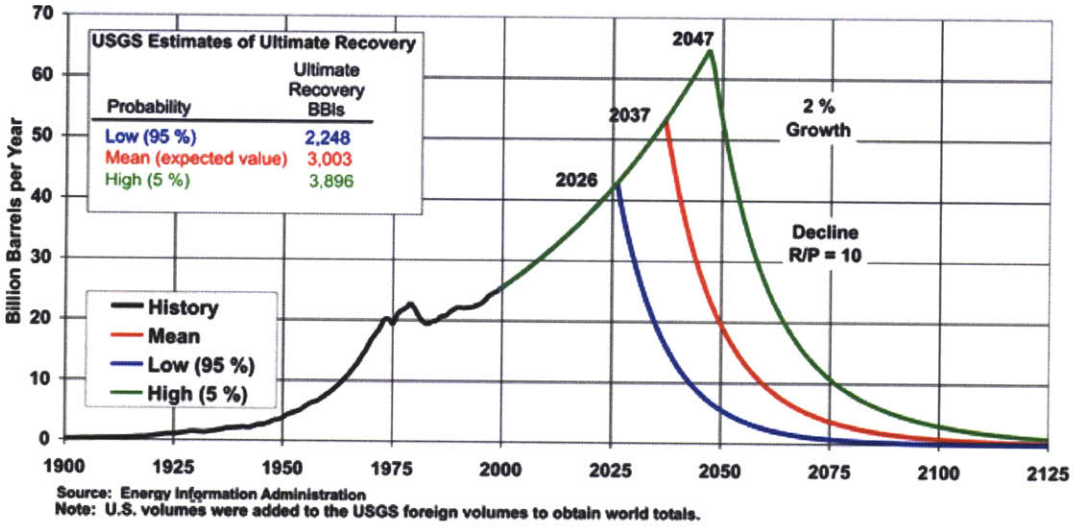

Figure 1-3: Projected global oil supply [29]

The data from the previous figures shows that oil will continue to be the most-used energy source worldwide for at least the next 20 years, with usage steadily increasing every year. It is thus important that research continue to be conducted into the safest ways to extract and produce oil.

1.1.2 Oil Production Today

Currently, 60 percent of the world's oil is produced by so-called giant oilfields - those with a capacity of at least 500 million barrels of oil. Of the 331 giant oilfields in existence today, almost 80 percent have plateaued in oil production and will soon decline or have already declined [36]. A majority of these giant fields are on land or shallow water, where oil wells are relatively easy to drill and produce. As these wells plateau, however, oil companies are increasingly exploring the more difficult-to-produce deep-water oil reserves.

The oil industry's first offshore well was drilled in 1947 in shallow water off the coast of Louisiana, but it wasn't until the late 1990's that offshore and deep-water

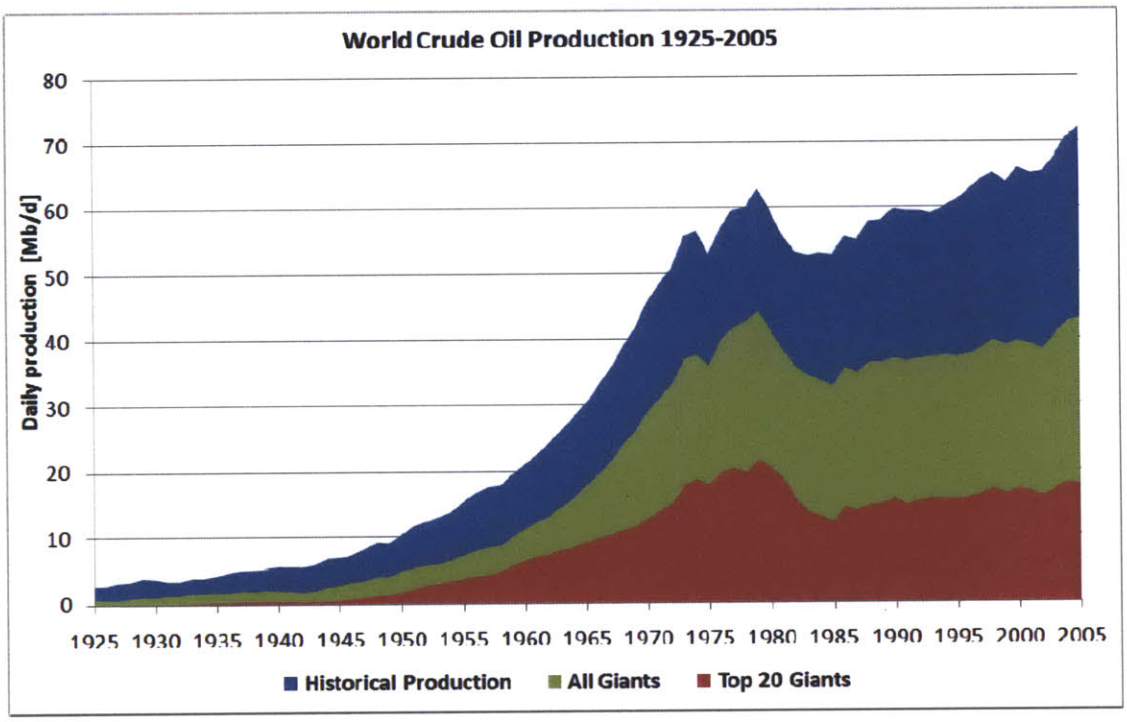

Figure 1-4: Projected global oil supply [36]

wells started becoming more popular. In 2007 there were 130 deepwater well projects and the number is continuing to rise [35]. In 2003 the oil company Chevron drilled a record-setting well in over 10,000ft of water and has plans in the future to drill wells up to 40,000 ft deep in up to 12,000ft of water [35]. By 2015 the company plans for deepwater wells to account for 25 percent of all offshore production.

1.1.3 Extraction Techniques

Most oil wells flow naturally near the beginning of their lives when the pressure at the well bottom is sufficient to overcome frictional pressure losses and atmospheric pressure at the surface. Over time wells can stop flowing for two main reasons:

- Reservoir pressure decreases because of loss of fluid
- Increase in oil density leading to increased frictional pressure losses in the well. Most wells produce some natural gas in addition to oil, and as the well ages less gas may be produced, leading to a more purely oil, higher-density fluid. [61]

Wells that do not flow naturally must be produced with artificial lift techniques. The main artificial lift techniques used are pumping and gas lifting. Pumping involves the use of a pump inserted downhole to increase the pressure at the bottom of a well. For shallow wells, sucker-rod pumping is the most common pumping form used. In sucker-rod pumping a positive-displacement plunger pump is inserted into the well bottom and connected to the surface with a rod (see figure 1-5). The horsehead moves up and down, pulling and pushing the rod to power the pump downhole. Sucker-rod pumps have been used at depths up to 14,500 ft [18], but are generally limited to lower depths (around 4000 ft or less) because of the increasing rod weight at high depths [50]. Sucker-rod pumps are also not well-suited to pumping oil with a high gas/liquid ratios.

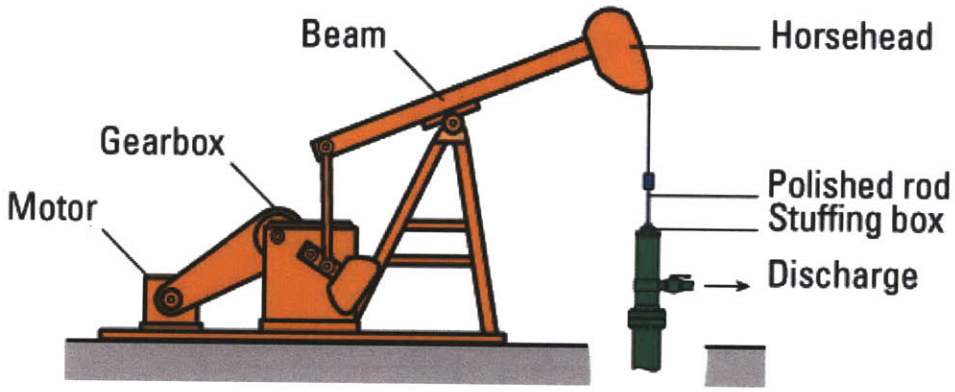

Figure 1-5: Projected global oil supply [52]

For deeper wells rodless pumps, such as electric submersible pumps (ESPs) and jet pumps, are more commonly used. In this technique usually a centrifugal, positive displacement, or hydraulic pump is inserted into the bottom of the well and powered by an electric wire or hydraulic fluid line running to the surface. Rodless pumps have been used at depths over 18,000ft, but they are susceptible to damage from high gas/liquid-ratio fluids, and corrosive and abrasive materials [50]. Because these pumps are integrated into the tubing, the entire tubing string must be pulled in the event of pump failure. This is a long and expensive procedure for deep off-shore wells.

The most well-suited artificial lifting technique for deep-water wells is gas lifting [61].

A gas-lifted well consists of an inner pipe called a tubing string connecting the reservoir to the surface and an outer pipe surrounding the tubing called a casing. The gap between the tubing and casing is referred to as the annulus. In gas-lifted wells, gas is typically injected through the well annulus and into the well tubing at a down-well location as close to the well bottom as possible (as shown in figure 1-6).

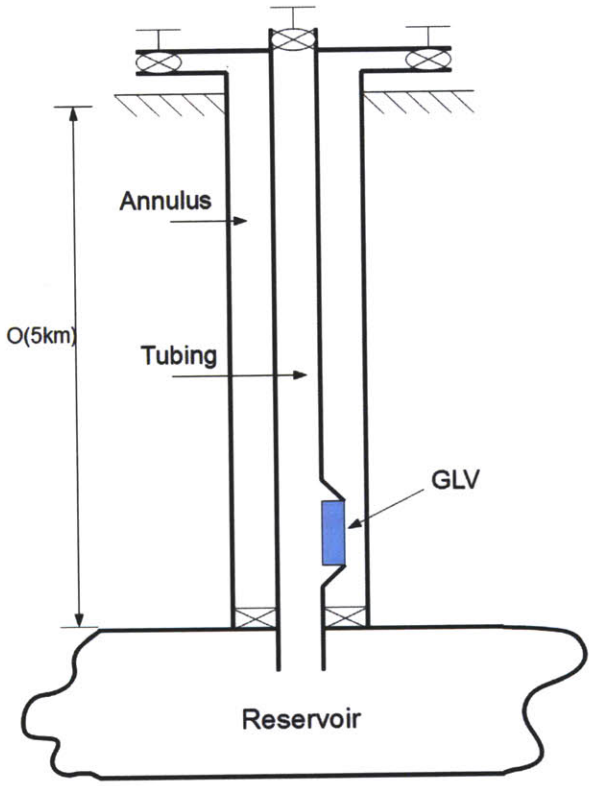

Figure 1-6: Schematic of oil well with gas lift valve (GLV). Top of figure represents sea floor.

The gas mixes with the oil in the tubing, aerating the oil and decreasing its density. This causes the oil to rise to the surface. There are several other methods to operate gas-lifted wells, but for this paper the most common method of gas injection into the annulus and production through the tubing is assumed.

The main advantages of gas lift for deep-water wells are [61]

- Gas lift can handle the high temperatures found at the bottom of deep wells
- Of all artificial lifting methods, gas lift is capable of lifting the greatest amount of liquid from any depth
- Gas lift allows the reservoir to be completely depleted of oil
- Gas lift can handle deviated or crooked wells
- Gas lift can handle wells with high amounts of formation gas where other pumping methods may not be possible
- Gas lift can handle corrosive materials.

For these reasons, gas lift is the most popular form of artificial lifting used in deep-water wells.

1.1.4 History of Gas Lift

The first use of gas lift was to remove water from mines in Chemnitz, Hungary in the mid 18th century [54]. Gas lift was first used in the oil industry in 1864 for wells in Pennsylvania. Called a 'well blower', the system consisted of an air-filled pipe connected to the tubing that blew compressed air into the bottom of the well to decrease oil density and increase well production rates [8]. In Texas around 1900 gas lift with air was first used in large-scale oilfield applications, and in 1920 natural gas replaced air as the lifting gas of choice because it had a lower risk of explosion.

Initially gas was injected essentially uncontrolled into the bottom of the well and gas lift application was limited to shallow wells because of low injection pressures attainable [61]. In the mid 1930s the invention of a spring-operated differential gas lift valve and the development of a stepwise unloading process consisting of multiple well injection points allowed gas lift to be used for wells of even greater depths. The spring-loaded differential valve opened if there was enough pressure difference between casing and tubing, and allowed a more controlled gas injection. These valves were fixed in place on the tubing. Other valves were developed that could be mechanically

opened from the surface [7], but these all had reliability problems, and if they failed the entire tubing had to be replaced to replace the valve.

In 1944 the first pressure-operated gas lift valve was patented by W.R. King [33]. This valve uses a pressurized bellows instead of a mechanical spring to control gas injection. Wireline retrievable valves were later invented, allowing the valve to be replaced in the event of malfunction without replacing the entire tubing.

1.1.5 Gas Lifting Today

Since 1900 over 25,000 patents related to gas lift valves have been issued in the US alone, but the basic idea of the King valve is still the most widely-used today [61]. Gas lift valves used today are one-way valves that allow gas to pass through to the tubing but prevent oil from passing through to the annulus. Most valves, like the king valve, contain a pressurized bellows valve and an internal check valve (see figure 2-1). These valves are called injection pressure operated (IPO) valves because the pressure of the injected gas creates the dominating force to open or close the bellows.

The bellows valve opens when the injection gas is pressurized above a threshold value, and the internal check valve prevents oil from passing through the gas lift valve into the annulus. The most common type of gas lift valve used in industry today is a wire-line retrievable IPO valve that is inserted downhole into a side-pocket mandrel (figures 1-8, 1-9).

This type of valve can be pulled up to the surface using a special wire-line tool if the valve needs maintenance or replacement. When installed, this valve is lowered into the tubing and into the side-pocket mandrel so that a hole in the side of the gas lift valve is close to the same level as a hole between the side pocket mandrel and the annulus (see figures 1-9, 1-10). Two O-rings above and below the gas lift valve side hole create a sealed chamber around the gas lift valve above and below the hole level. This allows gas injected through the mandrel side hole to still enter the gas lift valve even if the two holes are not exactly aligned. In this paper all gas lift valves will be assumed to be wire-line retrievable IPO valves.

Gas lift valves must be designed not only to allow gas passage and prevent oil

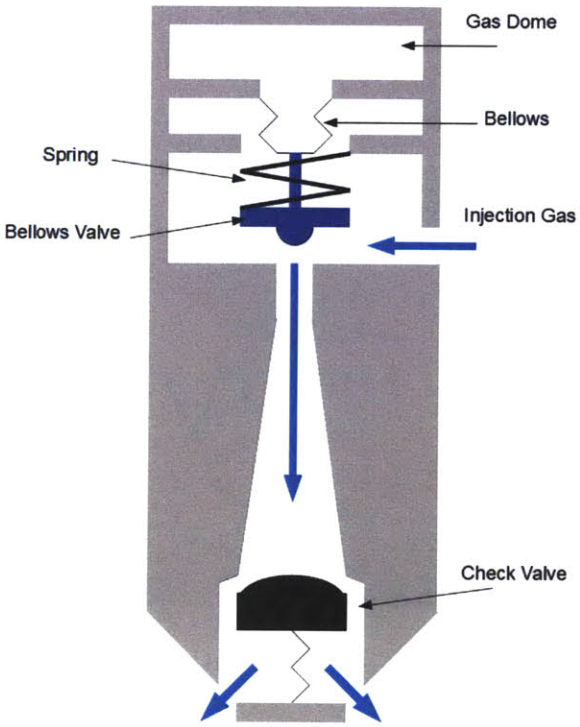

Figure 1-7: Gas lift valve schematic diagram

passage, but also for gas injection into wells to be started and stopped when needed. When a well is initially drilled, typically water or oil from the reservoir will partially fill the tubing and annulus, blocking gas injection. A special unloading process (figures 1-11, 1-12, 1-13) must be used to remove this liquid. To accommodate the unloading process, multiple gas lift valves are installed along the length of the well with gas lift valves lower in the tubing having bellows pressurized to lower pressures.

In the unloading process, gas is injected into the annulus at an initially low pressure and the pressure is gradually increased until the first valve begins passing gas. The pressure here is controlled by controlling the choke size of the injection. After the first valve begins passing gas, the gas mixes with the oil in the tubing and the hydrostatic pressure in the tubing drops, allowing the liquid level in the annulus to drop more until the second valve begins passing gas. With two valves now passing gas, the gas pressure drops and the top valve closes, leaving only the second valve

Figure 1-8: Picture of an actual gas lift valve, with cutaway view of bellows valve and check valve section.

passing gas. This passive process repeats until the bottom unloading valve is reached. At this point only the bottom valve is open and passing gas.

Proper function of gas lift valves is very important for the safety of the well and surface operations. If hydrocarbons flow through the wrong path (i.e. backflow from the tubing into the annulus, through a gas lift valve leak), they can reach the wellhead and create an undesired accumulation of high-pressure combustible material. Wrong manipulation of surface valves, procedures and accumulation of gases is thought to have caused the 1988 accident on the Piper Alpha North Sea production platform, which led to an explosion and fire killing 167 men [44]. With offshore wells being drilled thousands of meters below the ocean in extreme temperature and pressure conditions, repair and monitoring of gas lift valves is becoming more difficult. Thus, it is important to understand which valve conditions lead to failure modes and which valve parameters the failure modes are most sensitive to, and to use this knowledge to design valves that are safer and more reliable.

In this thesis, a quasi-steady state model for the entire gas-lift system is presented

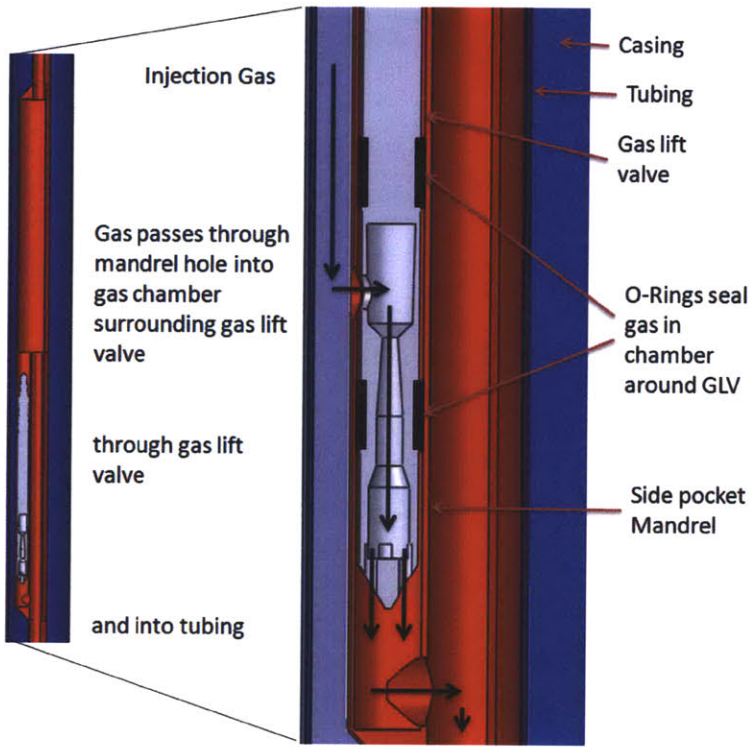

Figure 1-9: Close-up of gas lift valve in mandrel.

and sensitive parameters identified. Failure modes of the system and parameter values that lead to failure are identified using Monte Carlo simulation. Results are used to motivate the need for a positive-locking device in the gas lift valve to prevent oil from passing into the annulus in the event of system failure. A thermally-actuated positive locking valve is proposed, modeled, built, and tested.

1.2 Modeling Previous Work

Several models have been developed for gas lift valves with experiments to back up predicted behavior [70], [25], [5], [14]. Basic sensitivity analysis has been conducted on the bellows position relative to temperature and pressure changes [67]. Several models have also been developed for the two-phase oil-gas flow inside the tubing [4], [3], [41], [21]. Commercial software systems such as PROSPER [46] and OLGA [59] are also available for analyzing artificial gas lift valves. However, no work has been published giving a full sensitivity analysis and failure mode analysis of the entire gas

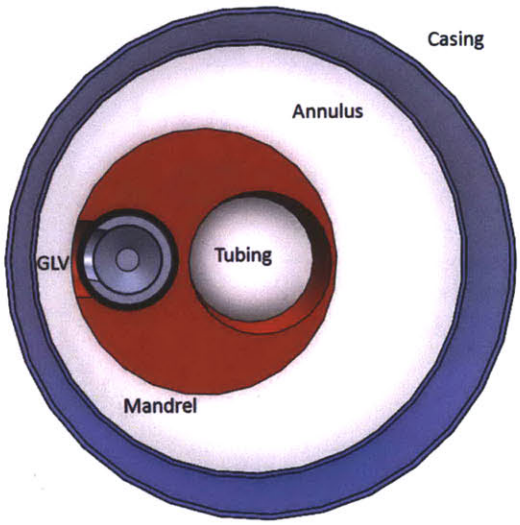

Figure 1-10: Gas lift valve

lift system (including gas lift valve, tubing, and reservoir). This systematic analysis is important because designers of new gas lift valves need to know which parameters are most important to consider in redesigning valves to be less susceptible to failure.

In this thesis a quasi-steady state model is developed for the entire gas-lift system. Sensitivity analysis is performed on the model and sensitive parameters are identified. Failure modes of the system and parameter values that lead to failure modes are identified using Monte Carlo simulation.

The goal in developing this model and program was to gain a deeper insight into the physical mechanisms at work. This will allow design improvements to be developed in future work.

1.3 Thermally-Actuated Positive Lock Prior Art

A patent review of thermally-actuated fluid valves reveals that this concept has been thought of as early as the 1930s, with about six different actuation techniques that all rely on a change in fluid temperature.

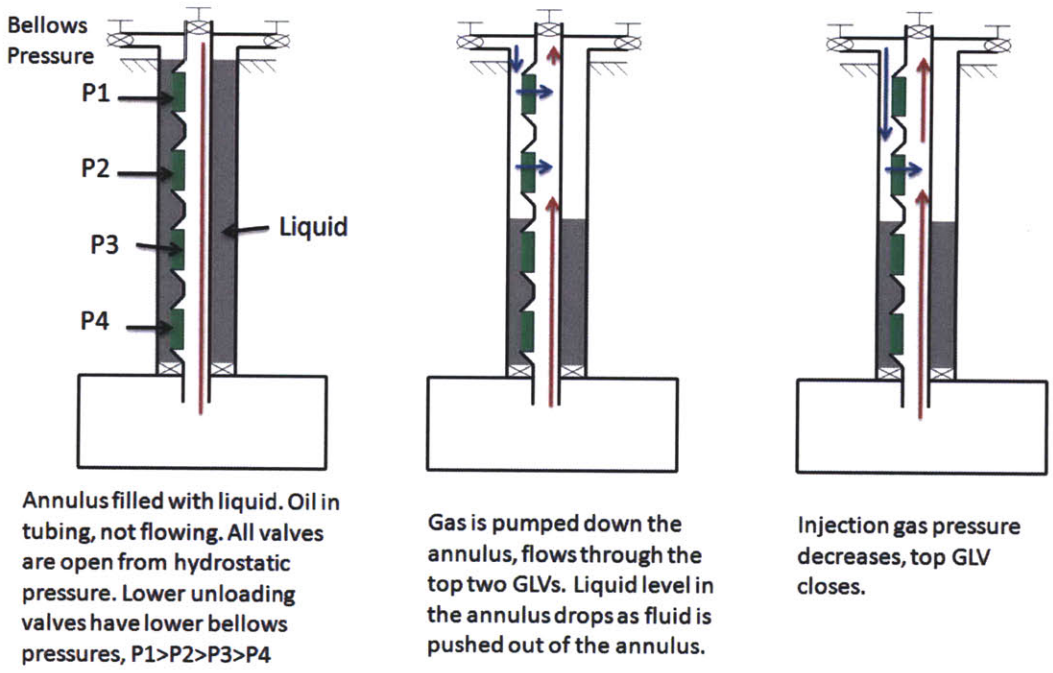

Figure 1-11: Unloading process

1.3.1 Bimetallic Strip

Several patents exist describing an actuation method relying on the movement of a bimetallic strip. A bimetallic strip is a strip of two different types of metal that are joined together. Because the different types of metal have different thermal expansion properties, one will expand more than the other when heated. Thus the bimetallic strip will bend when heated due to the differential expansion of the metals. This concept is used in [6], [48], and [45] to actuate gas valves.

1.3.2 Gas Expansion

Another actuation technique is based on the thermal expansion of gas at high temperatures. In [49] and [37], a valve is described that uses a gas-filled bellows which expands or contracts under different temperatures to open or close a gas valve. This valve is applied as a safety feature to gas-burning stoves.

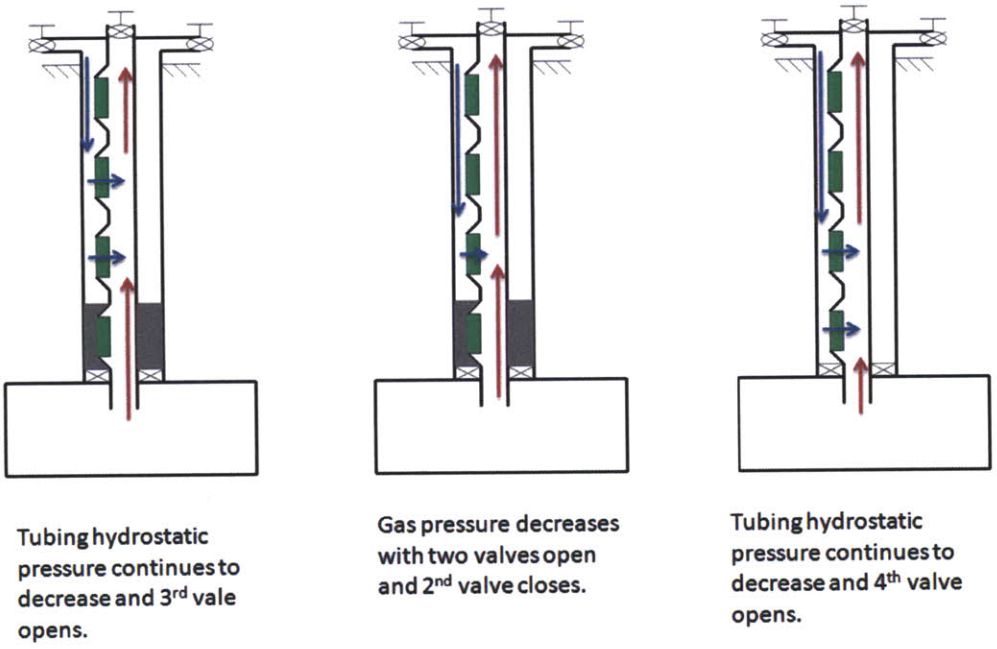

Figure 1-12: Unloading process

1.3.3 Fluid Expansion

Fluids, like gases, expand or contract under temperature changes and this has also been proposed as a valve actuation technique. In [63], a control fluid next to a diaphragm expands under heat and pushes the diaphragm to close a valve. This concept is applied to steam traps in factories. [47] proposes a wax-filled thermal actuator that expands or contracts under temperature changes to open or close valves, with an application to water temperature regulation between freezing and scalding.

1.3.4 Solid Expansion

One patent, [20], describes an actuation technique using a solid material with a high coefficient of thermal expansion. The material is wound into a helical spring and placed in a fluid flow. When the helix heats up it expands to choke the flow and it contracts when cooled.

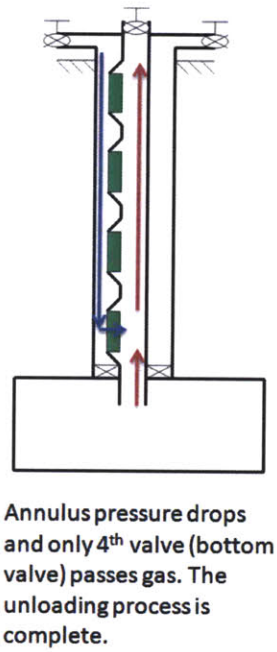

Figure 1-13: Unloading process

1.3.5 Dissolving Solid

A concept used in some smoke detectors relies on a solid material that dissolves when heated past a threshold temperature [31]. The dissolvable solid holds a valve open and dissolves when heated, allowing the valve to close.

1.3.6 Shape Memory Alloys

Shape memory alloys are materials that retain a memory of a high-temperature and low-temperature shape. These materials undergo a solid-state phase change at a specific threshold temperature to change between a Martensitic and Austenitic phase. For example, a helical spring made of a shape memory allow may be in a contracted state at all temperatures above a threshold transition temperature, and in an expanded state at temperatures below the transition temperature. Shape memory alloys will be described in more detail in chapter 4. [69] proposes multiple embodiments of shape memory alloy actuating valves and the claim covers 'a valve assembly with an open and closed position, means with which to bias the valve to one position, and a control member that may be temperature-actuated'. In [38], a shape-memory alloy

such as Nitinol is proposed to change between two distinct shapes when heated to actuate a valve. A shape memory alloy in the shape of a helix is proposed in [24]. The helix is placed in a fluid flow and attached to the valve seat. The helix expands or contracts based on the fluid temperature, and thus opens or closes the valve. In [62] a general claim is made for a subsurface valve actuated by a shape memory alloy for use in oil wells. The proposed embodiment of this valve is a spring-actuated gate valve fixed inside the tubing of the well.

1.4 Autonomous Fluid System Flow Control

The general goal of this thesis is to strengthen the reliability of one particular and important component of a larger autonomous fluid system, namely the gas distribution system of an oil well or set of wells. Future work may include studying the reliability of other autonomous fluid systems. One potential candidate is the larger fluid network of well platforms, wells, and gas distribution lines coupled with the oil refinery fluid network. A case study for this type of network is described in [39], where a 5000-well oilfield in Lake Maracaibo, Venezuela is controlled autonomously. Other examples include sewer systems, such as the Moscow sewer system fluid network studied in [13] and nuclear power plant coolant fluid systems, such as the system studied in [40].

1.5 Relevance to Current Events

Accidents are still occurring on oil rigs today, warranting continued research into improved well safety technology. On April 20th, 2010 the Deepwater Horizon oil rig operating in the Gulf of Mexico 41 miles off the coast of Louisiana exploded killing 11 men in what is thought to have been caused by a failed blowout preventer [23]. The accident occurred while the well was in the final stages of drilling a 6000m deep well in 1500m of water. The Deepwater Horizon had previously in 2009 drilled the world's deepest oil and gas well with a depth of over 10500m. A well blowout occurs when oil or natural gas flow up the well tubing uncontrolled and unexpectedly, possibly

igniting at the wellhead. A blowout preventer is a large set of valves placed at the wellhead and designed to seal off the tubing and casing in the event of a blowout. The valve has multiple redundancies, with hydraulic rams to block flow through the tubing, annular preventers to cut off flow through the annulus, and even a shearing device to cut through the entire piping system to close off the well [16]. Apparently none of these valves worked to completely seal off the well being drilled by Deepwater Horizon. The true cause of the disaster is still under investigation, but the potential exists to add a passive, thermally-actuated valve to the blowout preventer to increase redundancy. During well drilling the tubing is filled with mud to counteract the formation pressure. Because the blowout preventer is placed at the wellhead on the sea bottom and filled with mud, the temperature on the inside and outside of the blowout preventer would be close to freezing (0C). The reservoir temperature would be above freezing, thus if oil or natural gas suddenly began flowing up the tubing, the tubing would heat up. In this case a thermally-actuated positive-locking valve could passively shut off the well.

1.6 Outline

Chapter 2 covers a quasi-steady state pressure model of the gas lift system including the reservoir, riser, and gas lift valve. The model is validated using pressure profiles measured from several actual wells. Sensitive parameters of the model are identified. Failure modes of the system and parameter values that lead to failure modes are identified using Monte Carlo simulation.

Chapter 3 presents a design for a thermally-actuated positive locking mechanism that will actuate in the event of valve failure and prevent product from entering the annulus.

Chapter 4 details how well unloading and shut-in operations will be carried out with the positive locking mechanism in place.

Chapter 5 covers a steady state thermal model of the tubing and annulus temperature profiles and a transient state thermal model of the gas lift valve during

unloading and shut-in periods. These models are used to verify the feasibility of thermally actuating the positive lock.

Chapter 6 describes the construction of a physical prototype of the positive lock valve and experiments run to test the valve actuation under simulated failure scenarios.

Chapter 7 draws conclusions and describes future work.

Chapter 2

Quasi-Steady State Model

2.1 Modeling Assumptions

2.1.1 Valve

- The gas lift valve is injection pressure operated.
- A gas-filled bellows and spring are used in parallel.
- The bellows contains an incompressible gas dome.
- Side-forces on the bellows are small compared to the bottom force (by the small angle approximation for the folds in the sides of the bellows).
- No elastic deformation of bellows (also by the small angle approximation).
- The pressures at operation state will be such that the valve is in a quasi-steady state of completely open or completely closed. The transition between open and closed positions is not studied.

2.1.2 Gas-Fluid Mixture Above Valve

- The gas-fluid mixture is assumed to be homogeneous and in a quasi-steady state.

- The pipe is assumed to be well-insulated and thus the gas-fluid mixture is at a constant temperature equal to reservoir temperature. (Future model iterations will include temperature dependence).

2.1.3 Gas Inflow

- The injection gas pressure is set from the surface, and the mass flow rate of the injection gas into the tubing is dictated by the size of the valve opening.

2.1.4 Fluid Below Valve

- The fluid below the valve is pure oil (no water). This assumption is reasonable for new wells when little water is produced, but not for older wells which have higher water cuts [28].(Future model iterations will include non-zero water cuts).

2.1.5 Reservoir

- The reservoir is assumed to be cylindrical with pure oil inflow to the tubing.

- The reservoir pressure is assumed to be known from other sources and to remain constant.

2.2 Modeling Approach

Three constitutive equations of the fluid-mechanical system must simultaneously be satisfied: a differential equation of the well's pressure vs depth, an equation describing the oil mass flow rate from the reservoir into the tubing, and an equation relating the valve position to the pressure difference between the injection gas and the oil in the tubing.

2.2.1 Pressure

The pressure change in the tubing is a result of hydrostatic and frictional pressure losses. Because the fluid is assumed to be in a quasi-steady state, there are no acceleration pressure losses. Thus the pressure drop equation in the tubing is

$$\frac{dp}{dz} = \rho(z)g + \frac{f(v(z))\rho(z)v^2(z)}{2D} \tag{2.1}$$

with the boundary condition of surface pressure (which is controlled at the wellhead). Here p is pressure, z is depth, ρ mixture or liquid density, g is gravity, f is the friction factor, v is the mixture velocity, and D is the pipe diameter. This differential equation is applicable below and above the injection point. Below the injection point the density is the oil density while above the injection point the mixture density is given by

$$\rho_{mix} = \frac{\rho_g \rho_l}{q\rho_l + (1-q)\rho_g} \tag{2.2}$$

where ρ_g is the gas density, ρ_l is the liquid density, and q is the mixture quality, defined as the ratio of gas mass to total mixture mass [22].

The friction factor from equation (1) is determined by the Reynold's number of the fluid or mixture. The Reynold's number is a unitless measure of the ratio of inertial to viscous forces in a fluid and is given by

$$Re = \frac{\rho v D}{\mu} \tag{2.3}$$

where μ is the fluid viscosity. The flow is considered laminar for Reynolds numbers less than 2300 and turbulent for Reynolds numbers greater than or equal to 2300 [68]. For laminar flow the fluid friction factor is given by

$$f = \frac{64}{Re} \tag{2.4}$$

and for turbulent flow the friction factor is given by

$$f = \frac{1.325}{\ln^2(\frac{r}{3.7D} + \frac{5.74}{Re^{0.9}})} \tag{2.5}$$

where r is the pipe roughness and D is the pipe inner diameter [68].

2.2.2 Oil Flow from Reservoir

Oil flow out of the reservoir and into the tubing is driven by a pressure difference between the reservoir and the bottom of the wellbore. This pressure difference is related to the oil mass flow rate by Darcy's Law,

$$\dot{m}_l = \frac{\rho_l h k_{well}(P_{res} - P_{bot})}{B\mu_l \ln(\frac{r_e}{r_w} + S)} \tag{2.6}$$

where $\dot{m}_l$ is the oil mass flow rate, ρ_l is the oil density, μ_l the oil viscosity, h the reservoir thickness, B the fluid formation volume factor, r_e the distance from the wellbore to the constant pressure boundary of the well, r_w the distance from the wellbore to the sand face, S the skin factor, P_{res} the reservoir pressure, and P_{bot} the well bottom hole pressure [19].

2.2.3 Valve Position vs Flow and Pressure

The valve is modeled as an injection-pressure-operated pressurized bellows in parallel with a spring in tension. The bellows is connected to a pressurized dome of constant volume (see figure 2-1). The bellows itself is modeled as a series of frustums connected in an accordion-type fashion (see figure 2-2). If the temperature of the gas inside the bellows is assumed to remain approximately constant, then when the bellows compresses (ie when the gas lift valve opens), by the ideal gas law

$$P_{b1}V_{b1} = P_{b2}V_{b2} \tag{2.7}$$

where P_{b1} is the initial bellows pressure, V_{b1} is the initial bellows volume, P_{b2} is the final bellows pressure, and V_{b2} is the final bellows volume. The initial and final volumes are given by the frustum volumes. Thus, assuming the frustum radii remain

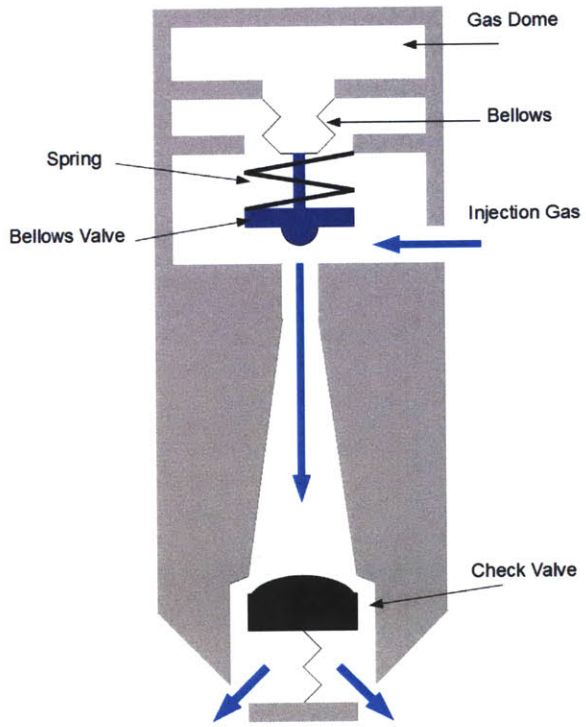

Figure 2-1: Gas lift valve model. Arrows represent injection gas flow

constant and only the heights change, the total elongation or compression of the bellows is given by the difference in heights. This simplifies to

$$E = \frac{V_D(P_{b1} - P_{b2})}{P_{b2}\frac{\pi}{3}(r_1^2 + r_1 R_1 + R_1^2)} + \frac{N h_1 P_{b1}}{P_{b2}} - N h_1 \tag{2.8}$$

where V_D is the dome volume, r_1 is the inner frustum radius, R_1 is the outer frustum radius, N is the number of frustums in the bellows, and h_1 is the height of each frustum.

Forces acting to open the valve are the injection gas pressure acting on the area of the bottom of the bellows and the oil pressure acting on the area of the bottom of the valve stem. Because the area of the bottom of the bellows is much larger than the area of the bottom of the stem, the valve is more sensitive to the injection pressure than the oil pressure. To determine the steady state position of the valve a free body diagram can be analyzed as given in Figure 2-3. By balancing the vertical forces on

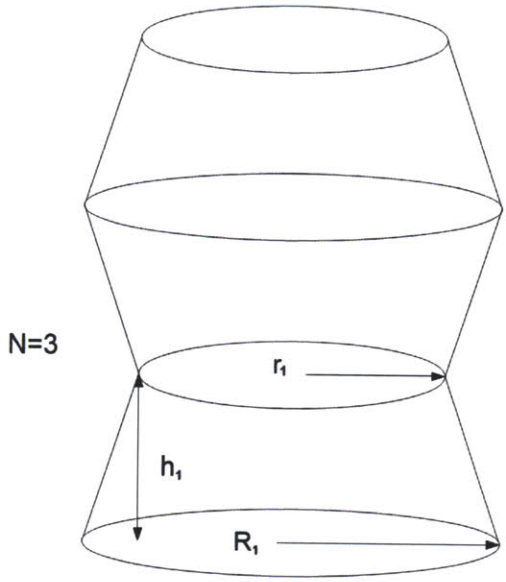

Figure 2-2: Frustum model of the bellows

the bellows, in the closed position the valve position equation is

$$F_{valve} = P_{b1}A_b + K_t\delta x_1 - P_{gas}(A_b - A_p) - P_{oil}A_p \tag{2.9}$$

where F_{valve} is the force between the stem and the valve, A_b is the area of the bottom of the bellows, K_t is the spring constant, δx_1 is the spring pre-stretch distance, A_p is the area of the bottom of the stem, and P_{oil} is the oil pressure at injection depth.

When the valve is open gas flows through the orifice and the valve stem is exposed to the gas pressure instead of the oil pressure. A new force balance yields

$$P_{b2}A_b + K_t(\delta x_2) = P_{gas}A_b \tag{2.10}$$

where δx_2 is the total length the spring is stretched, which is given by the equation

$$\delta x_2 = \delta x_1 + E \tag{2.11}$$

Combining equations (2.11), (2.10), and (2.8) yields the following quadratic equation the total spring stretch length

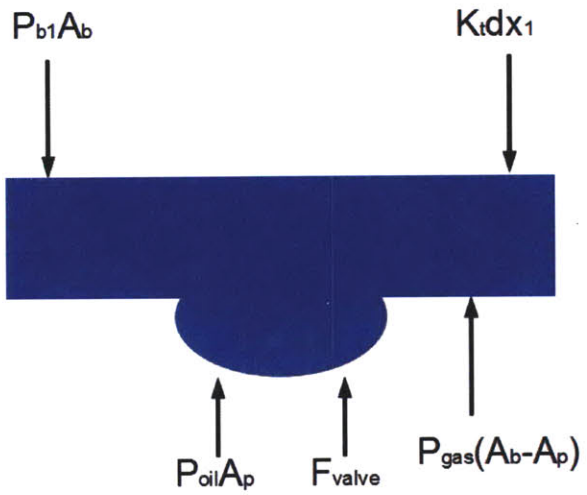

Figure 2-3: Bellows valve free body diagram

$$\begin{aligned} 0 &= (-K_t\chi)\delta x_2^2 + (K_t(\delta x_1 + Nh_1)\chi + K_t V_D + P_{gas}A_b\chi)\delta x_2 + \\ &\quad + (Nh_1\chi + V_D)P_{b1}A_b - P_{gas}A_b((\delta x_1 + Nh_1)\chi + V_D) \end{aligned} \tag{2.12}$$

where χ is defined as

$$\chi = \frac{\pi}{3}(r_1^2 + r_1R_1 + R_1^2). \tag{2.13}$$

Solving for δx_2 yields

$$\delta x_2 = \frac{K_t(\delta x_1 + NH_1)\chi + K_t V_D + P_{gas}A_b\chi}{2K_t\chi} \pm \sqrt{\beta} \tag{2.14}$$

where β is defined as

$$\begin{aligned} \beta &= \left(\delta x_1 + Nh_1 + \frac{V_D}{\chi} + \frac{P_{gas}A_b}{K_t}\right)^2 - 4\left(\frac{Nh_1P_{b1}A_b}{K_t} + \frac{V_DP_{b1}A_b}{K_t\chi}\right) - \\ &\quad - 4\left(P_{gas}A_b\left(\frac{\delta x_1 + Nh_1}{K_t} + \frac{V_D}{K_t\chi}\right)\right) \end{aligned} \tag{2.15}$$

The quadratic equation has two solutions and the positive real solution is chosen.

The position of the valve is then given by the elongation E from equation (2.8).

2.2.4 Injection Gas Flow

The flow of injection gas through the valve is modeled as orifice flow with the orifice area dependent on the valve position. When the valve is completely open the gas flows through an area equal to that of the valve orifice while when the valve is nearly closed the gas flows through only a small fraction of the same area.

The maximum gas flow rate is given by the compressible gas orifice flow equation:

$$\dot{m}_{max} = \frac{C_d \pi d_p^2}{4\sqrt{(1-(\frac{d_p}{d_v})^4)}} P_{gas} \sqrt{\left(\frac{2M}{RT_{inj}} \frac{\gamma}{\gamma-1} \left(\left(\frac{P_{oil}}{P_{gas}}\right)^{\frac{2}{\gamma}} - \left(\frac{P_{oil}}{P_{gas}}\right)^{\frac{\gamma+1}{\gamma}}\right)\right)} \quad (2.16)$$

where C_d is the discharge coefficient, d_p is the orifice diameter, d_v is the total valve diameter, M is the injection gas molar mass, R is the universal gas constant, T_{inj} is the injection gas temperature, and γ is the gas specific heat ratio [68].

To model the flow when the valve is in an intermediate position between completely closed and completely open the flow is assumed to asymptotically approach the maximum flow rate value. This asymptotic behavior can empirically be modeled with an arctangent curve.

$$\dot{m}_{gas} = \dot{m}_{max} \frac{2}{\pi} \arctan\left(\frac{x_1}{x_2} \tan\left(\frac{y\pi}{2\dot{m}_{max}}\right)\right) \quad (2.17)$$

where x_1 is the valve position and y is the flow rate when the valve position is at the value x_2.

2.2.5 Solving the Equations

Input Parameters

Table 2.3 below lists all input parameters that must be specified for this model.

Solution Algorithm

The three constitutive equations for pressure, valve position, and oil mass flow rate can be completely satisfied if the well bottom hole pressure is known. In this algorithm the bottom hole pressure is guessed and the three equations solved to yield a pressure profile of the well. The differential pressure equation has no analytical solution, so the Runge-Kutta numerical solution technique is used. The bottom hole pressure guesses have a lower bound of the hydrostatic pressure of the well if filled with pure gas above the injection point and pure oil below it. The upper bound is the reservoir pressure. With each guess, a surface pressure is determined for that guess and a curve of model surface pressure vs input bottom hole pressure is made. The surface pressure in reality will be either atmospheric pressure (if the well is open at the top) or a known pressure if a pressure-regulating device is used at the well head. Thus the bottom hole pressure guess that yields the known surface pressure is used.

2.3 Comparison with Experimental Data

To check the validity of the model, a pressure profile predicted by the model can be compared to pressure data from an actual well. Pressure surveys of two wells were provided by Chevron for comparison. The model takes 35 input parameters but not all of these parameters are given in the well pressure surveys. Nominal values are initially assumed for these remaining parameters, and the values are optimized within parameter ranges to yield a closer model match with the data. Figure 2-4 shows a pressure profile for a 2750 meter well with data taken between reservoir depth well head depth. Figure 2-5 shows a pressure profile for a 1000 meter well with data taken between reservoir depth and well head depth. Optimized parameter values are given in table 2.2.

1.	P_{gas}	Injection Gas Pressure
2.	P_{res}	Reservoir Pressure
3.	I	Injection Depth
4.	L	Well Depth
5.	D	Pipe Diameter
6.	B	Formation Volume Factor
7.	h	Reservoir Thickness
8.	r_e	Reservoir Radius
9.	r_w	Wellbore Radius
10.	k	Reservoir Permeability
11.	S	Skin Factor
12.	K_t	Bellows valve spring constant
13.	r_1	Bellows inner Radius
14.	R_1	Bellows outer Radius
15.	N	Number of Bellows Frustums
16.	dx_1	Initial Spring Stretch
17.	h_1	Initial Frustum Height
18.	V_D	Dome Volume
19.	P_{b1}	Initial Bellows Pressure
20.	γ	Gas Specific Heat Ratio
21.	C_d	Orifice Discharge Coefficient
22.	μ_L	Oil Viscosity
23.	ρ_L	Oil Density
24.	T	Temperature
25.	μ_g	Gas Viscosity
26.	r	Pipe Roughness
27.	P_{surf}	Surface well pressure
28.	K_c	Check valve spring stiffness
29.	A_b	Outside area of bellows bottom
30.	A_s	Area of stem of bellows valve
31.	A_d	Inside area of bellows bottom
32.	A_o	Area of orifice bottom
33.	y	Maximum check valve spring length
34.	y_0	Initial check valve spring length
35.	d	diameter of obstacle/debris

Table 2.1: Input Parameter Symbols and Descriptions

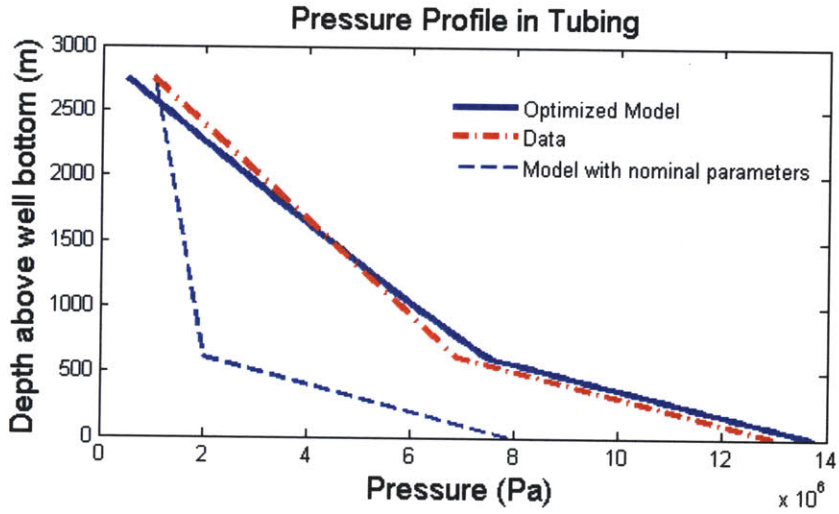

Figure 2-4: Pressure profile for 2750m well. Data taken between reservoir depth and surface.

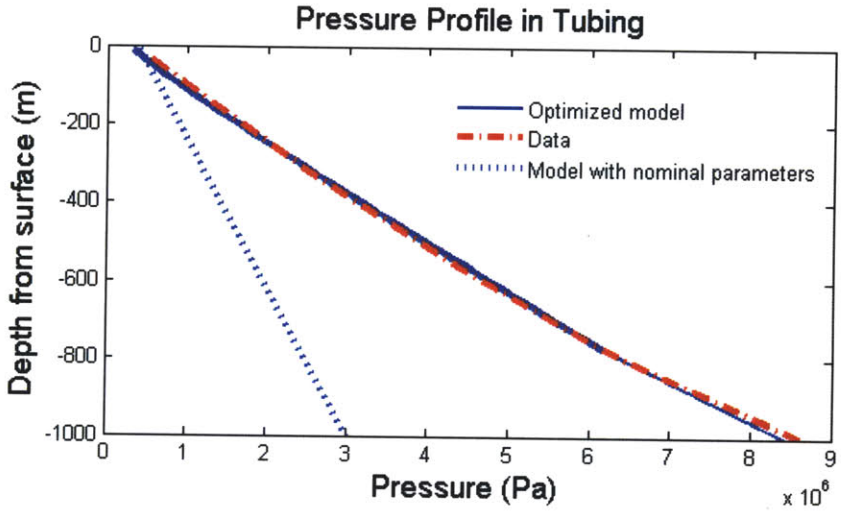

Figure 2-5: Pressure profile for 1000m well. Data taken between reservoir depth and surface.

The magnitude and shape of the modeled pressure profiles are reasonably close to the actual pressure profile. Pressures agree within 10 percent along the entire curves.

2.4 Parameter Sensitivity Analysis

The first step to improve the design of the gas lift valve is to understand the influence each input parameter value has on the important output parameters like oil mass flow rate and valve position [43]. The input parameters that are the most sensitive

to changes represent areas for potential design improvement. For example, if small changes in the bellows pressure lead to large changes in the valve position, then the bellows should be examined as an area for design modification. One way to determine which parameters are the most sensitive is to make a plot of output parameter change vs input parameter change with respect to nominal values for a range of input parameter changes. To compare parameters with different magnitudes of nominal values, the percentage change in output can be compared to the percentage change in input. In figure 2-6 the change in valve position from a nominal starting position is plotted against changes in individual input parameters. When the curve for a given parameter is flat at 0 percent output change this means the output is not sensitive to that parameter, while if the curve has a nonzero slope then the output is sensitive to the input change. In this case if the valve position changes by -100 percent, this means the valve completely closes. A discontinuity in the graph where the slope is nearly vertical represents a sharp change in valve position from open to closed as opposed to a gradual change. This could be caused by the input parameter crossing a threshold value which would immediately close the valve.

Figure 2-6 and additional plots for the remaining input parameters show that the valve position is sensitive to the parameters γ, C_d, r_1, R_1, N, h_1, V_d, P_{b1}, P_{gas}, P_{res}, D, and B.

There are apparently three types of sensitivities:

- Small changes in input have little effect but a threshold change causes the valve to close: γ, C_d, P_{gas}, D, B. This could be caused, for example, by the bellows spring bottoming out.

- Input changes result in roughly proportional changes in valve position: r_1, R_1, N, h_1, V_d, P_{b1}. These parameters directly affect the pressure on the bellows valve and will thus directly affect the valve position.

Parameter	Range of Values	Source	Fit Values Fig 2-4, Fig 2-5 * denotes known value
P_{gas}	$10^5 - 10^7$Pa	[7]	6.9x10^6*, 6x10^6
P_{res}	$10^7 - 10^9$Pa	[7]	3x10^8, 3x10^9
I	100-10^4 m	[7]	2140*, 1002*
L	100-10^4 m	[7]	2750*, 1067*
D	0.02-0.2 m	[7]	0.1016*, 0.0889*
B	1	[19]	0.9, 1.1
h	10-100 m	[19]	190, 200
r_e	100-1000 m	[19]	340, 410
r_w	0.02-0.2m	[19]	0.1, 0.1
k	$10^{-15} - 10^{-13}$ m^2	[19]	2x10^{-13}, 2.1x10^{-13}
S	0-1	[19]	0.001, 0.001
K_t	$10^3 - 10^5$ N/m	[7]	1.7x10^4,1.5x10^4
r_1	0.01-0.02 m	[7]	0.01, 0.012
R_1	0.01-0.02 m	[7]	0.017, 0.015
N	5-20	[7]	12, 15
dx_1	$10^{-5} - 10^{-3}$m	[7]	7x10^-4, 10^{-3}
h_1	0.001-0.01 m	[7]	0.006, 0.005
V_D	$10^{-3} - 10^{-5}$ m^3	[7]	5x10^{-4},5x10^{-4}
P_{b1}	$10^4 - 10^7$ Pa	[7]	4x10^5,4x10^5
γ	1-2	[68]	1.0, 1.3
C_d	0.1-1	[68]	0.7, 0.6
μ_L	0.01-0.1 Pa-s	[61]	0.1, 0.1
ρ_L	800-1000 kg/m^3	[61]	1000, 850
T	300-400 K	[61]	350*, 332*
μ_g	$10^{-6} - 10^{-5}$ Pa-s	[68]	9x10^{-6}, 1.7x10^{-5}
r	$10^{-5} - 10^{-4}$	[68]	5x10^{-5},5x10^{-5}
P_{surf}	$10^5 - 10^7$ Pa	[7]	10^6,10^6
K_c	$10^5 - 10^7$ N/m	[7]	2x10^5, 10^5
A_b	$10^{-4} - 10^{-3}$ m^2	[7]	6x10^{-4}, 5x10^{-4}
A_s	$10^{-6} - 10^{-3}$ m^2	[7]	2x10^{-4},3x10^{-6}
A_d	$10^{-4} - 10^{-3}$ m^2	[7]	9x10^{-4},7x10^{-4}
A_o	$10^{-4} - 10^{-3}$ m^2	[7]	6x10^{-4},5x10^{-4}
y	0.01-0.1 m	[7]	0.1, 0.15
y_0	0.01-0.1 m	[7]	0.3, 0.3
d	0-0.01m	[7]	0*,0*

Table 2.2: Optimized parameter values

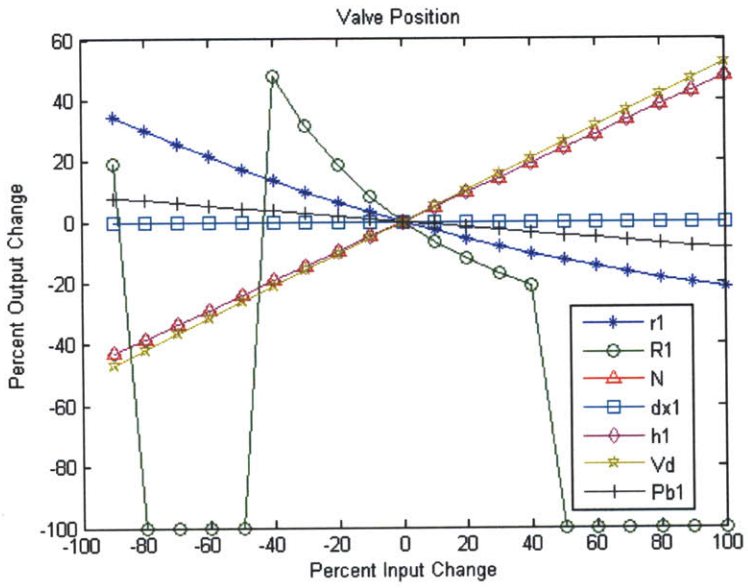

Figure 2-6: Percentage change in valve position vs percentage change in input parameters with respect to nominal starting values

- Input changes have no almost no effect on valve position: μ_L, μ_G, ρ_L, dx_1, h, r_e, r_w, k, S, K_t, P_{res}, I, L. Most of these parameters will effect the oil pressure, but because the oil pressure acts on a much smaller area of the bellows valve than the injection gas pressure, these parameters have very little effect on the valve position.

Similar plots can also be made for other output variables such as the oil mass flow rate (see 2-7).

This figure and figures for the remaining input parameters show that the oil mass flow rate is sensitive to μ_L, ρ_L, γ, h, k, r_e, r_w, B, D, and P_{res}. Figure 2-8 is a plot of the gas injection rate sensitivities and this and additional plots for the remaining input parameters show that the injection gas mass flow rate is sensitive to T, γ, R_1, P_{gas}, I, D, and P_{res}.

2.5 Failure Modes

The main mode of failure of the system is non-closure of the one-way check valve leading to oil flow into the annulus. From figure 2-3 the valve opens when $Fvalve$=0

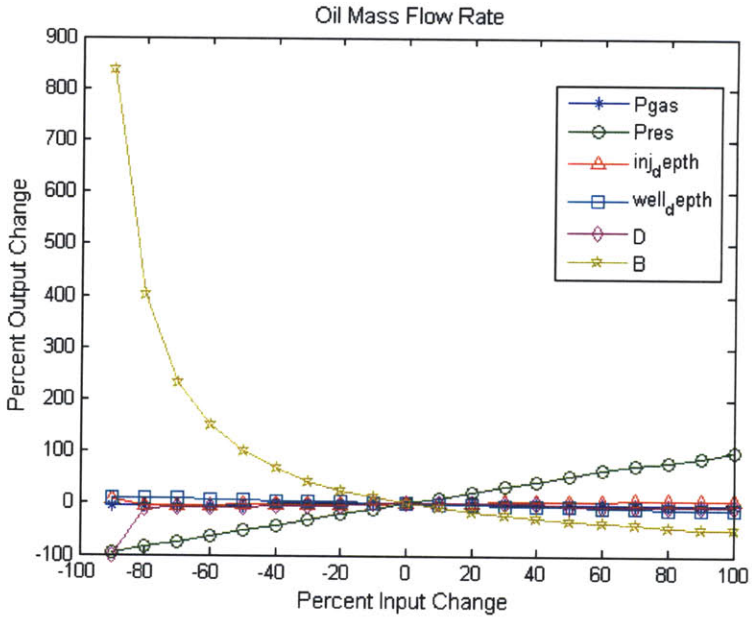

Figure 2-7: Percentage change in oil mass flow rate vs percentage change in input parameters with respect to nominal starting values

and the opening forces are greater than the closing forces, given by

$$P_{oil}A_p + P_{gas}(A_p - A_b) > P_{b1}A_b + K_t d_{x1} \tag{2.18}$$

When the valve opens and the oil pressure is greater than the gas pressure, oil will flow into the annulus if the one-way check valve fails to close. Non-closure of the check valve is mainly caused by the following:

- Debris stuck in main valve or check valve
- Incorrect injection gas pressure. If injection gas pressure is higher than valve opening pressure but less than oil pressure, this would cause the valve to open and oil would flow into the annulus. If a sensitive parameter of the system is modeled with an incorrect value then the model may miscalculate the required injection pressure for optimal flow.
- Bellows pressure too low. Valve could remain open.
- Corrosion of valve stem (main valve or check valve) to prevent uniform contact

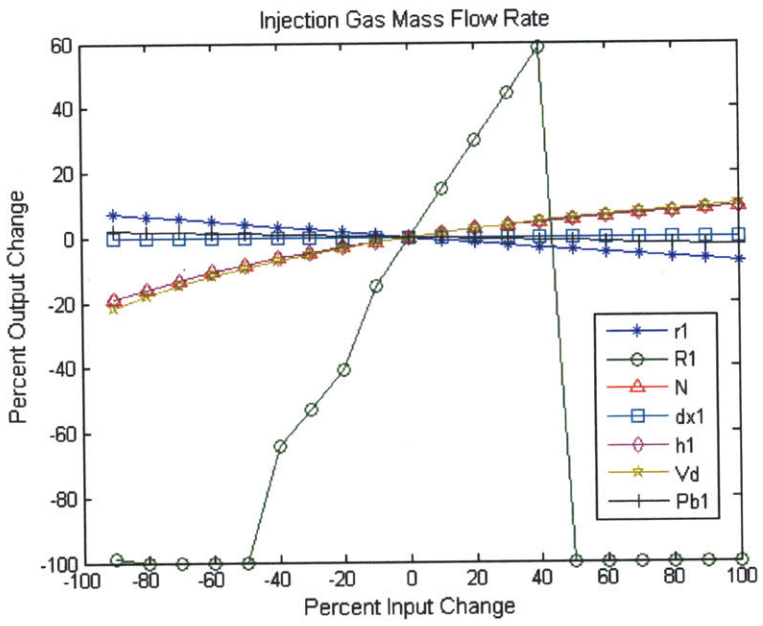

Figure 2-8: Percentage change in injection gas mass flow rate with respect to nominal flow rate vs percentage change in input parameters with respect to nominal values

with orifice. This allows oil to leak into the annulus.

2.6 Multi-Factor Failure: Monte Carlo Simulation

Failure will likely be a result of a configuration of multiple parameters, and it is thus informative to vary multiple parameters simultaneously in a Monte Carlo simulation to see which configurations lead to system failure [55]. For this simulation MATLAB software is used with code generated by the authors. Each of the 35 parameters is assigned a random value from a uniform distribution within +/- 90 percent of the nominal value, with a mean of the nominal value. The set of differential algebraic equations is then solved for this sample of input parameters, and if system failure results then the sample input parameter values are recorded. Histograms are made of individual parameter values that resulted in a failure configuration. For this simulation 250,000 samples were taken.

Of these samples the parameters that had non-uniform histogram distributions at failure were pipe diameter, injection depth, injection gas pressure, reservoir pres-

sure, and bellows outer diameter. Figure 2-9 shows that injection depth tends to be higher when the system fails while bellows outer diameter tends to be lower at system failure. Injection gas pressure and pipe diameter tend to be lower while reservoir pressure tends to be higher. Some parameters do not have definite correlations at failure. For example, bellows pressure values are uniformly distributed at failure so no correlations can be inferred. In each sample it is also possible for there to be relationships between pairs of parameters that lead to system failure. For the same Monte Carlo simulation the correlation coefficients between every pair of parameters was calculated for samples that led to system failure (see figure 2-10). The correlation coefficient, r is defined as

$$r = \frac{n\sum xy - \sum x \sum y}{\sqrt{\left[n\sum x^2 - (\sum x)^2\right]\left[n\sum y^2 - (\sum y)^2\right]}} \tag{2.19}$$

where n is the number of data points (in this case the 40000 failure configurations of the 250000 samples taken), x is the set of values of one parameter that lead to failure, and y is the set of values of a second parameter that lead to failure [32]. A correlation coefficient of zero means no correlation between the two parameters at failure while a coefficient of 1 or -1 means direct correlation between the two parameters at failure. Figure 2-10 shows that all correlation coefficients are less than 0.3, meaning that no pairs of parameters are highly correlated. However, some relationships can be determined from the 6 parameter pairs with correlation coefficients greater than 0.1. Figure 2-11 shows contour plots of failure frequency at different parameter pair values. A plot of parameter pair values was divided into a 10x10 grid and the number of failures in each grid square counted to generate the contour plots. These plots show regions of high and low failure probability. The cross markers in each plot signify approximate locations with least failure probability. For example, the lower right plot shows that failure is most likely for wellhead pressure greater than 10^6 Pa with injection gas pressure less than $2\text{x}10^6$ Pa. This could be because a higher wellhead pressure means that the oil at injection depth is at a higher pressure, and if the injection gas pressure is low than the oil pressure could exceed the gas pressure. This

could lead to oil passing into the annulus in the event of a leaky check valve.

From the upper left plot, failure is most likely for gas specific heat ratio around 1.5 with pipe diameter less than 0.02 m. The upper right plot shows that failure is most likely for injection gas pressure less than $4x10^6$ Pa with pipe diameter less than 0.04 m. The plot of pipe diameter versus reservoir pressure shows that failure is most likely for reservoir pressure greater than $2x10^8$ Pa with pipe diameter less than 0.02 m. From the middle right plot failure is most likely for pipe diameter less than 0.02 m with any wellhead pressure, and from the bottom left plot injection depths greater than 2000 m with injection gas pressure less than $2x10^6$ Pa has the highest likelihood of failure.

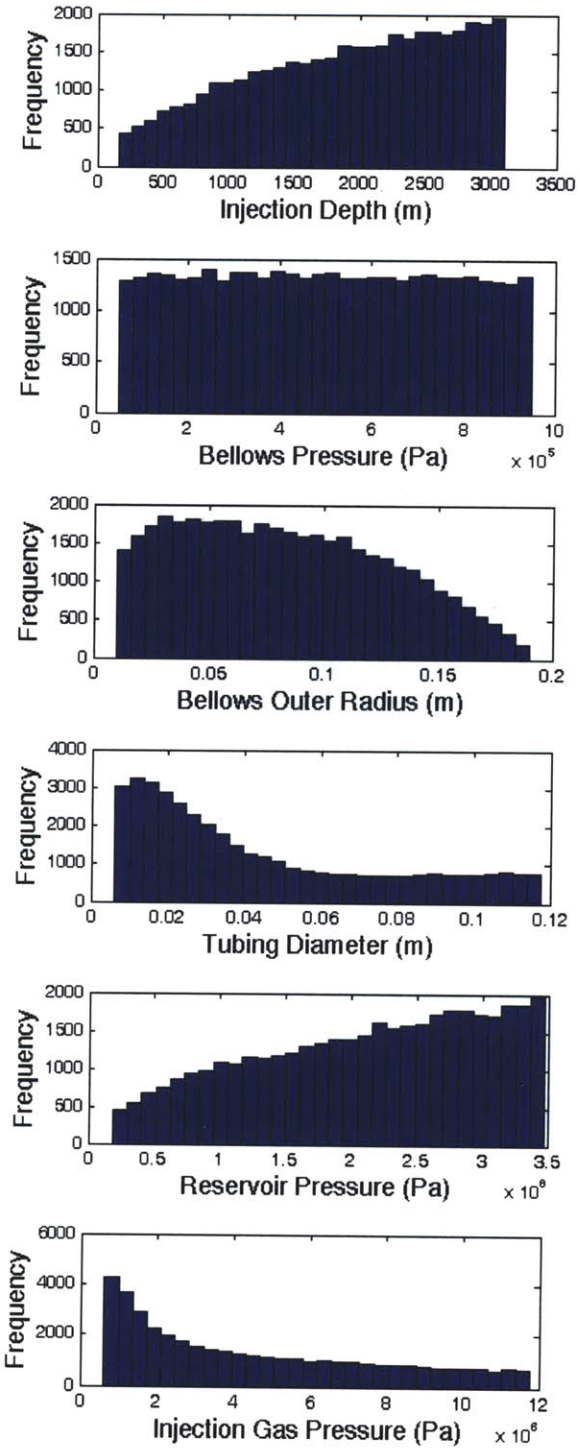

Figure 2-9: MC simulations. Histograms of bellows pressure, bellows radius, tubing diameter, reservoir pressure, and injection gas pressure at failure.

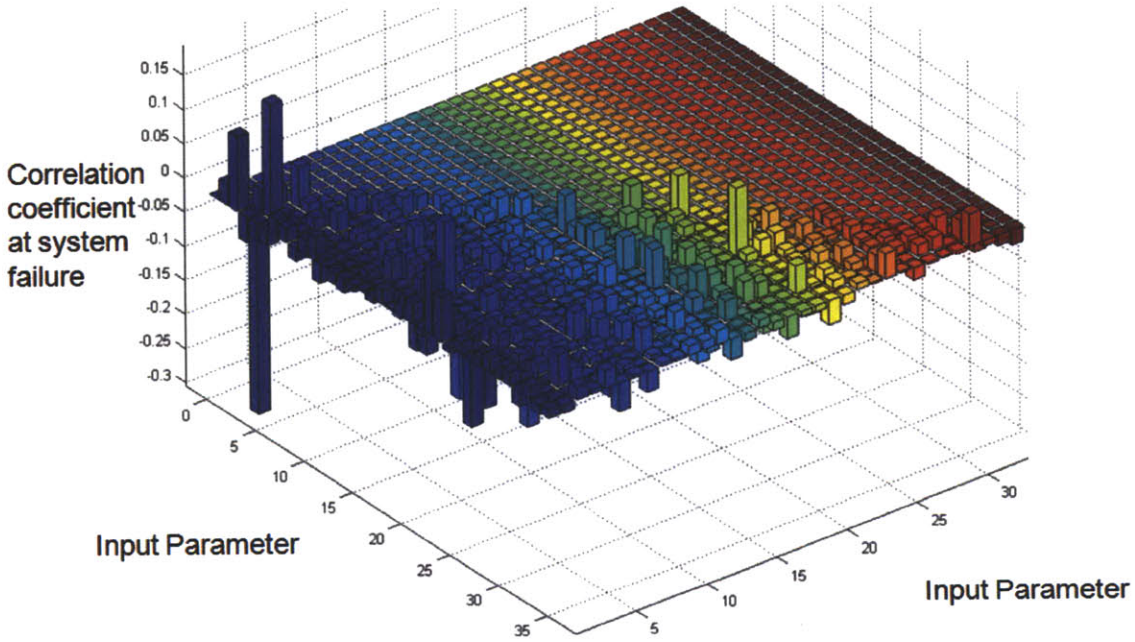

Figure 2-10: Correlation coefficients between two parameters at failure.

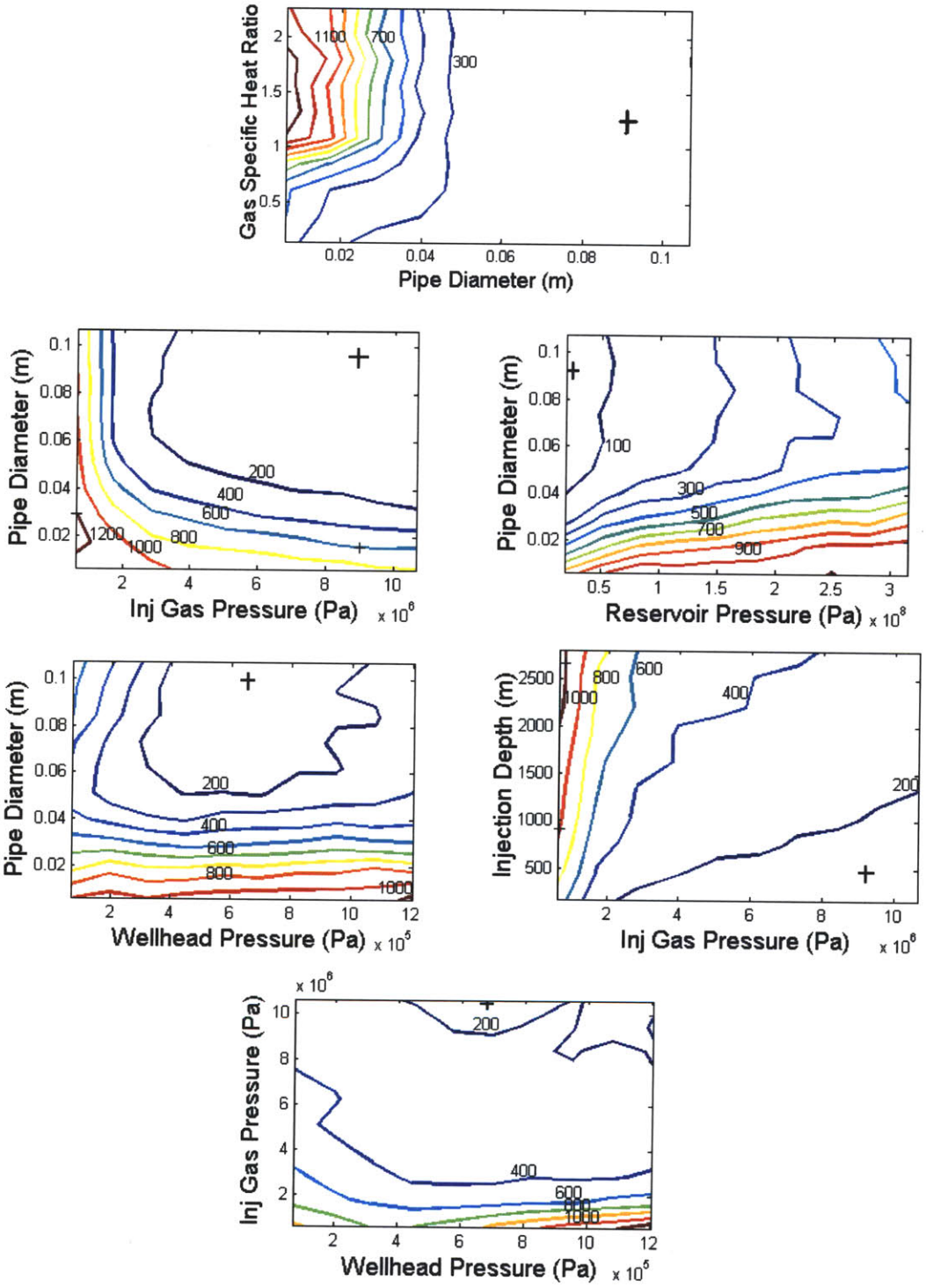

Figure 2-11: Contour plots of failure frequencies of input parameter value pairs. Input parameters with correlation coefficients greater than 0.1 are plotted. 40,000 failures were sampled.

Chapter 3

Positive Lock

3.1 System-Level Design

The overall mission statement for the positive lock as provided by Chevron was to create a positive locking device to prevent oil from entering the annulus through failure of the one-way check valve. The goal can be more clearly defined by a set of functional requirements and design parameters [60]. Any design that satisfies all of the functional requirements will fulfill the mission statement, and the design parameters specify how each functional requirement must be satisfied. In table 3.1 a list of functional requirement and design parameter pairs for the positive lock are given.

Functional Requirement	**Design Parameter**
Prevent oil from entering annulus in the event of non-closure of the one-way check valve	Zero oil passage through valve at operating pressures
Fit inside existing gas lift valve housing	Fits inside a XL-175 Schlumberger gas lift housing [51]
Passively actuated	Requires no surface communication to actuate
Compatible with current well operations	Allows for shut-in and unloading processes to occur as needed
Durable	Lifetime of at least 2 years

Table 3.1: Functional requirements and design parameters

3.1.1 Strategies

A design strategy is a general idea that satisfies all of the functional requirements but exact details of implementation are not yet determined. For the positive lock problem, four strategies were considered as outlined below.

1. Lock check valve in closed position. If oil begins passing through the gas lift valve, the orifice can be closed by locking closed the existing check valve. This strategy has the advantage that it does not add much complexity or additional moving parts to the system, and that oil pressure is acting to close the valve. The disadvantages are that debris can be caught in the check valve preventing closure, the check valve can still be eroded, and it may be difficult to unlock the valve during shut-ins.

2. Lock bellows valve in closed position in the event of oil passage through the gas lift valve. This strategy works even if the check valve is eroded or debris is caught in the check valve. The disadvantage is that the bellows valve seat can still be eroded by injection gas and the valve will be working against the oil pressure to close.

3. Use independent 3rd locking valve in the system that actuates to close off the orifice if oil begins to pass through the gas lift valve. This valve will only be used to lock the gas lift valve closed and thus will not be eroded by oil or injection gas like the check valve and bellows valve. The disadvantage of this strategy is that there is not much space to add a third valve in the gas lift valve.

4. Use new type of check valve and orifice geometry that channels backflowing fluids differently than inflowing fluids, possibly using a bistable switch. This strategy avoids the problems of check valve and bellows valve erosion, but is very complex and may be outside the scope of the project.

For each of these strategies the means with which the positive lock is actuated must be taken into account because this could affect whether the strategy satisfies all functional requirements. Four methods of actuation were considered:

1. Pressure-dependent: Oil pressure is different that injection gas pressure and thus if oil passes into the gas lift valve this pressure change could possibly be detected.

2. Flow-dependent: Gas always flows the same direction through the gas lift valve and thus any reverse flow could be assumed to be due to oil. This reverse flow could be detected and used to actuate the positive lock.

3. Corrosion-dependent: Oil is more corrosive than the injected gas and this property could be used to actuate a lock.

4. Temperature-dependent: Oil is hotter than injection gas and a temperature difference in the gas lift valve could indicate that oil is passing through the valve.

The bellows valve is already actuated based on a pressure difference between the oil and gas and a positive-locking valve acting also on this principle would likely encounter the same problems as the bellows valve. Similarly, the check valve already actuates based on reverse flow and a positive lock based on this strategy would likely encounter the same problems. A corrosion-dependent valve could only be actuated one time based on its dependence on some element corroding. Thus this strategy may be difficult to incorporate with shut-in processes, which could occur multiple times during the life of the well and valve. The temperature-dependent actuation strategy could potentially be actuated multiple times because it would not rely on a component of the valve corroding. Also, the temperature-dependent actuation is different than the actuation of any existing valves in the gas lift valve assembly, which is desirable from a safety perspective. For instance, the check valve my not actuate because the oil backflow is too low and the bellows valve may fail because of a leak in the pressurized bellows, but a temperature-actuated valve would not be susceptible

Category	Pressure	Flow	Corrosion	Temperature
Quality of Lock	0	0	+	+
Impact on Shutin Process	0	0	-	+
Impact on Unloading Process	0	0	-	+
Reliability	0	+	-	+
Scope	0	0	0	0
Sensitive to Small Oil Amounts	0	0	-	+
Detects Oil vs Gas	0	0	+	+

Table 3.2: Strategy Pugh Chart

to these same failure modes and would thus add an additional degree of reliability to the system.

Strategies were compared in a Pugh chart [60] (see table 3.1.1) on the basis of quality of positive lock, impact on current gas lift shutin and unloading procedures, reliability, scope, sensitivity to small oil amounts, and sensitivity to oil vs gas.

In this chart one strategy is chosen as the baseline and all other strategies are compared to it in each category. If the strategy is similar in performance to the baseline in the given category it is given a 0; if it is better than the baseline it is given a +; and if it is worse than the baseline it is given a -. When the columns of the chart are added up with a + considered +1 and a - considered -1, then the strategy with the highest total is the best strategy. The Pugh chart is mainly used as a qualitative tool, because some categories may actually be more important than others even though ratings are not weighted, but it can still be used to determine a superior strategy. In this case, the pressure-actuated valve is the baseline strategy which the other strategies are compared to. Based on this chart, the temperature-actuated valve strategy was selected as the best strategy for the positive lock.

3.1.2 Concepts

A concept is a more specific implementation idea of the strategy chosen. For the thermally-actuated independent third locking valve strategy concepts were developed

for thermal actuation and for the type of valve to use.

Thermal Actuation Concepts

Thermal actuation concepts generated are similar to those outlined in the thermal lock prior art section of chapter 1.

1. Gas expansion: based on the ideal gas law, for a given pressure, the volume of a gas will change as temperature changes, and this could actuate the valve.

2. Fluid or solid expansion: fluids and solids also change volume and shape with different temperatures, which could actuate the valve.

3. Dissolving solid: some solids dissolve when heated beyond a threshold temperature and this could release a valve.

4. Bi-metallic strip: as described in chapter 1, a bimetallic strip is a strip of two different types of metal that are joined together. Because the different types of metal have different thermal expansion properties, one will expand more than the other when heated. Thus the bimetallic strip will bend when heated due to the differential expansion of the metals, with the curvature of the bend directly proportional to the temperature difference relative to equilibrium temperature [64].

5. Shape memory alloy: as mentioned in chapter 1, shape memory alloys are materials that retain a memory of a high-temperature and low-temperature shape. These materials undergo a solid-state phase change at a specific threshold temperature to change between a Martensitic and Austenitic phase. A valve relying on shape-memory alloy actuation would be open below the threshold temperature and closed above the threshold temperature.

The actuation methods of gas expansion, liquid expansion, solid expansion, and the bi-metallic strip movement all rely on shape changes that vary continuously with temperature. These would be well-suited for a flow-regulation valve where an orifice

size needed to be changed over a continuous range of sizes, but not as well-suited to a flow-stopping valve that assumes only the discrete states of open or closed. An intermediate mechanical process would be needed to convert the continuous motion to discrete motion, and while possible, this would increase the complexity of the design.

The dissolving solid and shape memory alloy actuation concepts both rely on discrete state changes, which would be well-suited for the positive lock application. The dissolving solid concept, however, would rely on a permanent shape deformation and would not work for multiple actuations as may be needed in this application. The shape memory alloy concept would allow the valve to be actuated multiple times in a discrete manner, leading to a simple design that meets the functional requirements. Thus the shape memory alloy concept is chosen as the actuation method for the positive lock.

Third Locking Valve

Several different concepts were considered for the third locking valve as detailed below:

1. Gate Valve. This is a spring-loaded gate valve that deploys to seal off the gas lift valve orifice. No door is necessary and a shape-memory alloy spring can hold the gate closed or open (figure 3-1).

2. Double check valve. A second check valve in the venture orifice operates on the same principle as the bottom check valve, which is to seal the orifice when pushed upwards into an orifice section with smaller diameter than the valve diameter (figure 3-2) .

3. Swinging door valve. The door swings up and latches closed to seal off the orifice. A torsion spring can push the door closed (figure 3-3)

4. Pinch valve. This valve relies on a pinching effect on a flexible orifice to constrict the orifice size.

5. Ball valve. This is a sphere with a hole passing through the middle located in the orifice of the gas lift valve. In normal operation the hole lines up with the

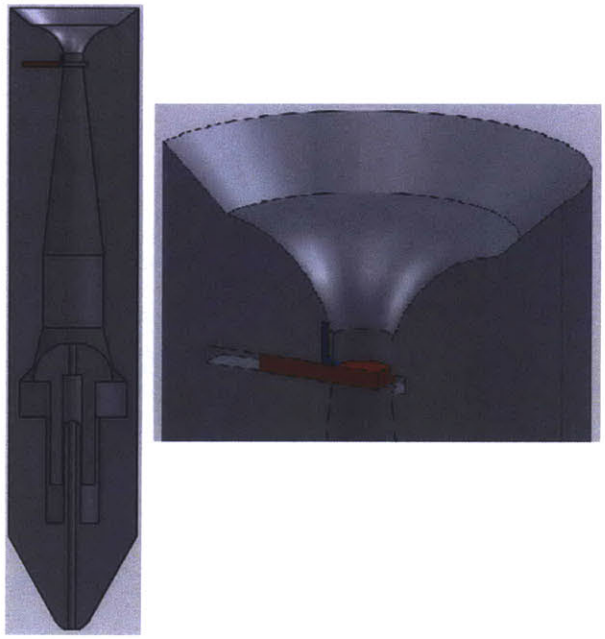

Figure 3-1: Gate valve concept

orifice, and in locked mode the hole is perpendicular to the flow, stopping the flow (figure 3-4).

A gate valve is designed primarily for flow regulation, not flow shut-off [57], but still can provide a strong seal and the force to open or close the valve is not acting against oil or gas pressure. However, the gate valve has the risk of jamming and the slots that the gate slides through could become eroded by injection gas, decreasing the seal strength. The gate valve also takes up a lot of space horizontally to fit inside the gas lift valve. By St Venant's Principle [34], the gate should always be held by a length equal to at least 3-5 times the thickness of the gate to constrain the gate's motion (figure 3-5). This length, in addition to a length long enough to span the orifice, must fit in the side of the gas lift valve. A standard 45-mm diameter gas lift valve has an orifice size of 6mm at the smallest constriction with 19.5 mm of material on each side. The gate valve must be at least 6mm (orifice size) plus 3-5 times the gate thickness plus any actuation elements. If the gate is even a few millimeters thick it will be very difficult to fit in the available gas lift valve width.

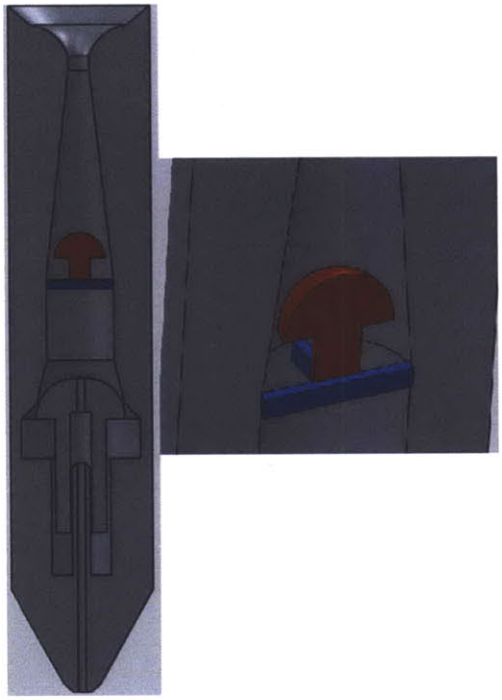

Figure 3-2: Double check valve concept

A second check valve in the gas lift valve orifice would provide a strong seal and is designed for flow shut-off [57]. The closing force would be helped by oil pressure though the valve would be held closed by the thermal actuator. This valve, though, adds considerable flow resistance to the orifice and would be subjected to the same erosion problems as the fist check valve in the system.

A swinging door valve will not add flow resistance in the open position and will mainly take up vertical space in the gas lift valve side (where more material is available), not horizontal space. However, this valve would be acting against pressures in the orifice when actuating, could potentially be eroded by injection gas during normal operation, and debris could prevent the door from closing.

A pinch valve relies on a flexible membrane that can be pinched mechanically or by fluid pressure. One advantage of pinch valve is that, if operated by fluid pressure, the valve can close around solid debris and still provide a strong seal [57]. However, the flexible membrane is not as corrosive-resistant as a metal valve and thus would likely not meet the durability functional requirement.

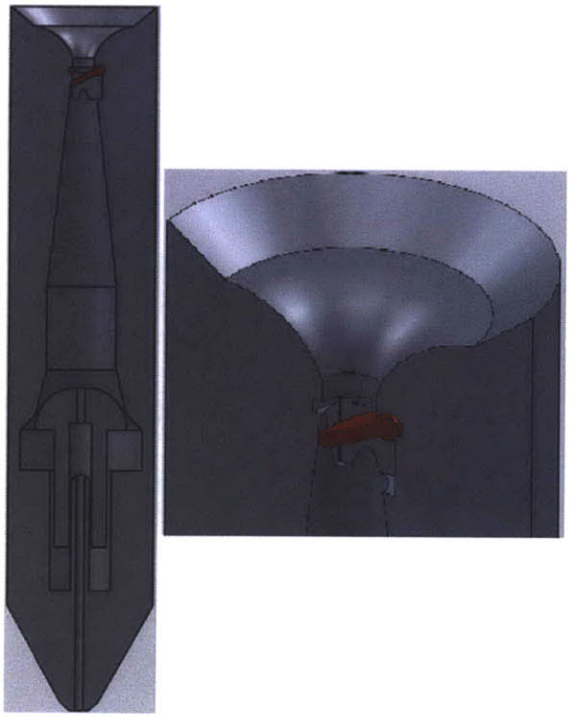

Figure 3-3: Swinging gate valve concept

A ball valve is a simple valve designed for flow shut-off applications. Actuation force would not work against gas or oil pressure. The valve can be sealed either by O-rings between the ball and housing or by a precise metal-to-metal contact between the ball and housing. While O-rings could corrode if exposed to oil or gas for a long enough time, they are very similar to the check valve O-ring seal which already exists in many gas lift valves. The metal-to-metal seal takes much more machining precision to make completely air-tight and is thus more expensive, though it resists corrosion for longer. The metal-to-rubber seal is cheaper because it requires less machining precision, though it has a shorter lifetime due to a lower corrosion resistance (typically around 2 years). The ball valve also would add only minimal flow resistance because the ball valve hole would be the same diameter as the venturi orifice.

The ball valve was ultimately chosen as the valve best suited to meet the positive lock functional requirements, and thus the final concept chosen was a thermally-actuated ball valve positive lock.

Figure 3-4: Ball valve concept

3.2 Thermally-Actuated Ball Valve Concept Details

The thermally-actuated ball valve concept involves a simple modification to an existing gas lift valve - no major redesign is required. In this concept a ball valve with cylindrical side extensions is located in the top section of the venturi orifice of the gas lift valve, just below the bellows valve (see figures 3-6 and 3-7). The side extensions have small stoppers sticking out, which constrain the valve motion to $\frac{\pi}{2}$ radians of rotation between vertical (fully open) and horizontal (fully closed). The ball valve is supported by sliding bearings on the outside of the stoppers. The ball valve sits in a spherical pocket and relies on a metal-to-metal water seal. The ball valve is actuated by shape memory alloy wires which are tied to the ball valve side extension, wrapped one-half revolution around the side extension, and attached to the gas lift valve housing below the side extension. The shape memory alloy is set to have a transition temperature A_s between the gas temperature and oil temperature. If oil begins passing through the gas lift valve, the entire gas lift valve will heat up, in turn heating up

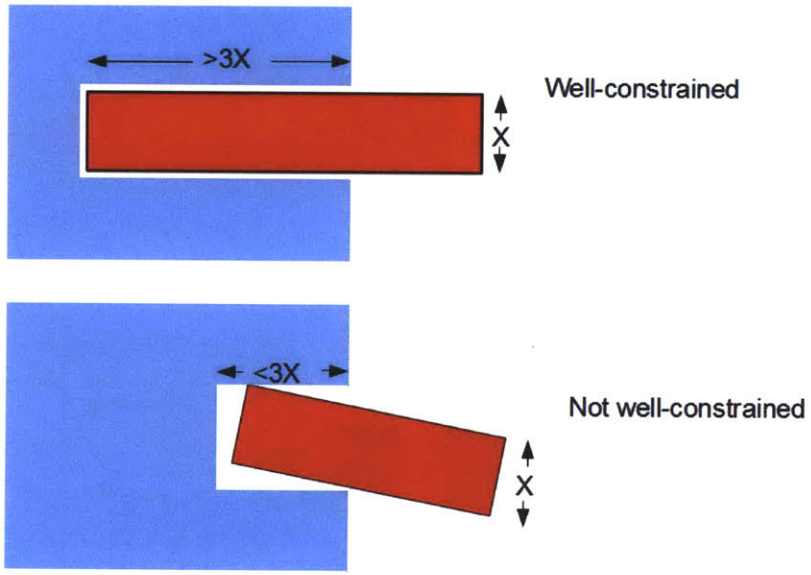

Figure 3-5: Illustration of St Venant's principle. In the top figure, the gate is held by a length greater than three times the gate thickness, and the gate is thus well constrained. In the bottom figure, the gate is held by a length less than three times the gate thickness and the result is gate misalignment.

the shape memory alloy wires. The wires contract in the Austenitic phase and will thus pull the ball valve into the closed position (see figure 3-8). Torsion springs are also wound around the ball valve side extensions. Thus, if the shape memory alloy cools and transitions to the Martensitic state, the wires will expand and the torsion springs will pull the ball valve back into the open position. Theoretically the valve could be actuated with shape memory alloy wire and torsion spring on only one side extension, but in this concept wire and torsion springs are located on both sides of the valve for redundancy.

3.2.1 Analysis of Thermally-Actuated Ball Valve Concept

Torque Balance

A free body diagram (figure 3-9) shows the balance of torques that determine the angular position of the ball valve.

In this figure, T_{spring} is the torque exerted by the torsion spring, F_{sma} is the pulling force of the shape memory alloy wire, r is the radius of the ball valve side extension,

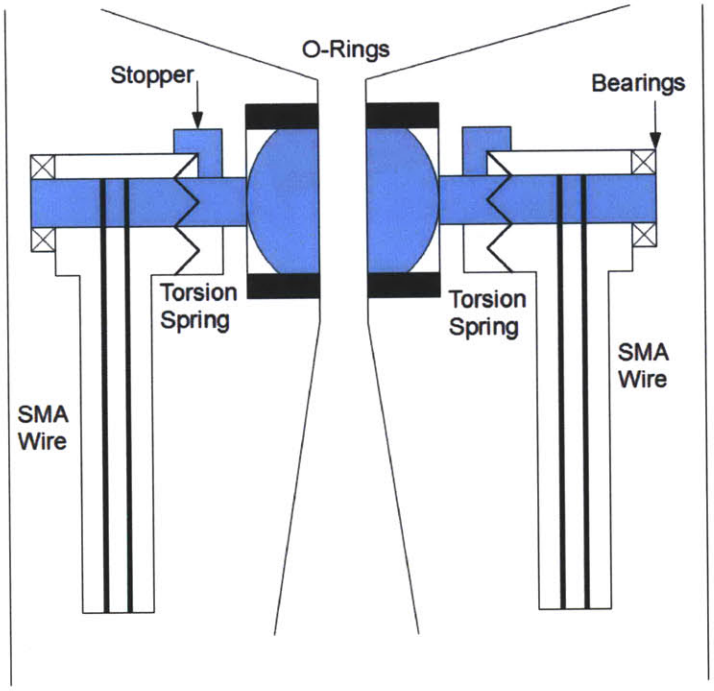

Figure 3-6: Ball valve diagram

and θ is the angular rotation of the ball valve relative to the vertical orientation. T_{spring} varies with rotation, given by

$$T_{spring} = -\kappa\theta \tag{3.1}$$

where κ is the torque constant of the spring. F_{sma} is a constant material property of the shape memory alloy wire. A torque balance of the system gives the equation

$$\frac{d^2\theta}{dt^2} = F_{sma}r - \kappa\theta \tag{3.2}$$

This equation can be used to determine the appropriate size and number of shape

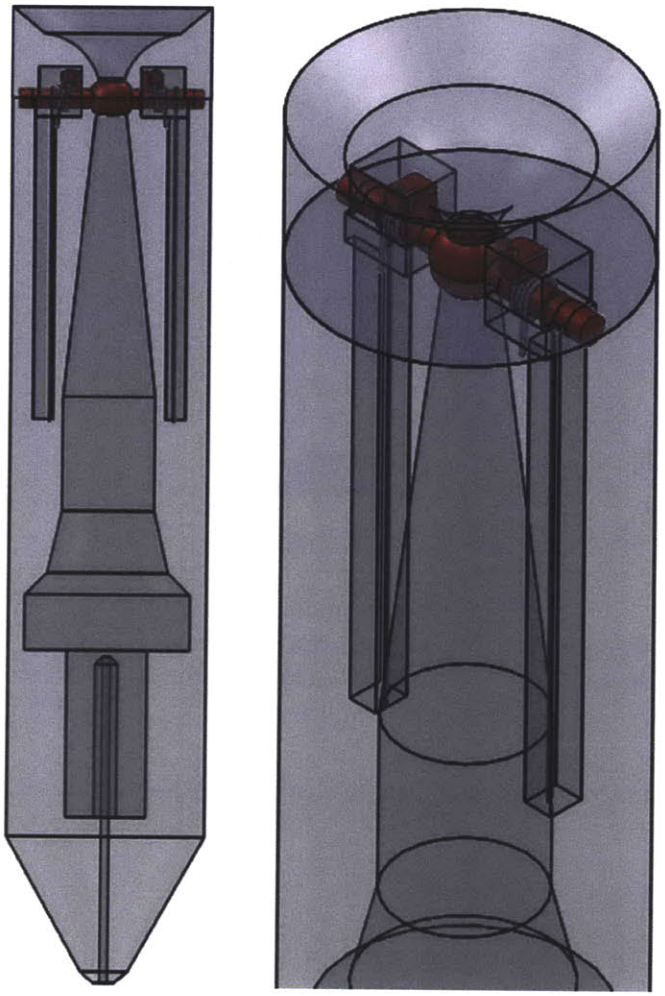

Figure 3-7: Ball valve 3D picture

memory alloy wires necessary to overcome the torque provided by the torsion spring. The maximum torque provided by the torsion spring will be at $\theta = \frac{\pi}{2}$ (the horizontal valve position). If θ is assumed constant with respect to time in this position, then the minimum shape memory alloy force required is

$$F_{sma} = \frac{\pi\kappa}{2r} \tag{3.3}$$

This force can be achieved by using thicker wire (thicker wire has a higher pulling force) and/or multiple wires (force is also directly proportional to the number of wires used.

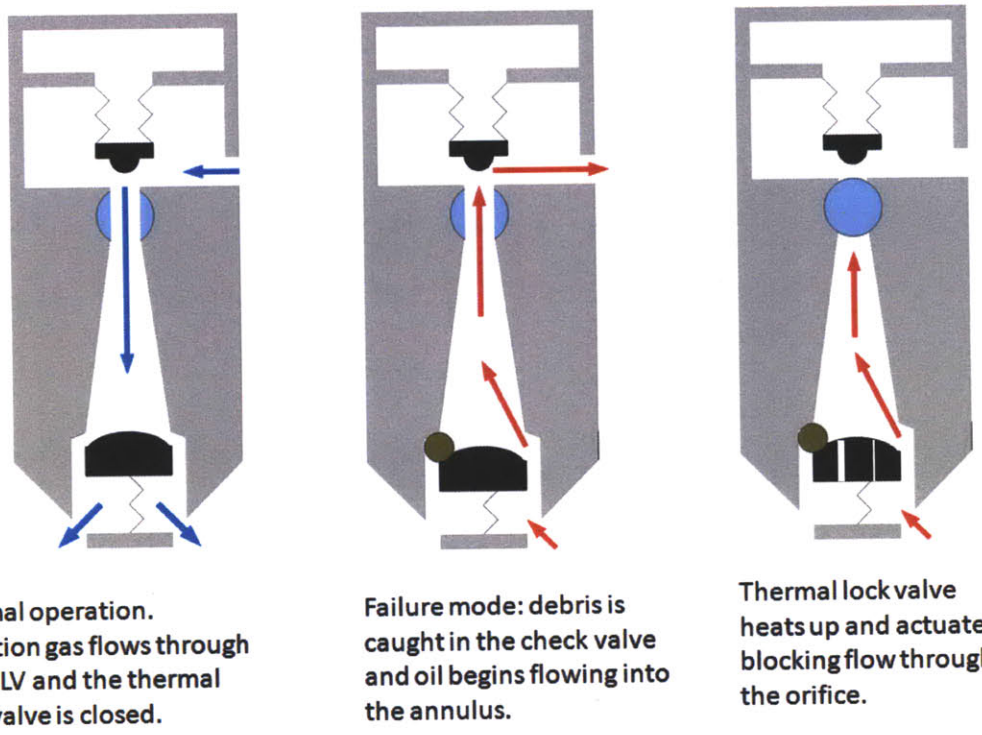

Figure 3-8: Thermal lock actuation after oil backflow through the gas lift valve.

Closing Angle

The ball valve will actually seal off the orifice before it turns a full 90-degrees of rotation, as shown in figure 3-10.

In this figure R is the radius of the ball valve, r is the radius of the orifice, and θ is the angular rotation of the ball valve with respect to vertical. Two right triangles can be drawn in the fully-closed diagram to determine the minimum angular displacement to close off the orifice (see figure 3-11).

From this figure,

$$sin\left(\frac{\theta}{2}\right) = \frac{r}{R} \tag{3.4}$$

which simplifies to

$$\theta = 2asin\left(\frac{r}{R}\right) \tag{3.5}$$

For the dimensions of the 1X scale gas lift valve positive lock this means a turning

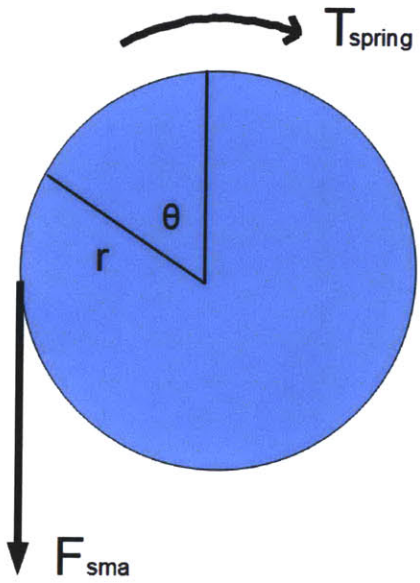

Figure 3-9: Ball valve free body diagram

angle of 74 degrees (1.28 rad) is necessary to close the valve. This required angle could be decreased by increasing the ball valve radius.

Wire Length

In the thermally-actuated ball valve concept the shape memory alloy wire must contract enough to rotate the valve by up to $\frac{\pi}{2}$ radians. Because the wire is partially wrapped around the ball valve side extension, this means a contraction length of $\frac{\pi}{2}r$. This can be represented mathematically as

$$\epsilon L = \frac{\pi r}{2} \tag{3.6}$$

where ϵ is the material strain of the shape memory alloy wire and L is the overall wire length. Thus the necessary wire length is directly proportional to the ball valve side extension radius, given by

$$L = \frac{\pi}{2\epsilon} r \tag{3.7}$$

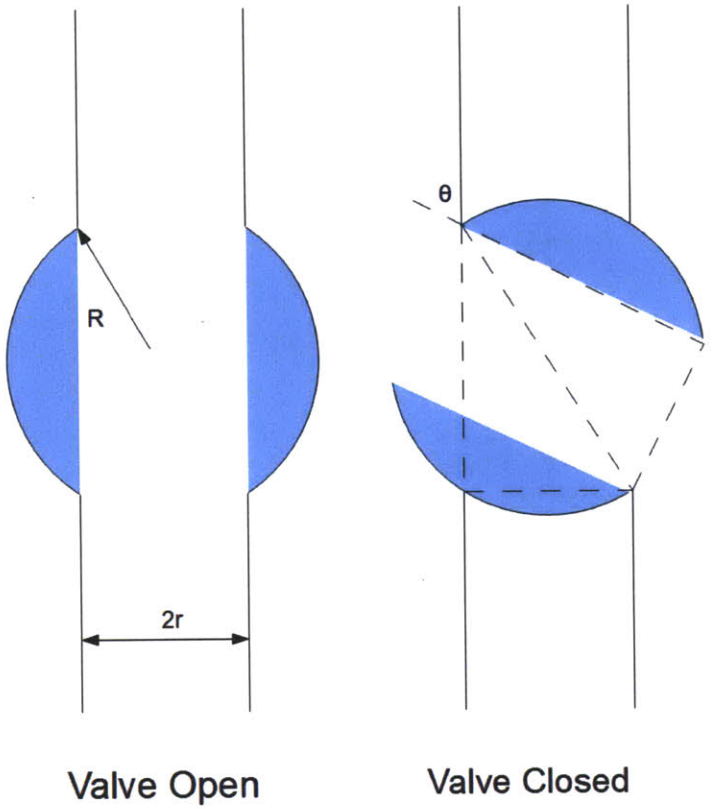

Figure 3-10: Ball valve closing diagram

Torsion Analysis

The shape memory alloy wire and torsion spring exert twisting forces on the ball valve and it is important to make sure these forces do not exceed the yield strength of the material or twist the valve at an angle that will affect performance. The shear stress in the material due to twisting is given by [9]

$$\frac{T}{J} = \frac{\tau}{r} \tag{3.8}$$

where T is the torque from the spring or shape memory alloy, τ is the maximum shear stress in the material, r is the radius of the valve side extension, and J is the torsion

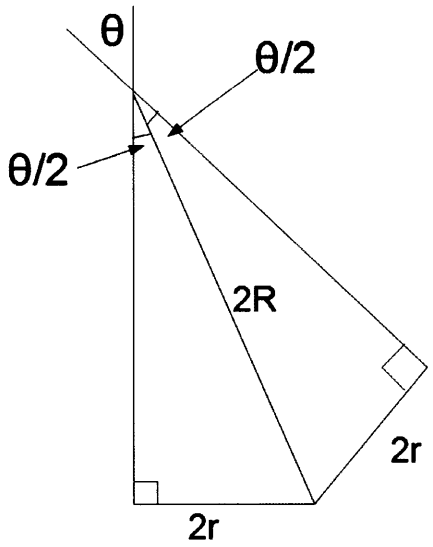

Figure 3-11: Ball valve closing analysis

constant. For a circle the torsion constant is

$$J = \frac{\pi r^4}{2} \tag{3.9}$$

Thus combining equations 3.9 and 3.8 gives the maximum twisting shear stress in the side extension due to the shape memory alloy wire as

$$\tau = \frac{2F}{\pi r^2} \tag{3.10}$$

The twisting angle is given by the equation [9]

$$\frac{T}{J} = \frac{G\phi}{l} \tag{3.11}$$

where G is the shear modulus of the material, ϕ is the angle of twist, and l is the length of the side extension between the application of the force (the attachment point of the shape memory alloy wire) and the opposing force (in this case, the stopper on the opposite side of the ball valve). This equation simplifies to

$$\phi = \frac{2Fl}{\pi r^3 G} \tag{3.12}$$

Equations 3.12, 3.10, 3.7, and 3.3 show that there is a tradeoff to consider when determining the radius of the side extension. A larger radius will result in a higher torque exerted by the shape memory alloy wire and thus fewer wires will be required. A larger radius also reduces the shearing and twisting effects on the side extension, but it also means longer wires are necessary to rotate the valve, which may not fit in the gas lift valve housing.

Dimensions for XL-175 Gas Lift Valve Housing

In the XL-175 gas lift valve housing the venturi orifice has a diameter of 6mm at the planned location for the ball valve. The ball valve will be stainless steel with a diameter of 10mm with 10mm-long side extensions of radius 2.5mm (see figure 3-12). A 6mm-diameter through hole will match the gas lift valve orifice size. A standard torsion spring with spring constant 0.1 $\frac{Nm}{rad}$ will be used. Bearings will be bronze sliding bearings and standard 0.5mm diameter, 5 percent strain, 35N pull-force Nitinol wire will be used for actuation.

Based on these dimensions and using equation 3.7, 78.5mm of wire will be needed to fully actuate the ball valve. Accounting for one wrap around the side extension this length will easily fit in the 100mm of available vertical space in the side of the gas lift valve housing. From equation 3.3 a force of 62.8N will be necessary to overcome the torsion spring torque. Thus 3 wires will be used on each side for a total force of 105N, with a safety factor of 1.7.

From equation 3.10, the maximum shear stress in the ball valve is $10MPa$, which is well below the yield stress of stainless steel (approximately 500 MPa [1]). The maximum angle of twist as given by equation 3.12 is 0.001 radians, based on a 73 GPa shear modulus of stainless steel [9]. This angle is not large enough to affect valve performance. Thus, the dimensions chosen for the ball valve fit inside the valve housing and allow the valve to be actuated and not overly stressed.

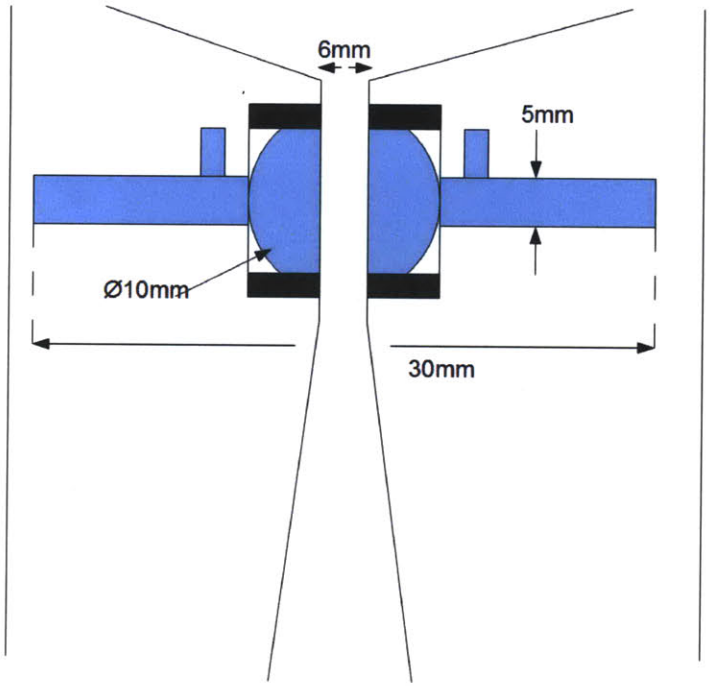

Figure 3-12: Ball valve dimensions

3.2.2 Design for Manufacture and Assembly

An XL-175 gas lift valve is divided vertically into 5 sections that screw together. The thermally-actuated positive lock will fit into the existing venturi orifice section between the check valve and the bellows valve (see figure 3-13).

To insert the ball valve assembly, the venturi orifice section will be cut horizontally through the middle of the narrowest section. Pockets for the ball valve will be CNC milled out of each side. Standard end mills will be used to cut out the rectangular pockets and ball end mills used to mill out the cylindrical side-extension slots and the hemispherical pockets for the ball valve.

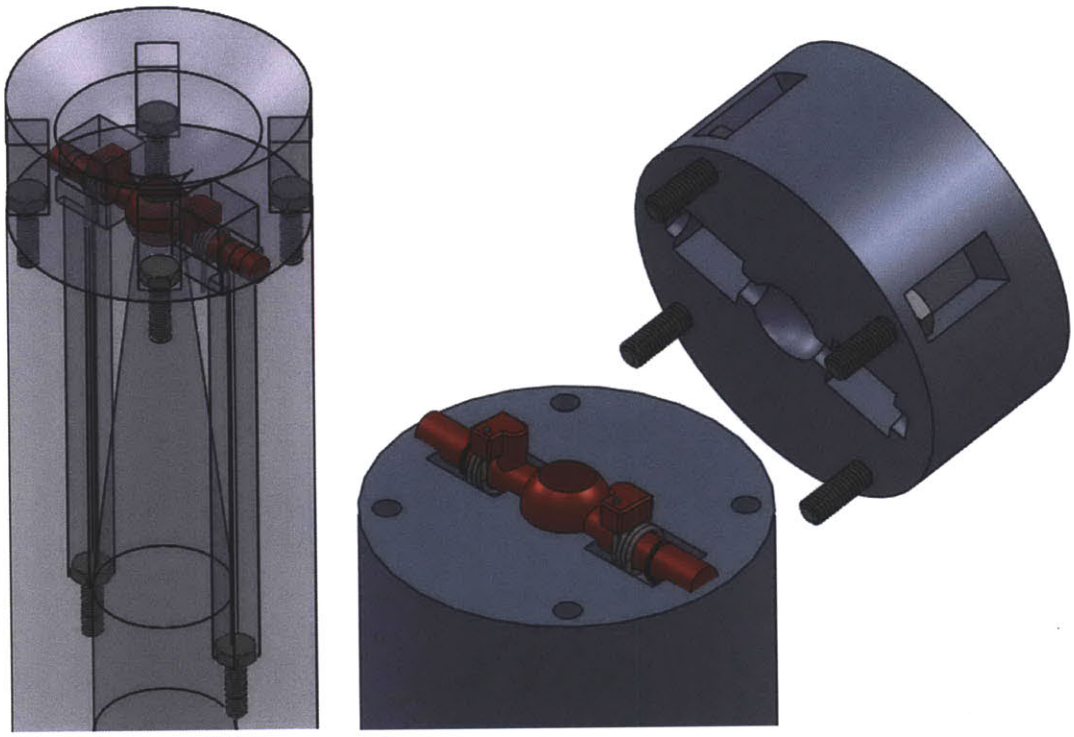

Figure 3-13: Ball valve solid model

To attach the Nitinol wire to the ball valve, a hole is drilled vertically through the ball valve side extension and the Nitinol wire is passed through the hole and tied into a knot on one end (see figure 3-14).

The wire is attached to the gas lift valve housing via a bolt screwed vertically in the housing. The wire is wrapped around the bolt and held in place by friction when the bolt is tightened against the housing. Both the knot and bolt attachment methods are recommended by Dynalloy for attachment of shape memory alloy wires. While the knot attachment method is simple with no additional moving parts and has been used in other shape memory alloy wire applications [12], it can be replaced with another bolt attachment at the ball valve side extension if experimental results find any slippage in the knot attachment.

A 180-degree torsion spring is used to bias the ball valve to the open position. The bottom end of the torsion spring fits into a hole drilled in the housing. The upper end fits into a hole drilled in the stopper and pushes the stopper to the open position (see figure 3-15). The stopper is press-fit into the ball valve side extension and has

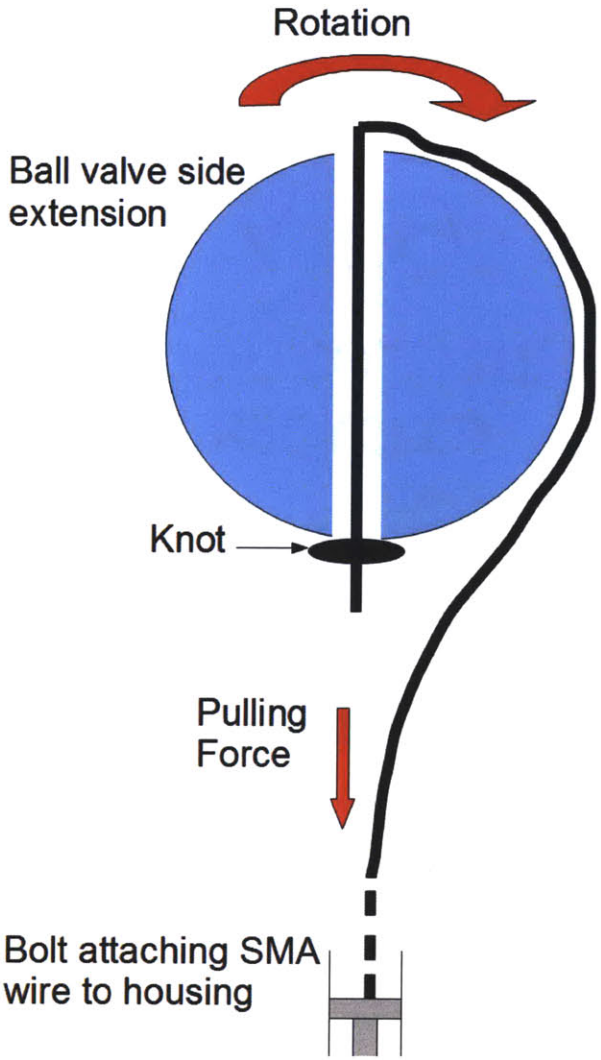

Figure 3-14: SMA attachment diagram

rectangular bottom profile so that it cannot twist out of place.

The two pieces housing the ball valve will be joined back together using bolts placed vertically in pockets on the outside of the gas lift valve. To test whether this connection will be strong enough for the application, stress analysis must be done on the bolts. The maximum force the bolts must withstand would occur in tension in the situation where the ball valve is closed and a pressure differential exists across the ball valve between oil pressure and injection gas pressure. Valves are generally designed for a pressure spread across the valve of $7x10^5$ Pa (100 psi) [61]. In this case the force pushing against the ball valve in the design case of the XL-175 gas lift valve

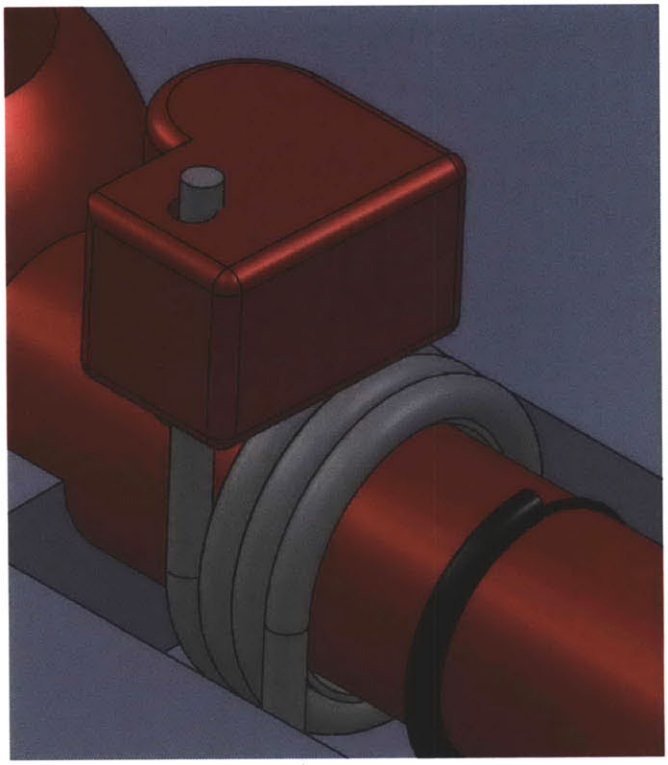

Figure 3-15: Torsion spring attachment

would then be the product of the pressure differential and the orifice area, which is about 20N.

In the current design, four 3-mm diameter stainless steel bolts are used to attach the housing sections. The stress on each bolt is given by

$$\sigma = \frac{F}{4A_{bolt}} \tag{3.13}$$

where σ is the stress, F is the force acting on each bolt, and A_{bolt} is the cross sectional area of each bolt. This gives a stress of 7x10^5 Pa in each bolt. The yield stress of stainless steel is approximately 10^8 Pa [2], giving a safety factor of approximately 150. Thus the bolted connection should withstand the design pressures.

In this design each bolt should be preloaded with a force equal to four times the maximum tensile force [56]. The preloading torque required is then given by the formula

$$F_p = \frac{4\pi\Gamma}{\frac{2l}{\epsilon} + 3\pi D_b \mu} \tag{3.14}$$

where F_p is the bolt preloading force, Γ is the preloading torque, l is the bolt lead, ϵ is the thread efficiency (usually between 0.2 and 0.9 depending on surface finish), D_b is the bolt diameter, and μ is the coefficient of friction (usually 0.3) [56]. For the design bolts (3mm diameter, 0.7mm per thread) this results in a preload torque requirement of 0.07 Nm, which is easily attainable.

Chapter 4

Shut-in and Unloading Procedures

4.1 Unloading

Only the gas lift valve at operating depth contains the thermally-actuated ball valve. The operating valve is the second lowest in the tubing, with an additional standard unloading valve located below the operating valve. During the unloading process the additional lower unloading valve is used to cool the thermal lock valve, as detailed in figures 4-1 and 4-2.

Initially the thermal-lock valve is at the hot steady-state oil temperature and the thermal lock is closed. Initially, because it is closed, the thermal-lock valve acts like a dummy valve and the unloading occurs exactly as normal until only the bottom valve is passing gas. At this point, gas is flowing past the thermal-lock valve and cools the valve by convection. When the thermal-lock valve cools sufficiently below the Martensitic transition temperature M_s, it begins to open and pass gas. Gas now flows through a larger total area (the bottom two valves), and the gas pressure thus drops. This causes the bottom gas lift valve to close. The thermal-lock valve bellows is pressurized to a lower pressure than the bottom gas lift valve and thus stays open passing gas. Now only the thermal-lock valve is passing gas as desired.

The thermal-lock operating valve is located approximately 15m above the bottom unloading valve so that it is far enough above to be retrieved by wireline techniques with current wireline accuracies, but not far enough to significantly affect well pro-

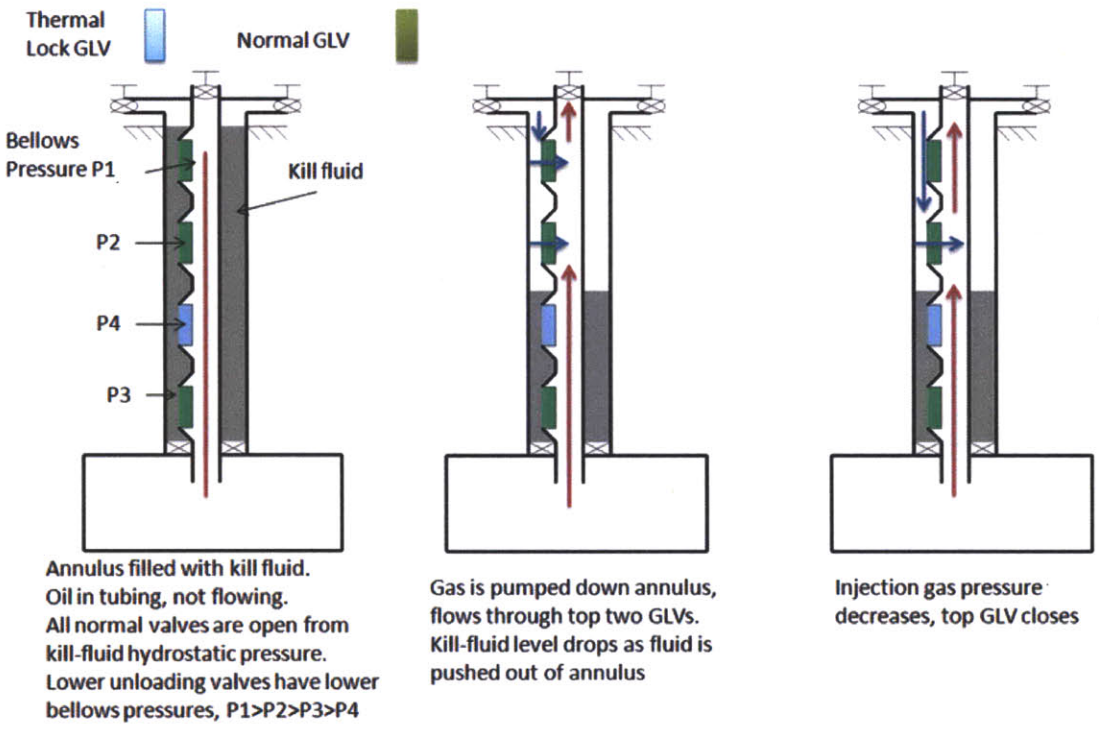

Figure 4-1: Unloading process with thermal lock

duction rates. In normal operation gas flows through the thermal-lock operating valve while all other gas lift valves remain closed.

4.2 Shut-in

During a shut-in, when injection of gas into the annulus is stopped, the thermal lock valve will heat up or cool down to a steady state temperature dependent on the oil temperature and ground temperature. If the valve heats up to a temperature greater than the transition temperature of the thermal lock, the ball valve will close. When the shut-in is complete, gas is injected first through the bottom unloading valve. The air circulates past the thermal lock valve, cooling it down. When the thermal lock cools below its transition temperature it opens and gas begins passing through the operating valve. Because gas is now passing through a larger combined opening, the

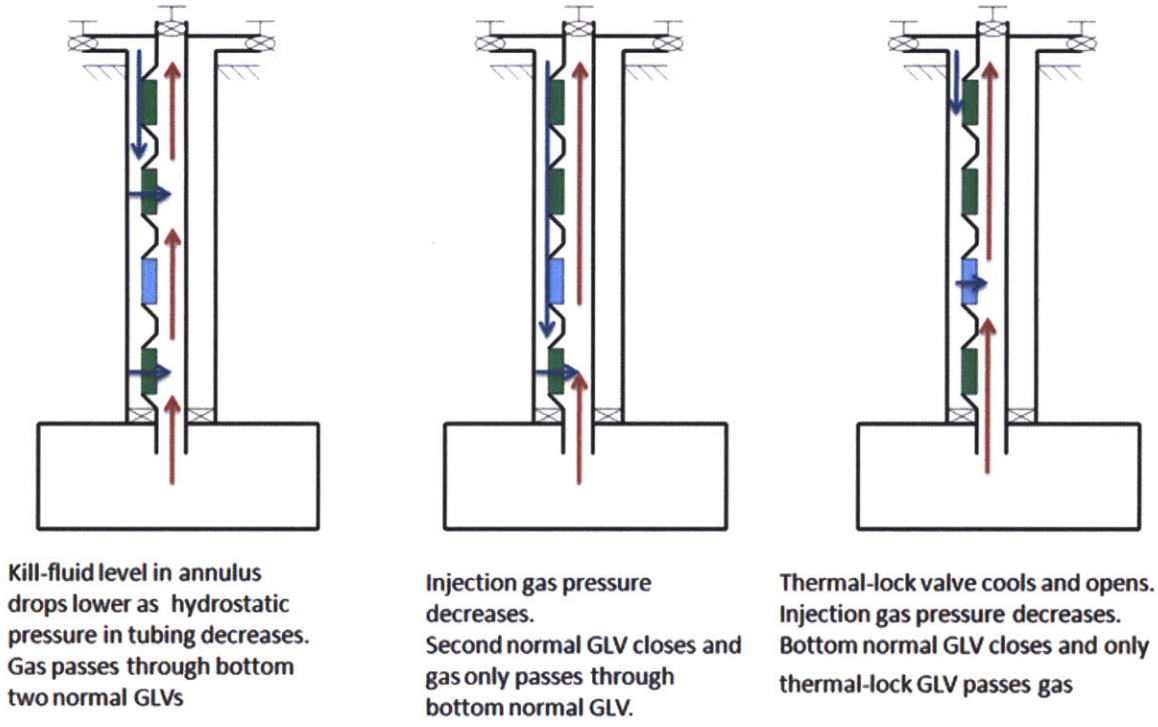

Figure 4-2: Unloading process with thermal lock

gas pressure drops and the lower gas lift valve closes. Thus the thermal-lock operating valve is the only valve passing gas.

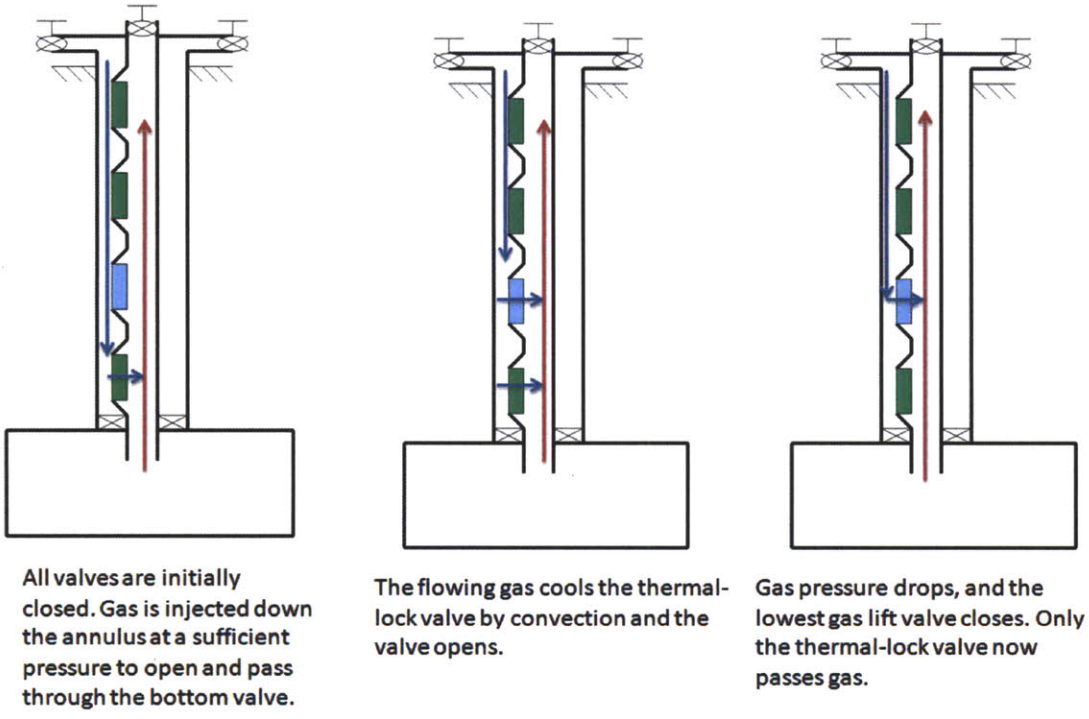

Figure 4-3: Shut-in process with thermal lock

Chapter 5

Thermal Lock Feasibility

5.1 Shape Memory Alloy Analysis

5.1.1 Background

Shape memory alloys are alloys that undergo a solid state phase change between a Martensitic low-temperature state and an Austenitic high-temperature state when heated or cooled. These alloys are said to have memory because they return to the same low-temperature shape whenever cooled to the Martensitic state and to the same high-temperature shape when heated to the Austenitic shape. The most popular shape memory alloy, Nitinol, made from Nickel and Titanium, was first discovered in 1958 by William Buehler at the Naval Ordinance Laboratory [15]. Numerous other shape memory alloys now exist such as InTl, CuAIZn, CuAlNi, CuSn, and AuCd, [15], with applications in robotic actuators, surgical tools, moldable glasses, fire sprinklers, and anti-scald water valves [30]. Of the most common shape memory alloys on the market, Nitinol is the most corrosion resistant, with similar corrosion behavior as stainless steel [11]. This is important for any component of a gas lift valve which could potentially be subjected to corrosive gases and liquids. Nitinol also has the highest working stress, highest strain, highest number of thermal cycles before degradation, lowest hysteresis [26], and is the most widely used and most easily commercially available SMA and is thus the alloy considered for this positive

lock design.

5.1.2 Properties

Shape memory alloys do not have a single transition temperature between Martensite and Austenite, but instead undergo a hysteresis, with different transition temperatures depending on whether the alloy is being cooled or heated. This hysteresis is shown schematically in figure 5-1, which plots strain (E) vs temperature (T). In this figure, when the alloy is being heated A_s represents the start of the transition from Martensite to Austenite and A_f represents the final transition to Austenite. When being cooled, M_s represents the start of the transition from Austenite to Martensite and M_f represents the final transition to Martensite.

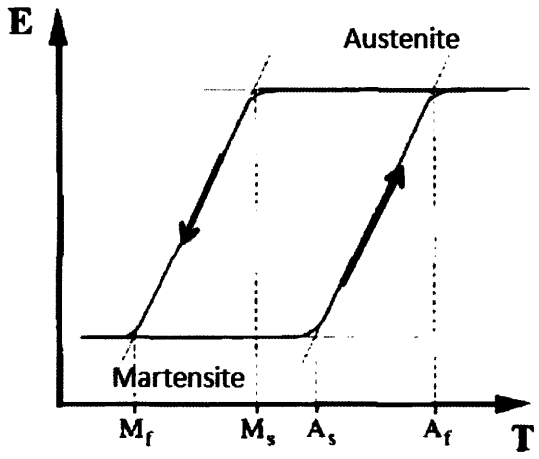

Figure 5-1: Shape memory alloy hysteresis [15]

The transition temperatures of a shape memory alloy depend on the proportion of each metal in the alloy. For instance, a Nitinol alloy of 55 percent Nickel and 45 percent Titanium will have different transition temperatures than a Nitinol alloy of 50 percent Nickel and 50 percent Titanium. Based on the alloy proportion, Nitinol can have transition temperatures within the range of $-150°C$ to $+100°C$ [53]. The hysteresis spread - the temperature difference between M_f and A_f - is between $2°C$ and $50°C$ for Nitinol depending on the alloy proportions [26], with the temperature spread between A_s and A_f less than half of the full hysteresis spread [11]. The

temperature spread between A_s and A_f is the important spread to consider when assessing whether an SMA will heat up sufficiently to transition when exposed to hot oil vs cool gas. For example, if the A_s - A_f spread is $10°C$ and the temperature difference between injection gas and oil is $15°C$, then the SMA will transition when heated from the gas temperature to the oil temperature.

Nitinol recovery does slightly degrade over time after repeated cycling, depending on preload, temperature, shape memory deformation and alloy composition. In general Nitinol is rated to over 100,000 thermal cycles [26]. In the gas lift application the Nitinol will only be actuated during unloading, shut-ins, and failure. Because unloading and shut-ins are not daily occurrences, with a functional requirement of a 2 year lifetime (as stated in chapter 3), the valve will likely see less than 1000 thermal cycles in its lifetime. Thus cycling degradation is not a major concern.

5.2 Steady State Thermal Model

In order for a thermally-actuated positive locking device to be feasible using Nitinol as the actuation element there must be sufficient temperature difference between the cold gas and hot oil to actuate the Nitinol. As discussed previously, Nitinol has a minimum hysteresis temperature spread of $2°C$ and thus there must be at least a $2°C$ temperature difference between gas and oil at injection depth.

In this section a model is derived for the steady state oil and gas temperature profiles in the well to determine the temperature difference between gas and oil at injection depth. This is a steady-state temperature model in space for the entire well. The next section will detail the transient thermal model, which is a thermal model in time for the gas lift valve temperature assuming the gas flow is instantaneously shut off and oil begins flowing through the valve (see figure 5-2.

5.2.1 Steady State Assumptions

Gas

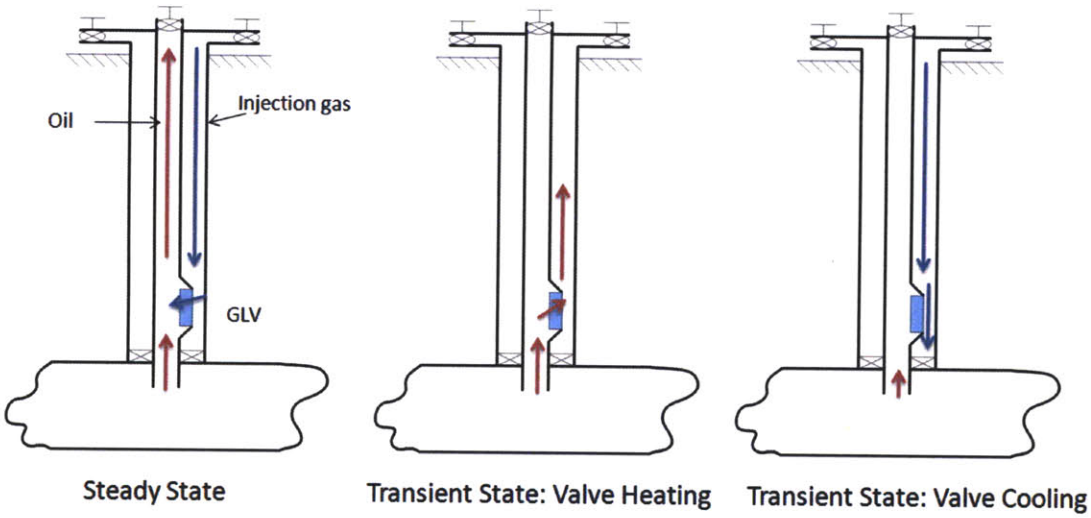

Figure 5-2: Heat transfer model for annulus control volume

- Steady state conditions
- Turbulent flow ($100 < Nu < 1000$ where Nu is the Nusselt number)
- Heating from ground and tubing by convection and conduction
- Surface gas temperature 300K
- Gas density is approximately constant down the annulus

Mixture

- Steady state conditions
- Turbulent flow ($100 < Nu < 1000$)
- Heat loss to annulus through convection and conduction
- Heat capacity and conductivity are weighted averages of gas and oil properties

$$c_{mix} = \frac{\dot{m}_{gas}}{\dot{m}_{mix}} c_{gas} + \frac{\dot{m}_{oil}}{\dot{m}_{mix}} c_{oil} \tag{5.1}$$

$$k_{mix} = \frac{\dot{m}_{gas}}{\dot{m}_{mix}} k_{gas} + \frac{\dot{m}_{oil}}{\dot{m}_{mix}} k_{oil} \tag{5.2}$$

where c_{mix} is the specific heat of the gas-oil mixture, $\dot{m}_{gas}$ is the gas mass flow rate, $\dot{m}_{mix}$ is the mixture mass flow rate, c_{gas} is the gas specific heat, $\dot{m}_{oil}$ is the oil mass flow rate, c_{oil} is the oil specific heat, k_{mix} is the mixture thermal conductivity, k_{gas} is the gas thermal conductivity, and k_{oil} is the oil thermal conductivity.

- Mixture temperature at injection point is a weighted average of gas and oil temperatures

$$T_{mix} = \frac{C_{gas}\dot{m}_{gas}}{C_{mix}\dot{m}_{mix}} T_{gas} + \frac{C_{oil}\dot{m}_{oil}}{C_{mix}\dot{m}_{mix}} T_{oil} \tag{5.3}$$

where T_{mix} is the mixture temperature, T_{gas} is the gas temperature, and T_{oil} is the oil temperature.

Ground

- Linear temperature profile, slope 25K per Kilometer [17]
- Surface ground temperature = surface gas temperature

Piping

- Cement insulation around annulus, 10cm thick
- Steel tubing and annulus pipes 1cm thick

5.2.2 Modeling Approach

In figure 5-3 a control volume is drawn around a section of the well annulus between the depths of x and $x+dx$. For simplicity the control volume of the half of the annular segment is represented in 2 dimensions as a rectangle. A 3-dimensional drawing of the control volume is shown in figure 5-4, where R_{case} is the casing inner radius, R_{tube} is the tubing inner radius, and dx is the height of the differential element. Heat is transferred into the control volume by convection and conduction through the casing wall, convection and conduction through the tubing wall, and mass flow into the top

of the control volume. Heat is transferred out of the control volume through mass flow out the bottom of the volume.

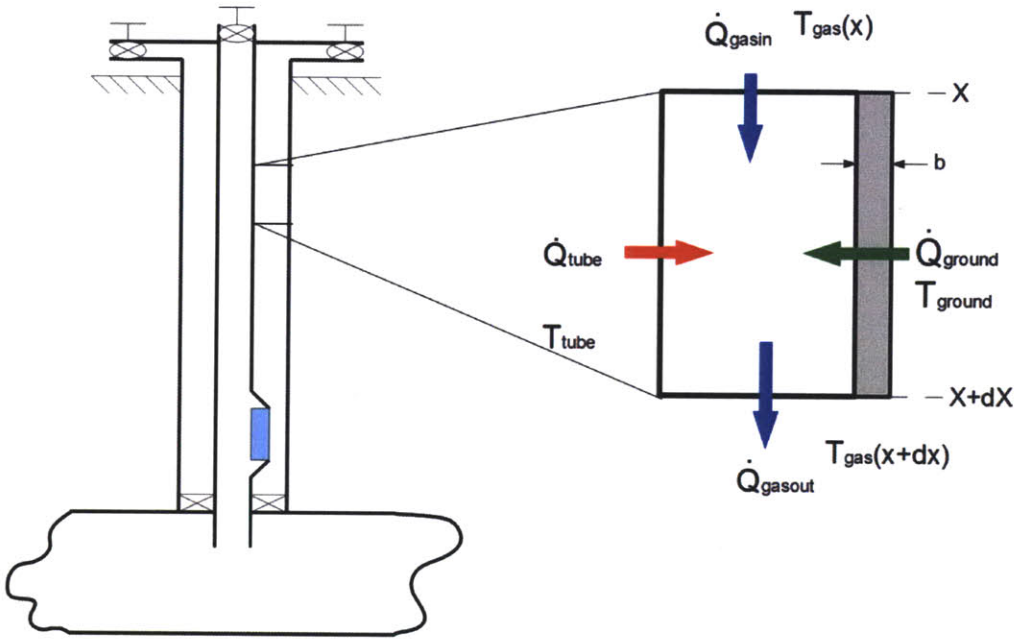

Figure 5-3: Heat transfer model for annulus control volume

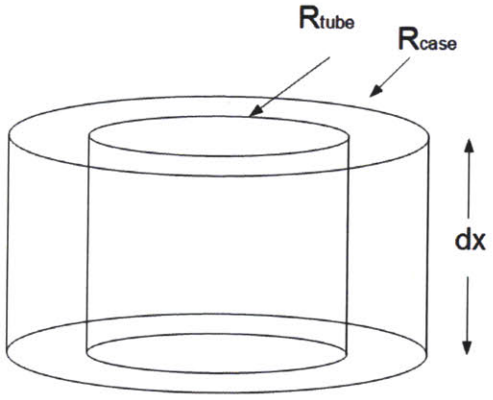

Figure 5-4: Annulus control volume 3 dimensional view

Heat transfer from the casing to the gas is given by

$$\dot{Q}_{ground} = \frac{(T_{ground}(x) - T_{gas}(x))}{R_{totg}} \tag{5.4}$$

where $\dot{Q}_{ground}$ is the heat transfer from the casing to the control volume, $T_{ground}(x)$

is the ground temperature at depth x, and $T_{gas}(x)$ is the gas temperature at depth x. R_{totg} is the total thermal resistance across the casing interface, which is the sum of the conduction and convection resistances,

$$R_{totg} = \frac{b}{k_{cem} 2\pi R_{case} dx} + \frac{1}{h_{ground} 2\pi R_{case} dx} \tag{5.5}$$

where b is the casing wall thickness, k_{cem} is the cement thermal conductivity, and h_{ground} is the convective heat transfer coefficient of the casing wall.

In these equations the ground temperature in Kelvin is assumed to be of the form

$$T_{ground}(x) = 273 + \frac{1}{40}x \tag{5.6}$$

where x is measured in meters below the surface. The convective heat transfer coefficient is given by

$$h_{ground} = \frac{Nuk_{gas}}{2R_{case}} \tag{5.7}$$

Heat transfer from the tubing to the gas is given by

$$\dot{Q}_{tube} = \frac{(T_{tube}(x) - T_{gas}(x))}{R_{tott}} \tag{5.8}$$

where $\dot{Q}_{tube}$ is the heat transfer from the tubing to the annulus, and $T_{tube}(x)$ is the tubing temperature at depth x. R_{tott} is the total thermal resistance across the tubing interface, which is the sum of the conduction and convection resistances,

$$R_{tott} = \frac{a}{k_{tube} 2\pi R_{tube} dx} + \frac{1}{h_{tube} 2\pi R_{tube} dx} \tag{5.9}$$

where a is the tubing wall thickness, k_{tube} is the tubing wall thermal conductivity, and h_{tube} is the convective heat transfer coefficient of the tubing wall given by

$$h_{tube} = \frac{Nuk_{mix}}{2R_{tube}} \tag{5.10}$$

Heat transfer through the control volume due to mass flow is given by

$$\dot{Q}_{outgas} - \dot{Q}_{ingas} = \dot{m}_{gas} c_{gas} \left(T_{gas}(x + dx) - T_{gas}(x) \right) \tag{5.11}$$

where $\dot{Q}_{outgas}$ is the heat transfer out the bottom of the control volume due to mass flow, $\dot{Q}_{ingas}$ is the heat transfer into the control volume due to mass transfer, $\dot{m}_{gas}$ is the gas mass flow rate, and c_{gas} is the gas specific heat.

The gas mass flow rate is calculated by

$$\dot{m}_{gas} = \frac{\rho_{gas}}{\rho_{oil}} R_s \dot{m}_{oil} \tag{5.12}$$

where ρ_{gas} is the gas density, ρ_{oil} is the oil density, and R_s is the gas-oil volumetric ratio at injection depth. The gas density can be calculated using the ideal gas law, assuming constant gas density from the surface,

$$\rho_{gas} = \frac{P_{gas} M_{gas}}{R T_{gassurf}} \tag{5.13}$$

where P_{gas} is the surface gas pressure, M_{gas} is the gas molar mass, R is the ideal gas constant, and $T_{gassurf}$ is the surface gas temperature.

An energy balance for the control volume yields the equation

$$\dot{Q}_{outgas} - \dot{Q}_{ingas} = \dot{Q}_{tube} + \dot{Q}_{ground} \tag{5.14}$$

Combining equations 5.11 and 5.14 and dividing both sides by dx yields

$$\dot{m}_{gas} c_{gas} \frac{\left(T_{gas}(x + dx) - T_{gas}(x) \right)}{dx} = \frac{\left(T_{tube}(x) - T_{gas}(x) \right)}{R_{tott} dx} + \frac{\left(T_{ground}(x) - T_{gas}(x) \right)}{R_{totg} dx} \tag{5.15}$$

In the limit as dx approaches zero, the left side of the equation becomes a derivative. Thus the new differential equation is

$$\dot{m}_{gas} c_{gas} \frac{dT_{gas}(x)}{dx} = \frac{\left(T_{tube}(x) - T_{gas}(x) \right)}{\frac{a}{k_{tube} 2\pi R_{in}} + \frac{1}{h_{tube} 2\pi R_{in}}} + \frac{\left(T_{ground}(x) - T_{gas}(x) \right)}{\frac{b}{k_{cem} 2\pi R_{out}} + \frac{1}{h_{ground} 2\pi R_{out}}} \tag{5.16}$$

A similar differential equation can be derived for a control volume in the tubing as shown in figure 5-5. For the tubing control volume, heat is exchanged between the tubing and annulus by conduction, and heat is exchanged into and out of the tubing by mass flow.

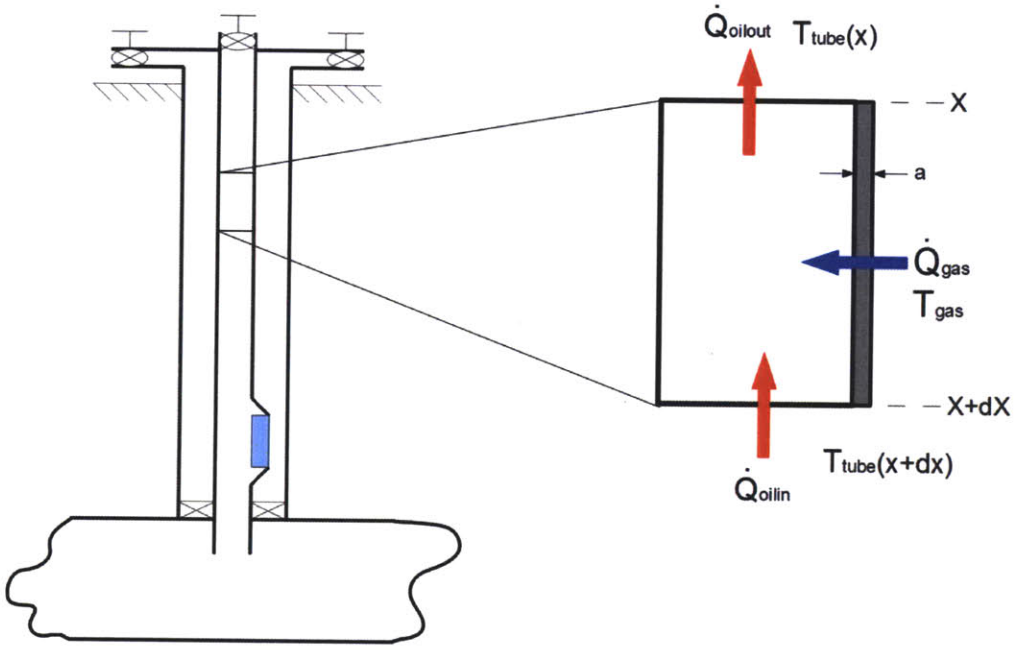

Figure 5-5: Heat transfer model for annulus control volume

Heat transfer between the annulus and tubing is equal to $\dot{Q}_{tube}$ calculated previously. Heat transfer through the control volume due to mass flow is given by

$$\dot{Q}_{outoil} - \dot{Q}_{inoil} = \dot{m}_{mix} c_{mix} \left(T_{tube}(x) - T_{tube}(x + dx) \right) \tag{5.17}$$

where $\dot{Q}_{outoil}$ is the heat transfer out the top of the control volume due to mass flow, $\dot{Q}_{inoil}$ is the heat transfer into the control volume due to mass transfer, $\dot{m}_{mix}$ is the oil mass flow rate, and c_{mix} is the oil specific heat. An energy balance for the control volume yields the equation

$$\dot{Q}_{outoil} - \dot{Q}_{inoil} = \dot{Q}_{gas} = \dot{Q}_{tube} \tag{5.18}$$

Combining equations 5.17 and 5.18 and dividing both sides by dx yields

$$\dot{m}_{mix}c_{mix}\frac{(T_{tube}(x)-T_{tube}(x+dx))}{dx}=\frac{(T_{tube}(x)-T_{gas}(x))}{R_{tott}dx} \tag{5.19}$$

In the limit as dx approaches zero, the left side of the equation becomes a derivative. Thus the new differential equation is

$$\dot{m}_{mix}c_{mix}\frac{dT_{tube}(x)}{dx}=\frac{(T_{tube}(x)-T_{gas}(x))}{\frac{a}{k_{tube}2\pi R_{tube}}+\frac{1}{h_{tube}2\pi R_{tube}}} \tag{5.20}$$

The Runge Kutta numerical integration technique is used to solve the pair of differential equations 5.20 and 5.16 to generate temperature profiles in the annulus and tubing. For each solution a bottom well mixture temperature is guessed and solution profiles generated. When the surface temperature of the annulus profile equals surface air temperature, the algorithm stops and the solutions are final.

5.2.3 Comparison with Experimental Data

To check the validity of the model, temperature profiles were compared to data from an actual well. A well temperature survey was provided by Chevron where data is for the temperature inside the tubing. Of the 17 parameters required for the model, 8 were provided by Chevron and 8 were standard values looked up in other sources (such as oil specific heat, oil thermal conductivity, etc.) (see table 5.1). The only unknown parameter was the Nusselt number of the well. The flow was assumed to be turbulent with a Nusselt number between 100 and 1000, and different Nusselt numbers were tried until the model matched the data.

Figure 5-6 shows the steady state well temperature profiles for a Nusselt number of 1000 and figure 5-7 shows profiles for Nusselt number of 100. For a Nusselt number of 1000 the mixture temperature profile agrees reasonably well with the data, with errors less than 5K along the entire curve.

The temperature difference at injection depth between the gas and oil is approximately 5K for a Nusselt number of 1000 (figure 5-6), but closer to 30K for a Nusselt

Parameter	Value	Units	Source
w	2500	m	Well Data
$\dot{m}_{mix}$	24	$\frac{kg}{s}$	Well Data
$\dot{m}_{gas}$	16.5	$\frac{kg}{s}$	Well Data
c_{gas}	2500	$\frac{J}{kgK}$	[10]
a	0.01	m	[7]
k_{tube}	50	$\frac{W}{mK}$	[2]
R_{tube}	0.0508	m	Well Data
b	0.362	m	[7]
k_{cem}	1.73	$\frac{W}{mK}$	[2]
R_{case}	0.1016	m	Well Data
c_{oil}	1841	$\frac{J}{kgK}$	[10]
k_{oil}	0.15	$\frac{W}{mK}$	[10]
k_{gas}	0.04	$\frac{W}{mK}$	[10]
T_{res}	356	K	Well Data
$T_{gassurf}$	300	K	Well Data
R_s	45	Unitless	Well Data

Table 5.1: Parameter values

number of 100 (figure 5-7). A temperature spread of 5K between gas and oil would be adequate for the correct alloy of Nitinol, while a temperature difference of 30K would be more than enough difference to cause a shape memory alloy to transition between Martensitic and Austenitic phases and actuate the positive lock proposed in chapter 3. Different wells will likely have different Nusselt numbers and temperature spreads and this would determine the appropriate Nitinol alloy to use.

5.3 Gas Lift Valve Transient Thermal Model: Valve Heating

The gas lift valve is considered to be in a transient thermal state during the beginning and end of shut-in periods, and during a failure situation where oil passes the wrong way through the valve into the annulus. A transient thermal model of the gas lift valve will determine how much time the valve will take to heat up or cool down to actuate the positive lock. This is a thermal model in time for just the gas lift valve and does not model transient temperature changes in the oil or gas above the gas

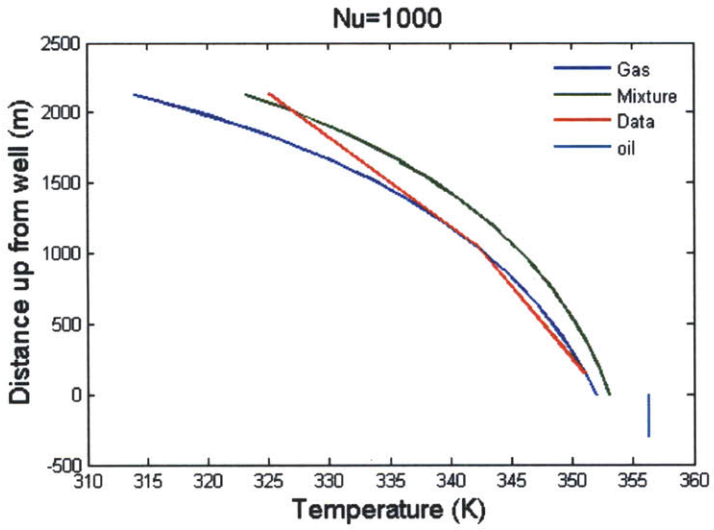

Figure 5-6: Steady state tubing and annulus temperature profiles

lift valve. This section details the modeling for the case where the gas lift valve is heating up (when oil passes through the valve during a failure situation). The following section details the modeling for the case where the gas lift valve is cooling down (after a shut-in when the well production is just beginning).

5.3.1 Assumptions

- The gas lift valve is a cylindrical lumped mass that heats and cools uniformly.
- The gas lift valve lumped mass has the thermal and mechanical properties of stainless steel.
- Gas surrounding the gas lift valve is heated equally by tubing and annulus heat exchanges.
- Heat exchanges from tubing and annulus to the surrounding gas are by conduction.
- Heat exchange from the surrounding gas to the gas lift valve is by convection.
- Tubing and annulus temperatures are constant at injection depth.
- Tubing temperature is equal to reservoir temperature at injection depth.

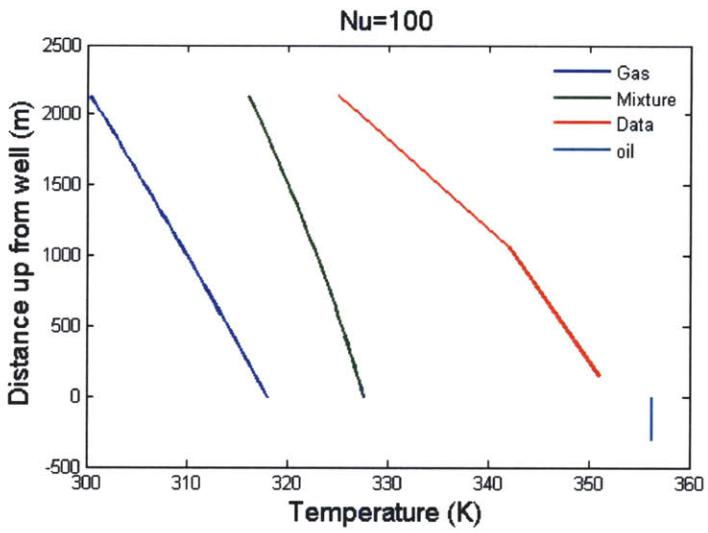

Figure 5-7: Steady state tubing and annulus temperature profiles

- Annulus temperature is equal to the average of tubing temperature and ground temperature at injection depth.
- Ground temperature varies linearly with depth with a slope of 25K per km [17]
- During failure, the temperature of the oil flowing through the valve is constant.

5.3.2 Energy Balance Equations

The gas surrounding the gas lift valve is heated by tubing and annulus heat exchanges, and cooled by heat exchange to the gas lift valve. This energy balance can be written mathematically as

$$\dot{Q}_{tube} + \dot{Q}_{an} - \dot{Q}_{GLV} = m_g c_g \frac{dT_g}{dt} \tag{5.21}$$

where $\dot{Q}_{tube}$ is the heat transfer from the tubing to the gas, $\dot{Q}_{an}$ is the heat transfer from the annulus to the gas, $\dot{Q}_{GLV}$ is the heat transfer from the gas to the gas lift valve, m_g is the mass of the gas surrounding the GLV at a given time, c_g is the gas specific heat, T_g the gas temperature, and t time.

The gas lift valve is heated by heat exchanges with the surrounding gas and, in the event of a failure scenario, from oil in the orifice. This can be written mathematically

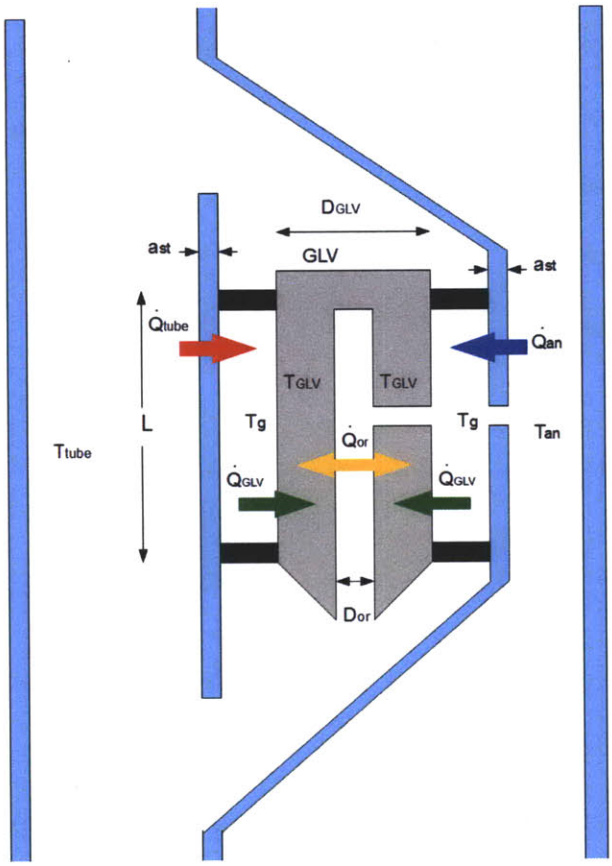

Figure 5-8: Gas lift valve transient heat transfer model

as

$$\dot{Q}_{GLV} + \dot{Q}_{or} = m_{GLV} c_{GLV} \frac{dT_{GLV}}{dt} \tag{5.22}$$

where $\dot{Q}_{or}$ is the orifice temperature (it may be oil or gas), m_{GLV} is the gas lift valve mass, c_{GLV} is the gas lift valve specific heat, and T_{GLV} is the gas lift valve temperature.

The conductive heat exchange $\dot{Q}_{tube}$ is driven by the temperature difference between the tubing and gas and is given by

$$\dot{Q}_{tube} = (T_{tube} - T_g) K_{st} \frac{\left(\frac{1}{2}\pi L D_{GLV}\right)}{a_{st}} \tag{5.23}$$

where K_{st} is the conductive heat transfer coefficient of steel, L is the height of the gas lift valve, D_{GLV} the diameter of the gas lift valve, and a_{st} the wall thickness of

the tubing pipe.

The conductive heat exchange $\dot{Q}_{an}$ is driven by the temperature difference between the annulus and gas and is given by

$$\dot{Q}_{an} = (T_{an} - T_g) K_{st} \frac{\left(\frac{1}{2}\pi L D_{GLV}\right)}{a_{st}} \tag{5.24}$$

The convective heat exchange to the gas lift valve $\dot{Q}_{GLV}$ is driven by the temperature difference between the gas and the gas lift valve and is given by

$$\dot{Q}_{GLV} = (T_g - T_{GLV}) \pi D_{GLV} L h_g \tag{5.25}$$

where h_g is the convective heat transfer coefficient of the gas.

The convective heat exchange from the orifice to the gas lift valve $\dot{Q}_{or}$ is driven by the temperature difference between the orifice and the gas lift valve and is given by

$$\dot{Q}_{or} = (T_{tube} - T_{GLV}) (\pi D_{GLV} L h_{oil} + C_{massflow}) \tag{5.26}$$

where h_{oil} is the convective heat transfer coefficient of the oil and $C_{massflow}$ is a constant proportional to the mass flow rate of the oil or gas flowing through the valve.

5.3.3 Governing Differential Equation

The energy balance and heat exchange equations can be combined to give one governing differential equation for the gas lift valve temperature,

$$A_1 \frac{d^2 T_{GLV}}{dt^2} + A_2 \frac{dT_{GLV}}{dt} + A_3 T_{GLV} = B_1 \frac{dT_{tube}}{dt} + B_2 T_{tube} + B_3 T_{an} \tag{5.27}$$

where

$$A_1 = \frac{m_g c_g m_{GLV} c_{GLV}}{\pi D_{GLV} L h_{gas}} \tag{5.28}$$

$$A_2 = m_g c_g + \left(\frac{m_{GLV} c_{GLV}}{\pi D_{GLV} L h_{gas}}\right)\left(\frac{K_{st}\pi L D_{GLV}}{a_{st}} + \pi D_{GLV} L h_{gas}\right) + \frac{m_g c_g D_{or} h_{oil}}{D_{GLV} h_{gas}} \quad (5.29)$$

$$A_3 = \frac{K_{st}\pi L D_{GLV}}{a_{st}} + \left(\frac{K_{st}\pi L D_{GLV}}{a_{st}} + \pi D_{GLV} L h_{gas}\right)\left(\frac{D_{or} h_{oil} + C_{massflow}}{D_{GLV} h_{gas}}\right) \quad (5.30)$$

$$B_1 = \frac{m_g c_g D_{or} h_{oil}}{D_{GLV} h_{gas}} \quad (5.31)$$

$$B_2 = \left(\frac{K_{st}\pi L D_{GLV}}{a_{st}} + \pi D_{GLV} L h_{gas}\right)\left(\frac{D_{or} h_{oil} + C_{massflow}}{D_{GLV} h_{gas}}\right) + \frac{K_{st}\pi D_{GLV} L}{2 a_{st}} \quad (5.32)$$

$$B_3 = \frac{K_{st}\pi D_{GLV} L}{2 a_{st}} \quad (5.33)$$

If tubing temperature is assumed to be constant and equal to reservoir temperature at injection depth and annulus temperature is assumed to be constant and equal to the average of ground temperature and tubing temperature at injection depth then the governing differential equation simplifies to

$$A_1 \frac{d^2 T_{GLV}}{dt^2} + A_2 \frac{dT_{GLV}}{dt} + A_3 T_{GLV} = B_2 T_{res} + B_3 \frac{1}{2}\left(T_{res} + T_{ground}\right) \quad (5.34)$$

where T_{res} is the reservoir temperature and T_{ground} is the ground temperature at injection depth.

5.3.4 Solution

The differential equation in 5.34 is linear and thus has an analytical solution of the form

$$T_{GLV} = C_1 e^{r_1 t} + C_2 e^{r_2 t} + C_3 \tag{5.35}$$

where

$$r_1 = \frac{-A_2 + \sqrt{A_2^2 - 4A_1A_3}}{2A_1} \tag{5.36}$$

$$r_2 = \frac{-A_2 - \sqrt{A_2^2 - 4A_1A_3}}{2A_1} \tag{5.37}$$

and

$$C_3 = \frac{B_2 T_{res} + B_3 \frac{1}{2}(T_{res} + T_{ground})}{A_3} \tag{5.38}$$

The valve is assumed to initially be the same temperature as the annulus gas (because annulus gas is passing through and around the valve, and this temperature is initially constant). These assumptions translate into the initial conditions

$$T_{GLV}(t = 0) = T_{an}(t = 0) \tag{5.39}$$

$$\frac{dT_{GLV}}{dt}(t = 0) = 0 \tag{5.40}$$

These initial conditions give the following values for the coefficients of the differential equation

$$C_1 = -\frac{r_2}{r_1} \frac{\frac{1}{2}(T_{res} + T_{ground}) - \frac{B_2 T_{res} + B_3 \frac{1}{2}(T_{res} + T_{ground})}{A_3}}{1 - \frac{r_2}{r_1}} \tag{5.41}$$

$$C_2 = \frac{\frac{1}{2}(T_{res} + T_{ground}) - \frac{B_2 T_{res} + B_3 \frac{1}{2}(T_{res} + T_{ground})}{A_3}}{1 - \frac{r_2}{r_1}} \tag{5.42}$$

5.4 Transient Thermal Model: Valve Cooling

The gas lift valve will be cooled at the end of a shut-in period when well production is being restarted. In this situation injection gas flowing past the outside of the gas lift valve will cool the valve through convection. The gas lift valve is assumed to have an initial temperature equal to the oil temperature. The energy balance equations for the cooling situation will be the same as for the heating situation except that there will be no heat transfer from the orifice to the gas lift valve ($Q_{or} = 0$) and the heat transfer between the annulus and the gas surrounding the gas lift valve will have an additional convection term, namely

$$\dot{Q}_{an} = (T_{an} - T_g) K_{st} \frac{\left(\frac{1}{2}\pi L D_{GLV}\right)}{a_{st}} + (T_{an} - T_g) \frac{1}{2}\pi L D_{GLV} h_c \tag{5.43}$$

where the area that convection is occurring is approximated as half of the lateral surface area of the gas lift valve and h_c is the convective coefficient of cooling in the annulus, given by the Dittus-Boetler correlation [71]

$$h_c = \frac{k_{gas}}{D_{char}} \left(0.023 Re^{0.8} Pr^{0.3}\right) \tag{5.44}$$

where k_{gas} is the gas thermal conductivity, D_{char} is a characteristic length assumed to be the difference in length between the casing inner diameter and the tubing outer diameter, Re is the Reynold's number of the flow, and Pr is the Prandtl number of the flow. The Reynold's number is defined in chapter 2 and the Prandtl number is defined as

$$Pr = \frac{c_p \mu}{k_{gas}} \tag{5.45}$$

where c_p is the gas specific heat and μ is the gas dynamic viscosity.

5.5 Transient Temperature Plots

Nominal values as described in chapter 1 are assumed for the 35 parameters used in this model with $C_{massflow}$ set to zero to simulate worst case slowest rise time. The reservoir temperature is set to 360K and the annulus initial temperature 350K. The transient temperature profile for heating is plotted in figure 5-9.

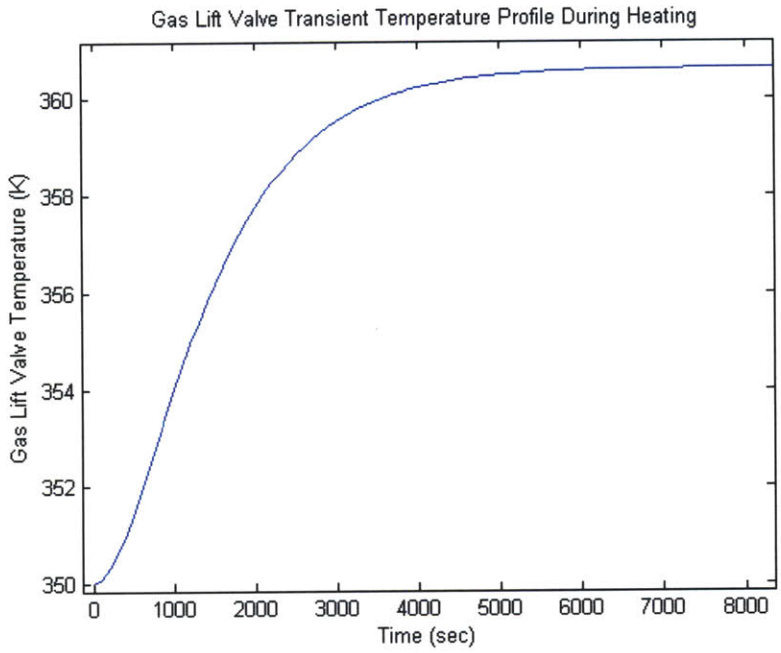

Figure 5-9: Gas lift valve transient heat transfer model heating time profile

In this scenario the 90 percent rise time is approximately 3000 seconds, or slightly under an hour. The initial temperature is equal to annulus temperature because injection gas is flowing through and around the valve. The final temperature is approximately reservoir temperature because hot oil is flowing through the valve.

For the cooling scenario, nominal values as described in chapter 1 are assumed for the 35 parameters, with a Reynolds number of 10000 (turbulent flow), reservoir temperature of 360K, and injection gas temperature of 350K. Figure 5-10 shows the gas lift valve temperature profile over time.

The 90 percent rise time to reach steady state is approximately 3000 seconds in this scenario as well. The temperature of the valve starts at approximately reservoir temperature and cools to a temperature between annulus and reservoir temperature.

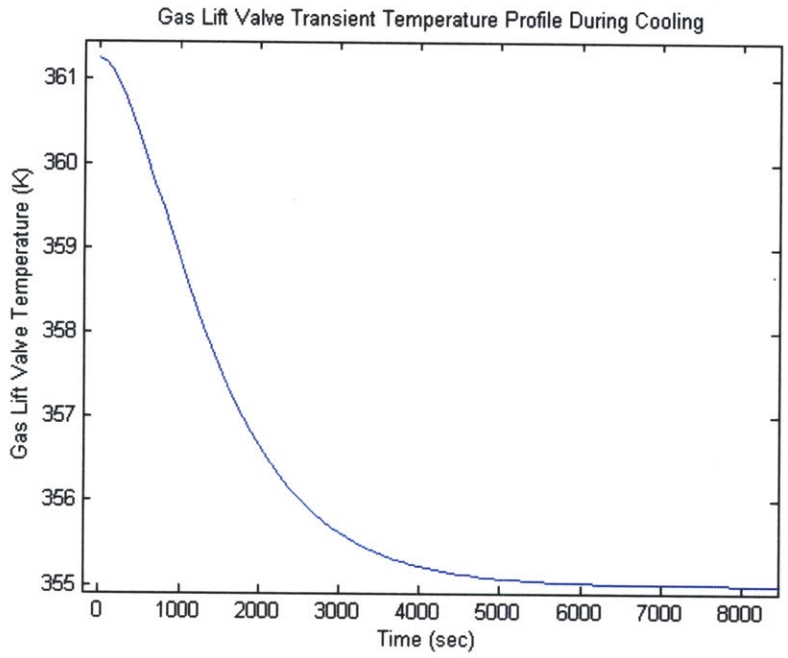

Figure 5-10: Gas lift valve transient heat transfer cooling time profile

5.6 Sensitivity Analysis

One way to determine which parameters rise time is the most sensitive to is to make a plot of rise time change vs input parameter change with respect to nominal values for a range of input parameter changes. To compare parameters with different magnitudes of nominal values, the percentage change in output can be compared to the percentage change in input. In figure 5-11 - 5-13 the change in rise time from a nominal starting value are plotted against changes in individual input parameters.

These figures show that the parameters that valve temperature rise time is most sensitive to are pipe thickness a_{st}, pipe conductivity K_{st}, gas convection coefficient h_{gas}, gas specific heat c_{gas}, gas mass surrounding valve m_{gas}, gas lift valve diameter D_{GLV}, and gas lift valve length L.

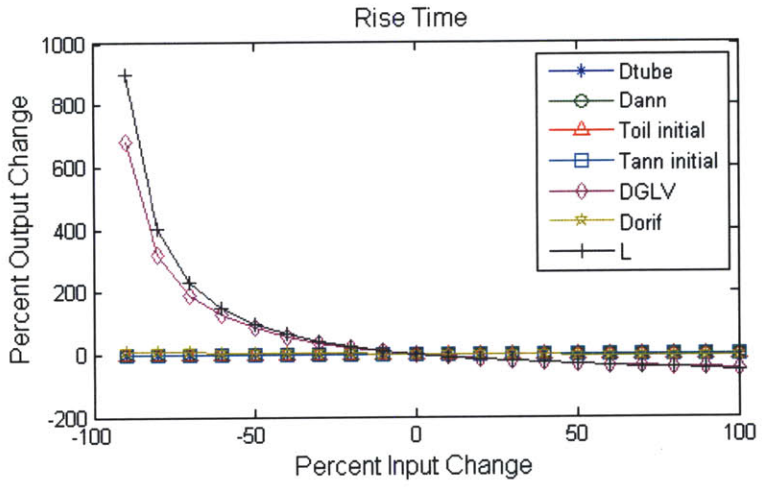

Figure 5-11: Gas lift valve transient heat transfer model sensitivity analysis

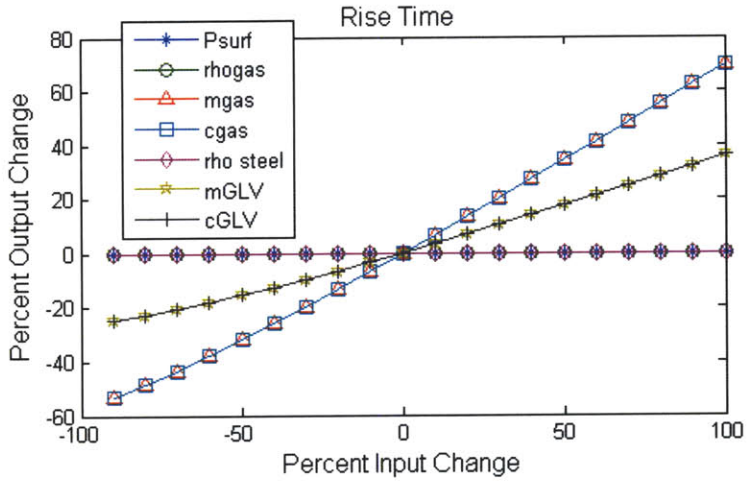

Figure 5-12: Gas lift valve transient heat transfer model sensitivity analysis

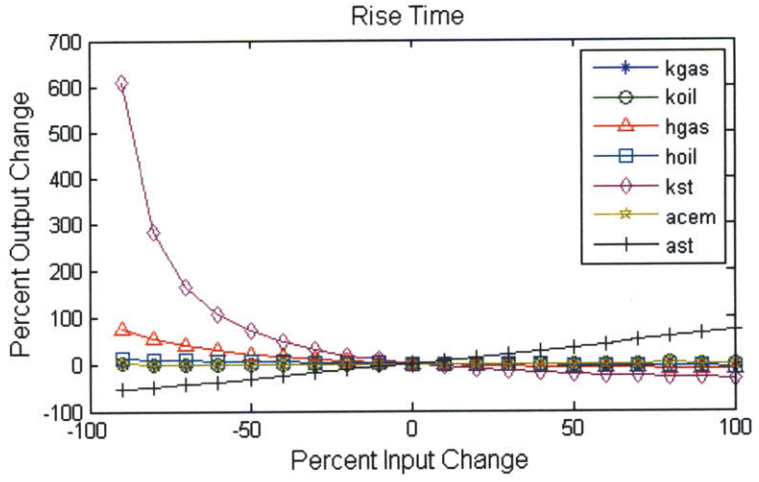

Figure 5-13: Gas lift valve transient heat transfer model sensitivity analysis

Chapter 6

Prototype and Experimental Results

To test the feasibility and performance of the positive lock concept, a scaled prototype positive lock is created and tested under simulated oilwell temperatures. The purpose of the prototype is to demonstrate that the ball valve will actuate when exposed to hot liquid above the shape memory alloy Austenitic transition temperature and when cooled below the Martensitic transition temperature. The Austenitic transition temperature was provided by Dynalloy as 70C for the wire and the Martensitic transition temperature as 45C.

6.1 Prototype

For ease of machining the prototype is constructed out of plastic at a 3X scale from the dimensions of an XL-175 gas lift valve. The top part of the prototype is constructed out of clear acrylic to allow valve actuation to be seen, while the bottom section is constructed out of Delrin because of its ease in machining. The prototype housing consists of a cylinder representing the section of the gas lift valve between the check valve and the bellows valve (see figure 6-1)

A straight cylindrical hole is located vertically through the housing for liquid to pass through. A second side hole is located next to the central hole extending from

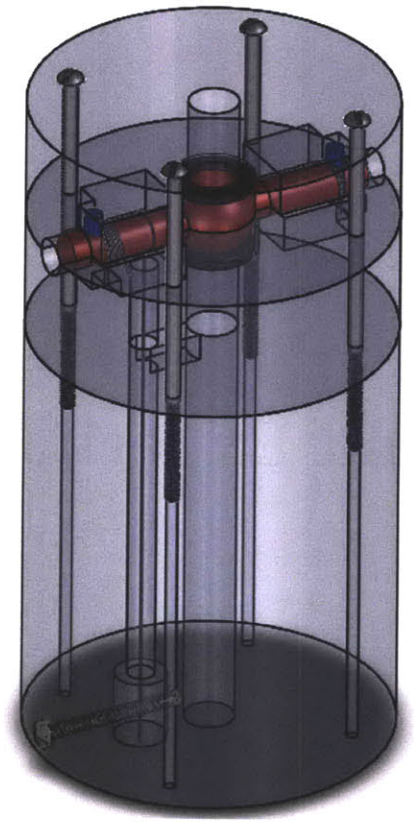

Figure 6-1: Prototype valve solid model

the bottom of the housing to the ball valve side extension. This second hole allows hot water to flow over and heat up the shape memory alloy wire (see figure 6-2). A connecting hole allows hot liquid to flow from the shape memory alloy hole back into the main gas lift valve orifice. In the actual valve the shape memory alloy wire will heat up over time through conduction of the metal housing, but for the plastic prototype this heating is simulated by allowing the wire to contact the hot liquid to heat up.

The housing is cut horizontally into three sections. The ball valve is located between the top two sections with the connecting hole located between the middle and bottom sections. The valve is actuated only on one side by Nitinol wires (while the actual valve assembly will have actuation on both sides of the ball valve for redundancy, only one side is necessary for a prototype to demonstrate the concept). The Nitinol wire used is Flexinol brand, A_s transition temperature 70C, produced by Dynalloy [12].

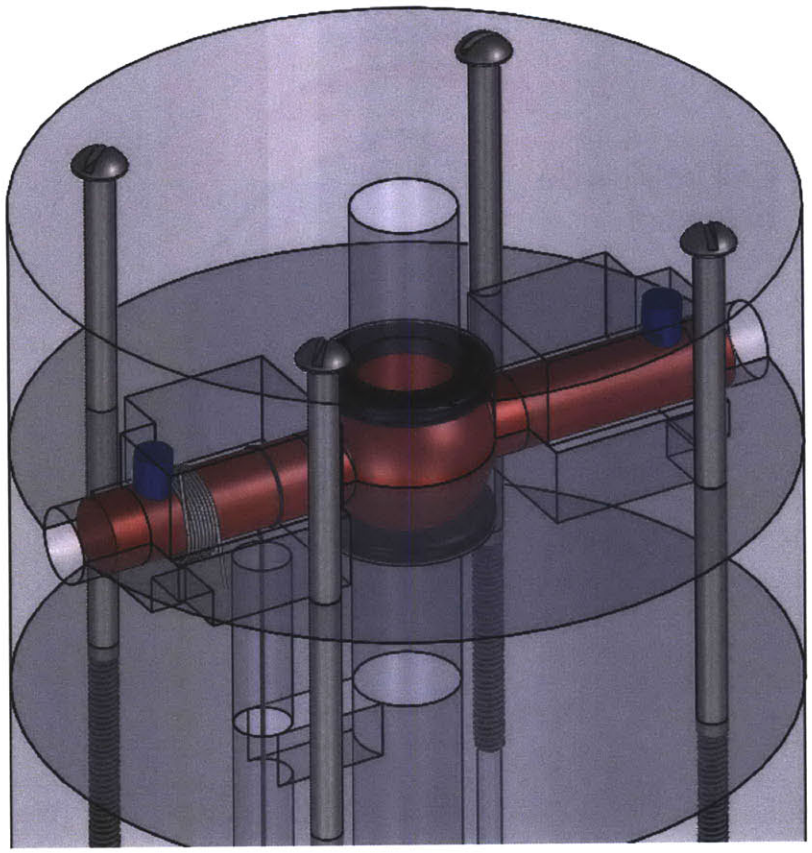

Figure 6-2: Prototype valve solid model

The Nitinol is attached to the ball valve side extension as described in chapter 3. The wire is then wrapped one half revolution around the ball valve side extension and passes through the side hole to the bottom of the housing. The bottom end of the wire is fixed to the prototype housing via a bolt passing horizontally into the housing (see figure 6-3).

The bolt presses the wire against the housing side, securing it in place. Both attachment methods are recommended by Dynalloy for attaching shape memory alloy wires.

Tight seals are created at the entrance and exit of the ball valve by using rubber O-rings. The ball valve sits in a cylindrical cavity with O-rings on the top and bottom that deform to press tightly against the ball valve (see figure 6-2).

Valve housing parts are machined using a CNC mill to cut out pockets. The ball valve is machined on a CNC lathe.

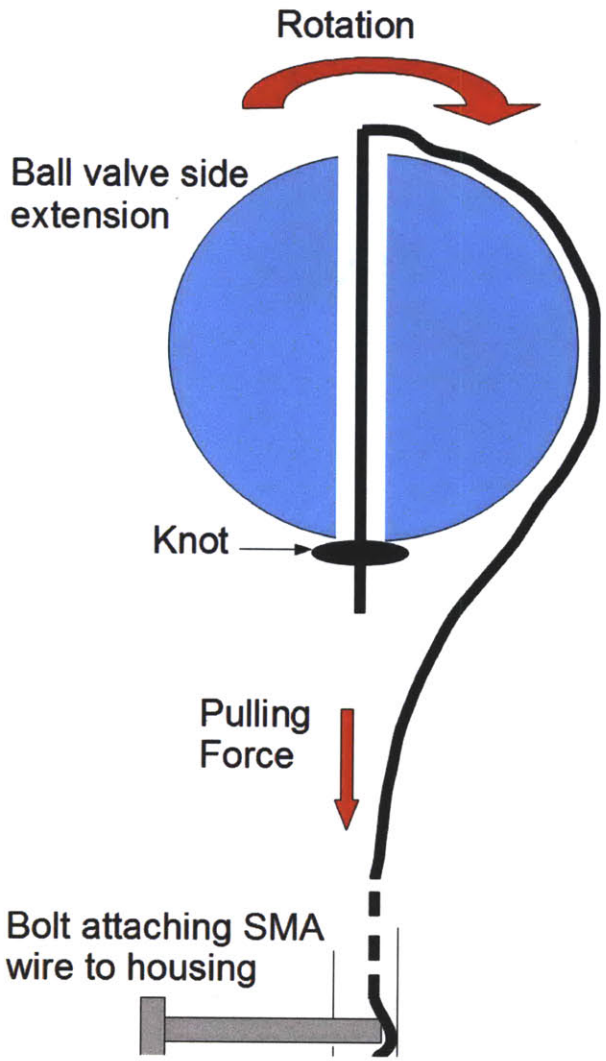

Figure 6-3: SMA attachment diagram

Before final assembly of the prototype, a mock-up was constructed to test the valve actuation (see figure 6-5).

The ball valve was propped up on sliding bearings and the torsion spring and shape memory alloy wires attached in a similar manner as the final design, with two 78mm strands of wire as needed to provide full actuation and overcome the torque of the torsion spring. As indicated by the manufacturer, the Flexinol wire can be heated up not only by conduction, but also by resistive heating by passing an electric current through it. This provides a quick and easy way to test the wire actuation behavior. The 0.5mm-diameter wire used requires a current of 4 amps to actuate [12]

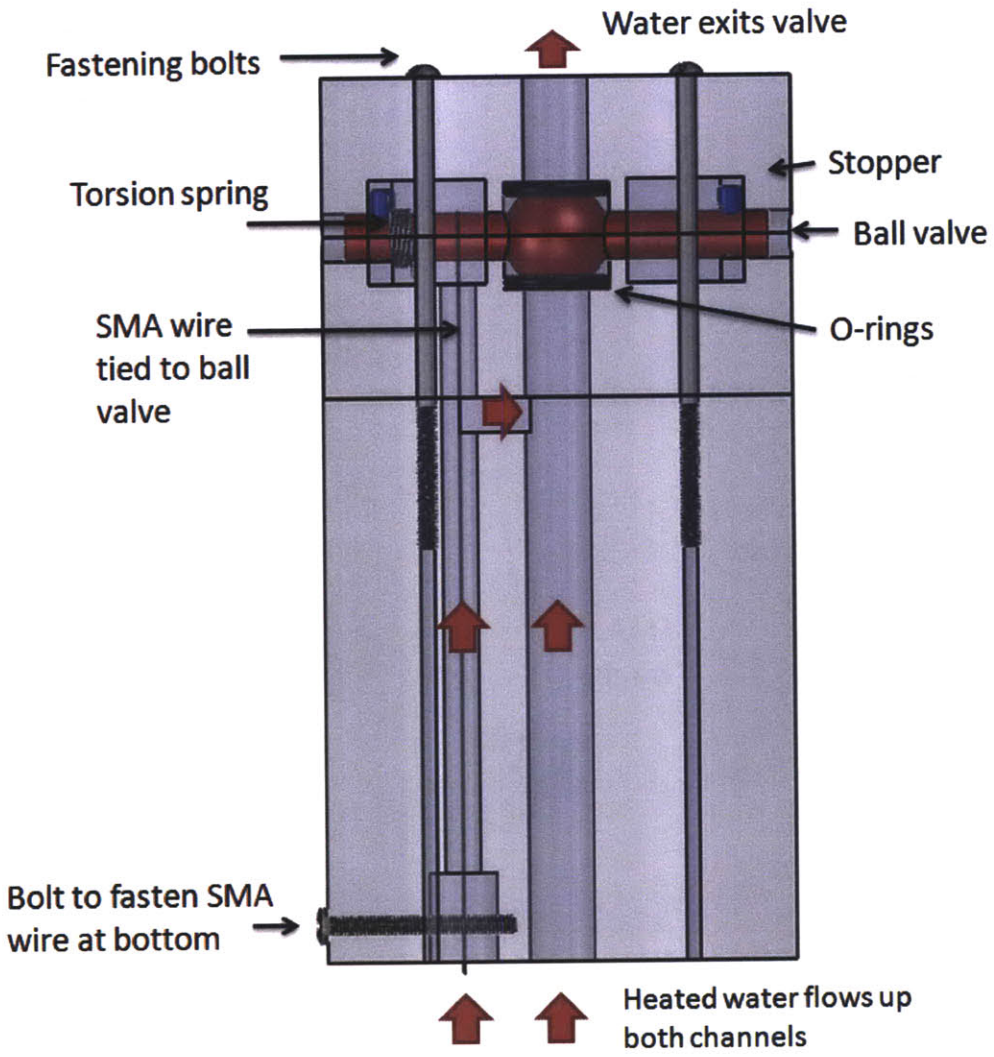

Figure 6-4: Prototype valve fluid flow diagram

and has a resistance of 0.04 $\frac{\Omega}{mm}$. Thus the resistance of the 78mm wire is 1.28 Ω and a voltage of at least 3.125V is required to pass the necessary current through the wire. Three 1.2V AA batteries were connected to the wires to provide a voltage drop of 3.6V. The wires contracted as expected for an angular displacement of the valve of approximately 90 degrees. This mockup showed that the valve will indeed rotate as expected when the shape memory alloy wire contracts. It also showed that two wires provide enough force to overcome the torsion spring force. The final prototype is shown in figure 6-6.

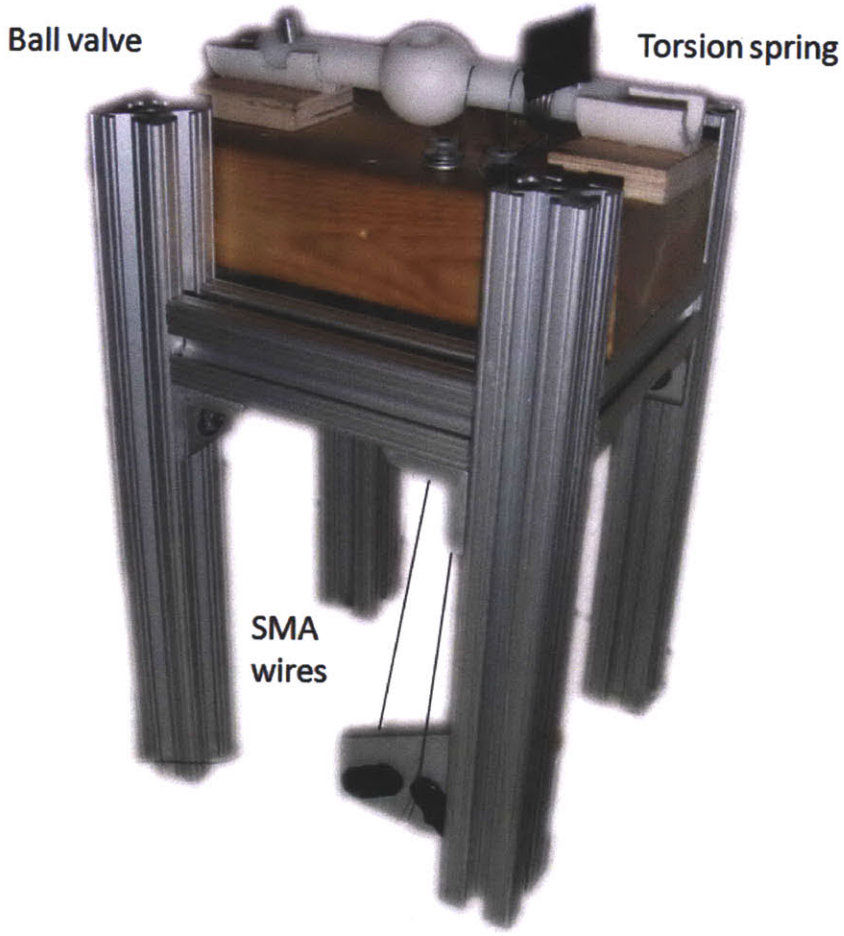

Figure 6-5: Prototype valve mock-up

6.1.1 Scaling Justification

One possible question with using a larger-scale prototype is how the performance of the prototype will compare to the performance of the actual-scale valve. The prototype valve will be tested for actuation time, actuation temperature, and hysteresis behavior. For this prototype, the shape memory alloy wire is being heated directly by the fluid instead of by conduction through the gas lift valve housing. Thus the size of the housing in the prototype will not affect the variables being tested in the experiment.

Future prototypes may allow the shape memory alloy wire to be heated by conduction through the gas lift valve housing, and in this case the scale of the prototype will be more important. Non-dimensional numbers can be used to directly compare

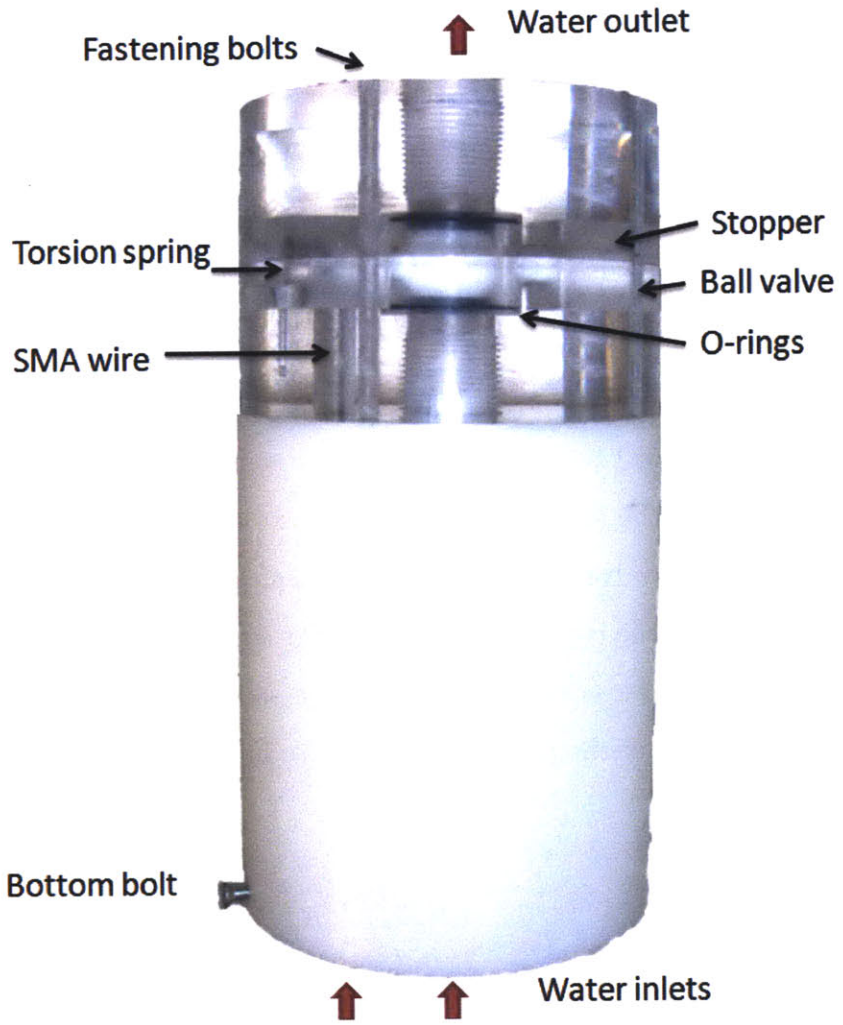

Figure 6-6: Final prototype

thermal properties of prototypes of different scales. In this case the transient heating rate of the gas lift valve housing is the property of interest, and the Biot number [27] is a useful non-dimensional number to characterize this. The Biot number is the ratio between heat transfer at the surface of a body to the heat transfer inside the body, and is given by the equation

$$Bi = \frac{hL_c}{k} \tag{6.1}$$

where Bi is the Biot number, h is the convective heat transfer coefficient at the body surface, L_c is the characteristic length (usually the ratio of the volume to surface

area of the body), and k is the thermal conductivity of the body. If the Biot number is much less than one, then this means the heat transfer through conduction inside the body is much greater than heat transfer through convection on the body surface and the body heats up uniformly with negligible temperature gradients inside. If the Biot number is much greater than one, then heat transfer through convection is much greater than heat transfer through conduction and the body will not heat up uniformly. Thus if the Biot number is similar for the actual valve housing and for the scaled prototype housing, the thermal properties can be assumed to be very similar.

The next prototype will be made out of stainless steel so should have the same thermal conductivity as the actual valve. If the Reynolds number of the flow around the outside of the gas lift valve is assumed to be the same in the 1X scale valve and 3X scale prototype, then by the convective heat transfer coefficient analysis in chapter 5, the convective heat transfer coefficients will be the same. The characteristic length will be given by the ratio of the prototype volume to lateral surface area, which for a cylinder is

$$L_c = \frac{\pi R_p^2 L_p}{2\pi R_p L_p} = \frac{R_p}{2} \tag{6.2}$$

where R_p is the prototype radius and L_p is the prototype length. Using parameter values outlined in chapter 5, the Biot number of the 1X scale gas lift valve is 0.04 and the Biot number for a 3X scale prototype would be 0.06. Both of these values are more than an order of magnitude less than 1, which means heat transfer will be similar in the 3X scale prototype as in the 1X scale gas lift valve.

Another potential issue with the scaled prototype is the difference in frictional forces required for the valve to turn. The prototype uses an O-ring seal with plastic-on-plastic bearings and this may yield different static and kinetic frictional forces than in the full scale design which will have a metal-on-metal orifice seal and metal-on-metal sliding bearings. This difference in frictional forces that must be overcome to actuate the valve will affect the shape memory alloy wire diameter and number of wires necessary to actuate the valve, with higher wire diameter or more wires needed

Sensor	Measurement	Rating	Output
Pressure Transducer	Water Pressure	0-2$x10^5$Pa	0-10V
Flow Meter	Water Volumetric Flow Rate	3-50GPM	4-20mA
Thermocouple	Water temperature	0C to 260C	0-5V
Inclinometer	Ball Valve Angle	± 75 degrees	0-5V

Table 6.1: Sensor Details

to overcome higher frictional forces.

A final potential issue with the scaled prototype is that the pressures and flow rates in the initial proof-of-concept experiments may not be as high as those experienced in actual oil wells. A future prototype made out of stronger materials could be tested under these higher pressure and flow rate conditions.

6.2 Experimental Setup

The experimental setup is designed to test the actuation temperature and hysteresis behavior of the prototype valve and to act as a proof of concept of the thermally-actuated ball vale. A schematic diagram of the setup is shown in figure 6-7 and actual experimental setup pictures in figures 6-8 and 6-9.

Water is pumped from a storage tank, through a water heater, through the prototype valve, and back into the water storage tank. A pressure relief valve is located on the input side of the prototype valve to allow water to pass around when the positive lock closes. A thermocouple senses the water temperature at the valve outlet. A tilt sensor is mounted to the ball valve end extension to record the ball valve position (see figure 6-10).

A pressure transducer is mounted near the pump outlet to allow closed-loop control of the pump speed. Pipes are made of aluminum because of its ability to withstand temperatures in excess of 70C as are necessary to heat up the SMA wire.

Tables 6.2 and 6.2 give details about the individual sensors, and table 6.2 gives details about the water heater and water pump.

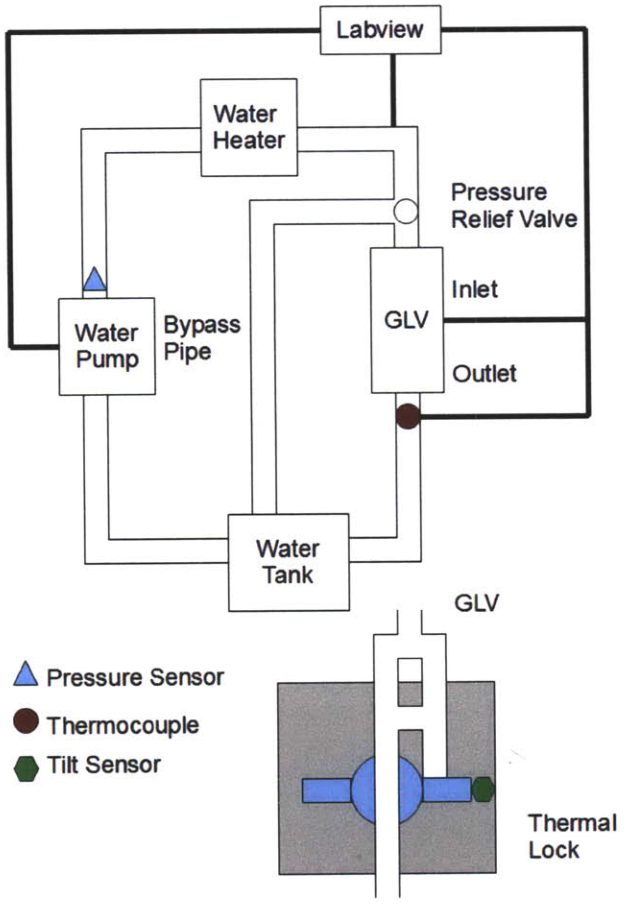

Figure 6-7: Schematic of experimental setup

The Labview software/hardware program is used to acquire data from the sensors and supply necessary power for the sensors. The water heater is plugged into a standard 120VAC wall outlet. The centrifugal pump is supplied with a closed-loop PID controller that relies on a pressure measurement at the pump outlet to control the flow. The set pressure of the controller is manually input as desired.

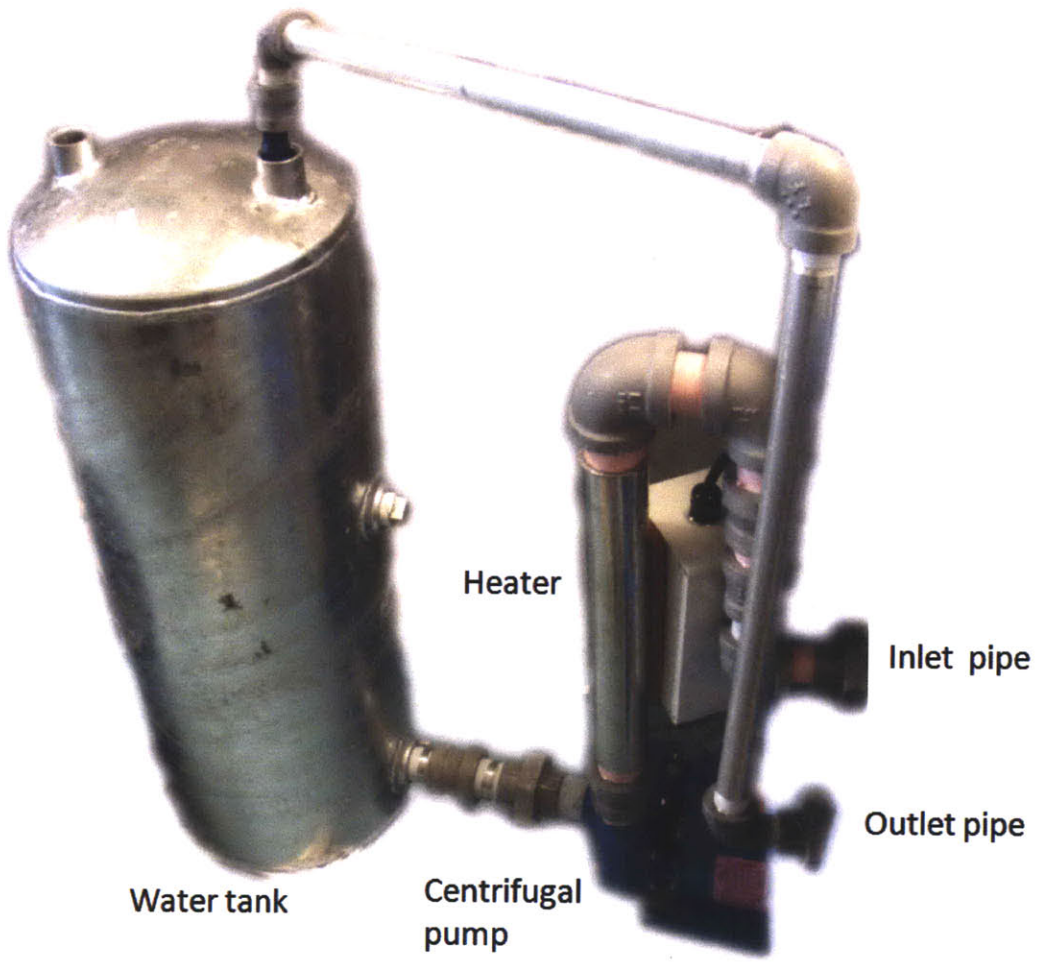

Figure 6-8: Water tank, pump, and water heater

6.2.1 Sensor Calibration

Pressure Sensor

The pressure sensor provided with the Aquavar pump controller was only rated to a temperature of 70C, which was too low for several experiments planned. A high-temperature pressure transducer rated to 125C was used instead. The pressure sensor 4-20mA output was converted to a pressure output by the Aquavar pump controller. The pressure sensor outputs a certain starting current at zero pressure, and this must be accounted for when reading the pressure given by the pump controller. At atmospheric pressure the pump controller output 320 kPa, thus all pressure readings must be shifted down by 320 kPa for correct calibration (so that a reading of 0 Pascals

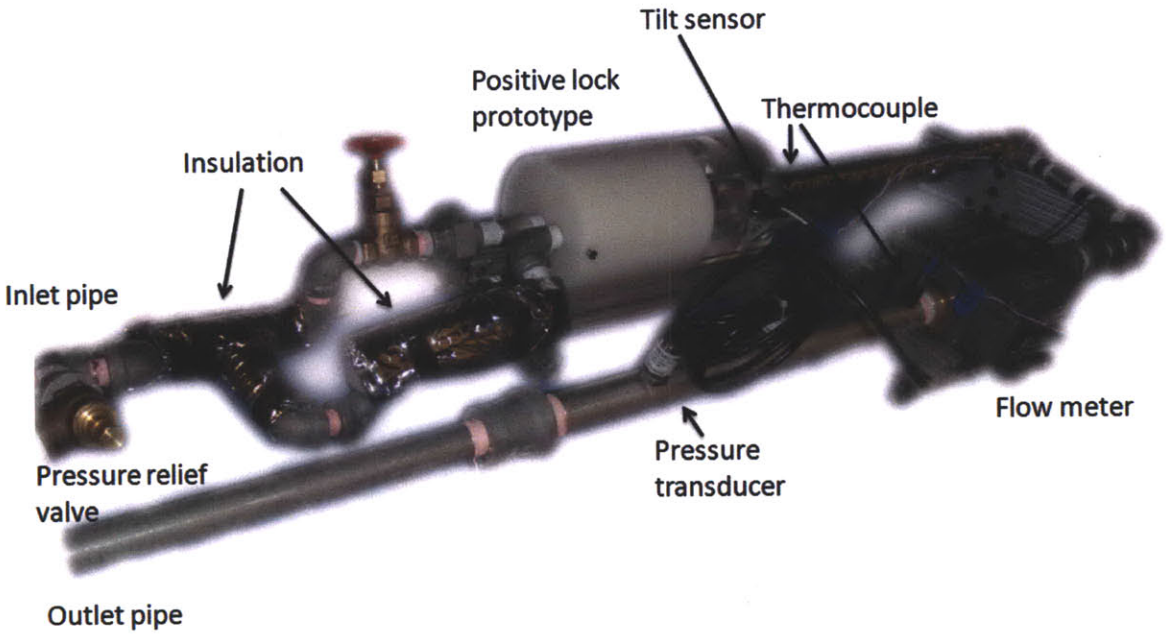

Figure 6-9: Prototype valve, thermocouples, flow meter, and pressure transducers

Sensor	Manufacturer	Model
Pressure Transducer	McMaster-Carr	2388K21
Flow Meter	Omegadyne	FLR8340D
Thermocouple	National Instruments	746061-01
Inclinometer	Crossbow	CXTA01

Table 6.2: Sensor details

corresponds to zero pressure in the pipe relative to atmospheric pressure).

Inclinometer

As specified by the manufacturer, the inclinometer gives a voltage output reading proportional to the sine of the one-dimensional tilt angle relative to vertical, given by the equation

Component	Input	Rating	Manufacturer	Model
Centrifugal Pump	240VAC	Flow to 50GPM	Goulds	GL 3642
Pump Controller	240VAC	PID pressure control	Aquavar	04168321
Water Heater	120VAC	Up to 88C	Omega	FTH1500120

Table 6.3: Component details

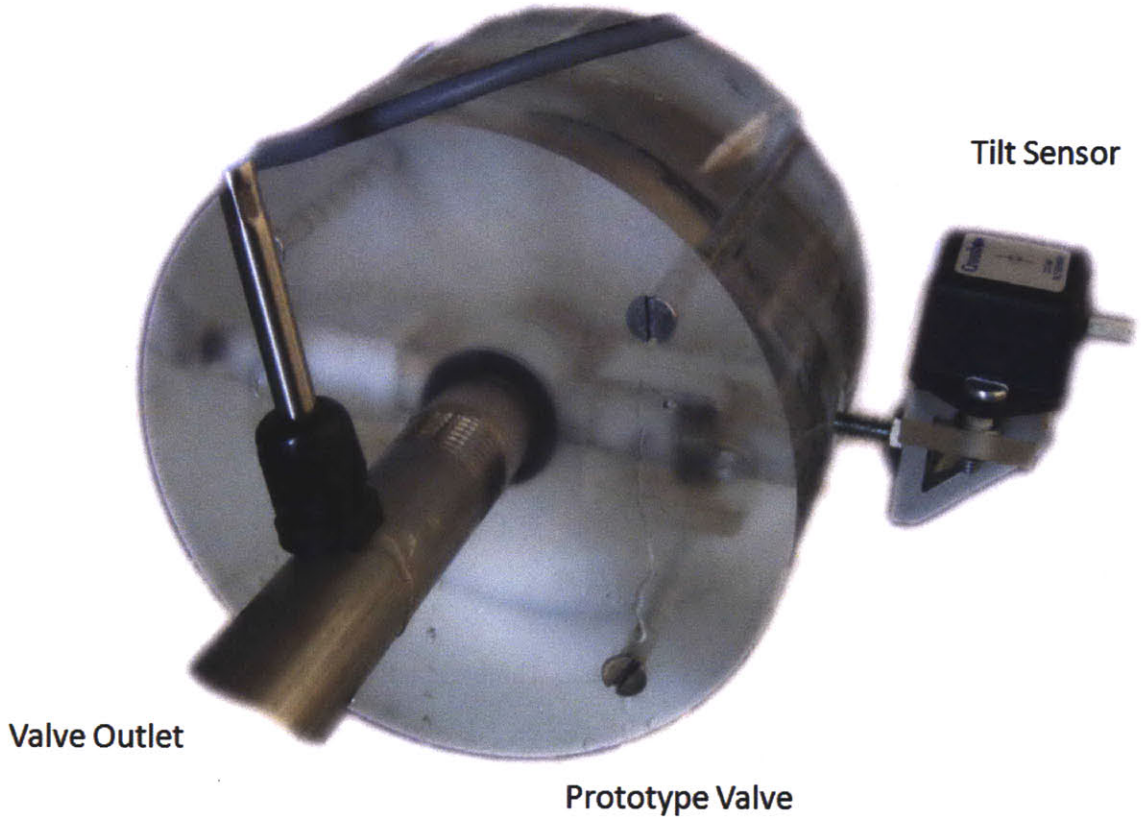

Figure 6-10: Tilt sensor mounting

$$sin(\theta) = \frac{V - V_0}{S} \tag{6.3}$$

where θ is the tilt angle, V is the output voltage, V_0 is the zero-angle voltage, and S is the sensitivity (V/degree). The sensitivity given by the manufacturer is 35 mV/degree and the zero-output voltage was measured to be 2.3V. Thus the equation for the tilt angle is

$$\theta = sin^{-1}\left(\frac{V - 2.3}{0.035}\right) \tag{6.4}$$

When tested with no other electrical power sources on, the inclinometer output had very little noise. However, the signal was very noisy when the pump and heater were drawing power. To eliminate the noise, a low-pass filter was applied to the output data to filter out signals at a higher frequency than the data sampling rate.

The filter used is an order 5 lowpass digital Butterworth filter with normalized cutoff frequency 0.003 radians/sec [42].

Thermocouple

T-class thermocouples were used which came compatible with the Labview hardware. Labview software came with built-in conversion capabilities to convert the T-class thermocouple output to the temperature reading in degrees Celsius, so no independent calibration was necessary.

6.3 Experimental Results

In the first experiment, water was pumped through the test setup at a controller set pressure of 70 kPa with the water heater on. The ball valve was attached to the prototype housing with 4 Nitinol wires. As the water heated up the bolts attaching the top housing of the prototype were manually loosened to account for a squeezing effect created by the differential expansion of the plastic and rubber, which was acting to clamp the ball valve in place. The temperature was allowed to reach 80C, 10C above the shape memory alloy transition temperature, and then the pump and heater were turned off. The gas lift valve was then allowed to cool back to room temperature and the experiment repeated four more times. The next four times the pump controller was set to a pressure of 35 kPa for a lower water flow rate. Figure 6-11 shows the time profiles of the ball valve angular displacement and the gas lift valve temperature as measured by the water temperature at the valve outlet.

The plots show the ball valve turning closed when the temperature rises to between 70C and 85C, then turning open as the temperature drops below 45C in each trial. In the second two trials the temperature momentarily spiked higher to between 90C and 100C. Based on observations during the experiment, this is likely because the flow rate was set so low that water was almost not flowing, and water near the heater was able to boil, creating steam. The steam then surged through the pipes and caused a brief temperature spike.

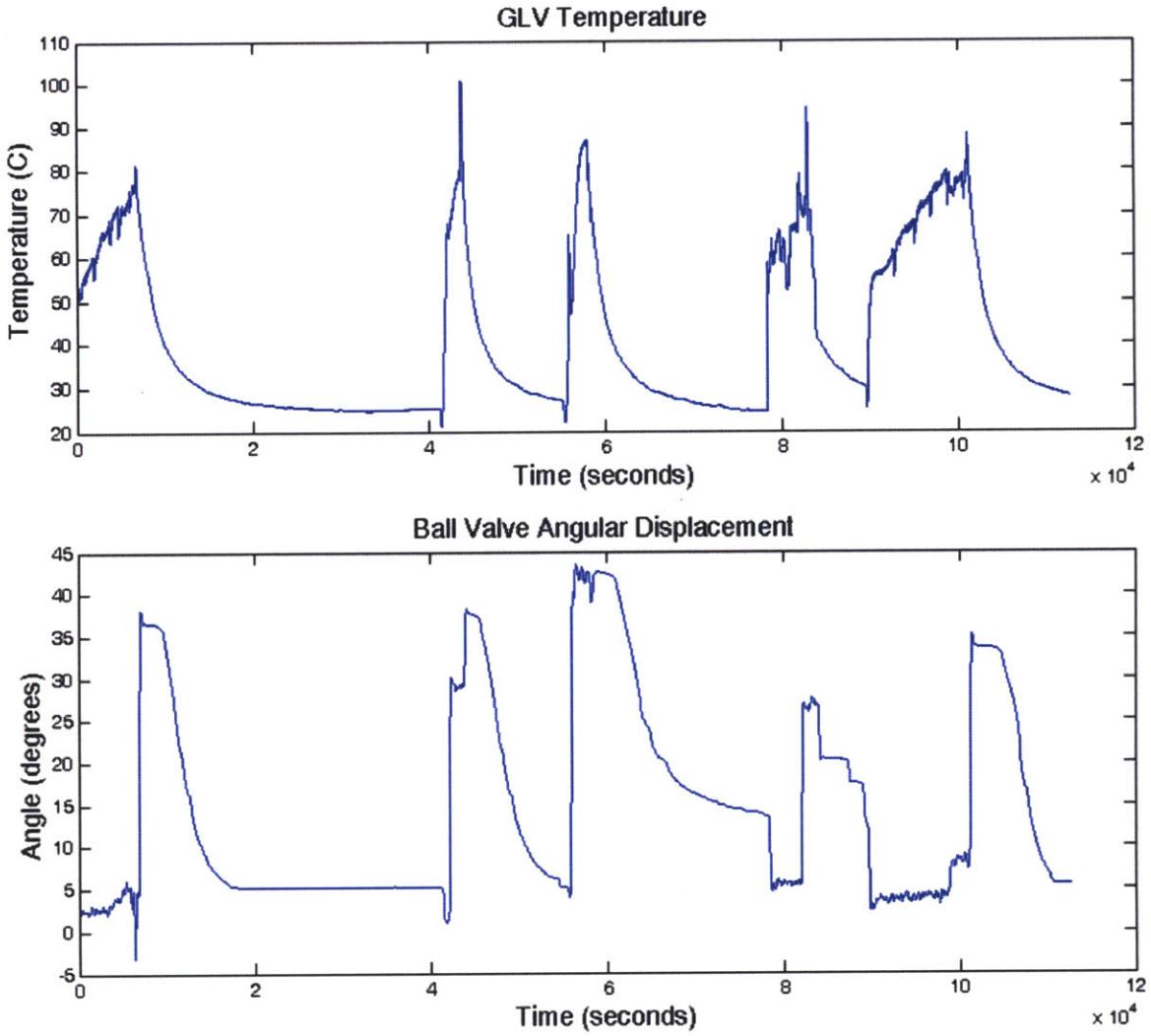

Figure 6-11: Ball valve temperature time profile

Figure 6-12 shows the angular displacement hysteresis plots of the ball valve as a function of temperature for the trials 4 and 5.

The hysteresis plots show that the ball valve turns closed when it is heated to between about 70C and 85C, and begins opening when it is cooled to below 45C. In each plot the ball valve started at an angle of approximately 0 degrees, opened to between 35 and 40degrees, and then closed to 5degrees. A slightly stronger torsion spring may need to be used to completely close the valve the remaining 5 degrees. The tilt sensor experienced considerable noise with the pump and other electronics on during the heating up phase, which is evident in the upper left cornere of the graphs.

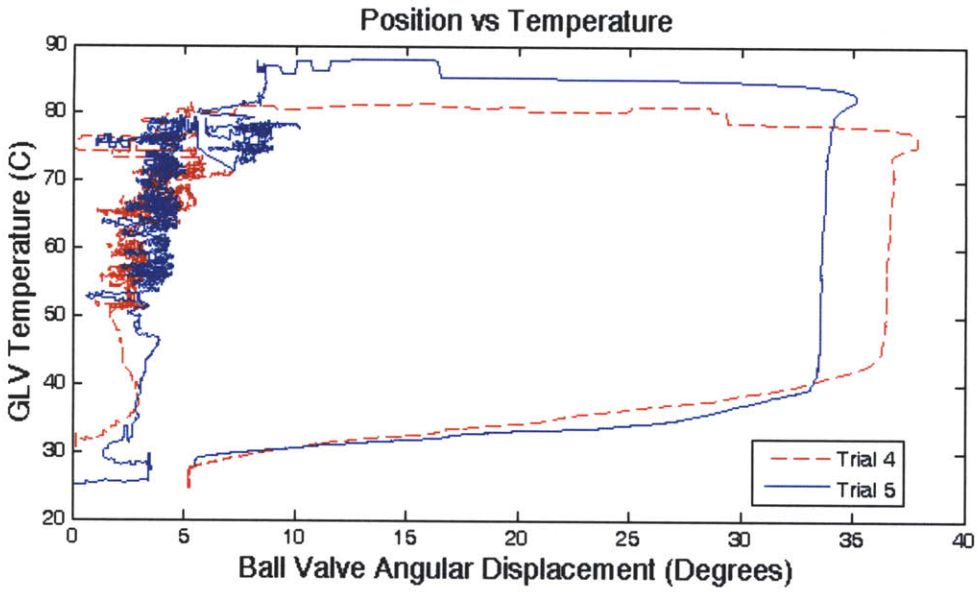

Figure 6-12: Ball valve hysteresis for trials 4 and 5

The Butterworth low-pass filter was able to remove most, but not all, of the noise. The hysteresis temperature spreads in these graphs between Austenitic and Martensitic transition temperatures are approximately 30C-40C. In future experiments, different shape memory alloys could potentially be used to attain a smaller temperature spread.

6.3.1 Discussion of Results

The experimental results show that it is possible to thermally actuate a ball valve to turn closed with 40 degrees of angular displacement, and to thermally actuate the valve to reopen within 5 degrees of its original position. The Austenitic transition temperature was found to be between 70C and 85C (when the valve begins to close), and the Martensitic transition temperature approximately 45C (when the valve begins to open). These transition temperatures agree with the temperatures listed by the manufacturer, Dynalloy.

The valve did not attain the full 90 degree angular displacement it was designed for, and several factors could have affected this. First, it was not anticipated that the differential expansion of the plastic housing and metal bolts would clamp the ball valve in place as strongly as it did, and this could have added additional friction

which was difficult for the shape memory alloy wires to overcome. Second, the wires may not have achieved the full 5 percent strain that was designed for.

Nevertheless, an angular displacement of 40 degrees would still be sufficient to completely close off the orifice if a larger ball valve radius is used, as described in the analysis in chapter 3.

Future iterations of the thermally-actuated ball valve design should use the same material for all housing and attachment components to eliminate the differential cooling problem. Additionally, a longer shape memory alloy wire or larger ball valve radius can be used to ensure the valve completely closes off the orifice. A different tilt sensor could also be used to acquire less noisy data.

Chapter 7

Conclusions

This thesis has modeled and studied the failure modes of gas lift valves and designed and constructed a thermally-actuated positive-locking safety valve that actuates in the event of gas lift valve failure. Sensitive gas lift system parameters and parameter values that lead to valve failure were identified. Preliminary proof-of-concept testing was performed on the positive lock and steady-state and transient thermal modeling used to demonstrate feasibility of the design in oilwell conditions.

7.1 Summary of Work

Chapter 1 introduced the problem. The current state of world oil production was examined and it was shown that deep-sea oil production is becoming increasingly important to meet projected global oil demands. Various oil extraction techniques were detailed and gas-lift was shown to be the best suited for many deep-sea production operations. Gas lift production was explained in detail and the Piper Alpha disaster used to motivate the study of gas lift failure modes and the design of a positive-locking safety valve for existing gas lift valves. A literature review was detailed for existing work on gas lift system modeling and for thermally-actuated safety valves.

Chapter 2 developed a quasi-steady state pressure model of the gas lift system including the reservoir, riser, and gas lift valve. The model was validated using pressure profiles measured from several actual wells. Sensitive parameters of the

model were identified. Failure modes of the system and parameter values that lead to failure modes were identified using Monte Carlo simulation.

Chapter 3 presented a design for a thermally-actuated positive locking mechanism that would actuate in the event of valve failure and prevent product from entering the annulus. Functional requirements for the valve were identified and strategies developed for positive lock location and means of actuation. Ultimately a thermally-actuated lock independent from the bellows or check valve and located in the venturi orifice was chosen. Concepts were developed for the type of valve and type of thermal actuation and a ball valve with side extensions actuated by a shape memory alloy wire was chosen.

Chapter 4 detailed how unloading and shut-in operations will be carried out with the positive locking mechanism in place.

Chapter 5 developed a steady state thermal model of the tubing and annulus temperature profiles and a transient state thermal model of the gas lift valve during unloading and shut-in periods. These models were used to verify the feasibility of thermally actuating the positive lock and to determine the time required for the positive lock to heat up and cool down during failure scenarios and shut-in/unloading scenarios.

Chapter 6 detailed the construction of a physical prototype of the positive lock valve and experiments run to test the valve actuation behavior under simulated failure scenarios.

7.2 Future Work

7.2.1 Experimental Testing

Experimental results have shown that the positive lock can successfully close off the gas lift valve orifice in a failure scenario. Future testing is needed to further understand valve behavior in the cooling scenario, as well as to understand valve lifetime and seal strength. Figure 7-1 shows a proposed experimental setup to conduct further

valve testing.

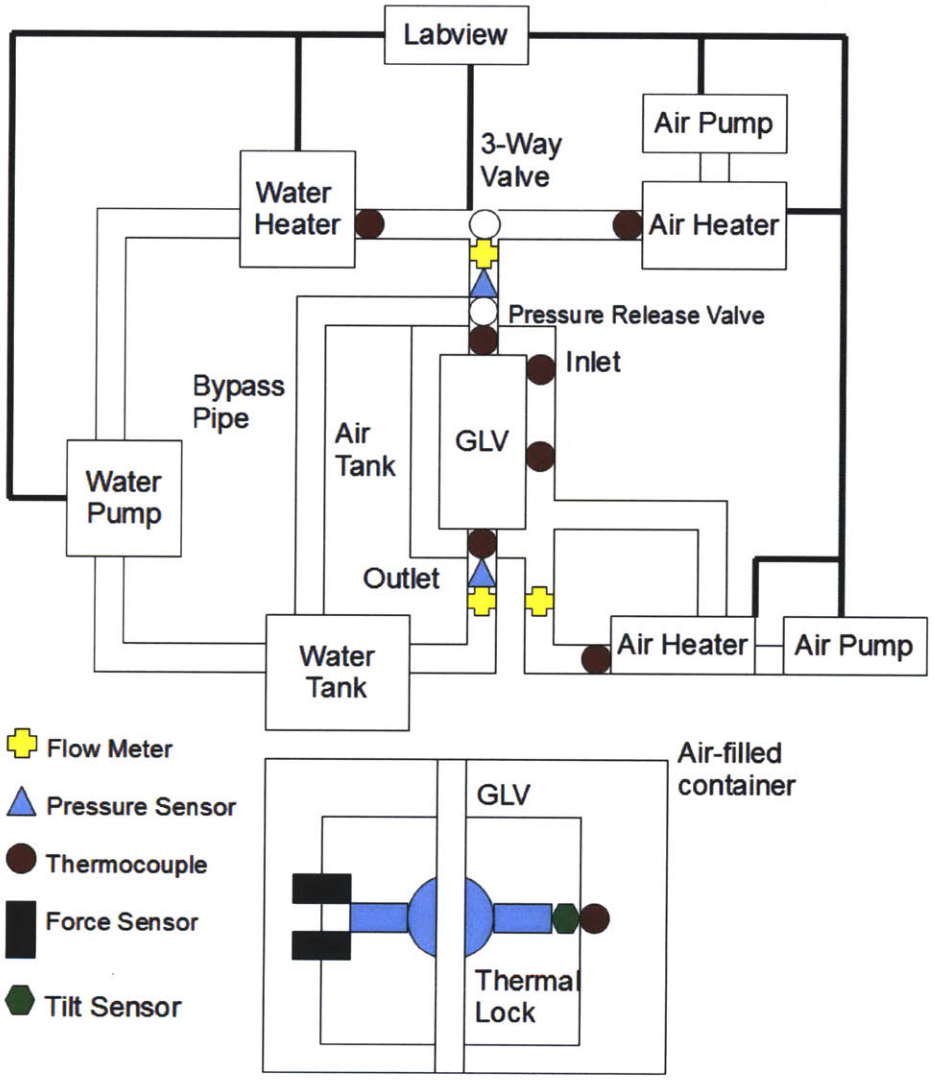

Figure 7-1: Future Experimental Setup

This setup is similar to the one detailed in chapter 6 of this thesis.As before, the prototype represents the valve section between the gas injection port below the bellows stem and the exit port below the check valve. Two force sensors are attached to one of the ball valve side extensions to detect when the valve begins opening and with how much force it seals the orifice. Temperature-controlled air or water can be

pumped through the GLV. A three-way valve at the GLV inlet controls the medium passing through the GLV. A bypass pipe allows liquid or air to pass around the GLV if the thermal lock is closed (this prevents a dangerous pressure buildup in the experiment). A holding tank at the outlet of the GLV stores water that has passed through and is ready to be cycled through the system again. Abrasive fluid, such as a fluid-sand mixture, will be pumped through the valve in some experiments to test corrosion resistance. Thermocouples are located inside the air-filled chamber, at the GLV inlet and outlet pipes, at the air- and water-heater inlet and outlet pipes, and at the surface of the GLV to record temperature values. Pressure and flow sensors are located at the inlet and outlet of the GLV. The three-way valve, air heaters, air pump, water heat, water pump, thermocouples, pressure sensors, flow sensors, and force sensors are controlled and monitored using Labview. This test setup is designed to be able to test different positive lock concepts if needed. Proposed experiments are detailed below:

1. Test actuation time during simulated failure for various air, liquid, and ground temperatures:

    - Cool air of known temperature is pumped through the GLV.
    - The three-way valve is switched and hot water of known temperature is pumped through the GLV.
    - Force sensors indicate when thermal lock begins to actuate, when it is fully actuated, and with how much force it pushes closed
    - When thermal lock is actuated, water pump is stopped
    - If injected hot water builds up pressure beyond a certain threshold while the thermal lock is actuated but before the pump is stopped, fluid will pass into the bypass pipe.
    - Test is repeated for different combinations of injection air temperature, hot water temperature, and air chamber temperature

2. Test opening and closing actuation time during simulated shut-in for various air, liquid, and ground temperatures. This will be a hybrid experiment enabled by real-time control of system temperatures and flow rates. Transient temperature models of the GLV will be used to control the physical GLV temperature to create a very realistic shut-in simulation.

    - Cool air of known temperature is pumped through the GLV.
    - Air chamber is kept at a constant, known temperature
    - Air pump is stopped (simulating a shut-in) and no fluid or air is pumped through the GLV.
    - GLV bulk temperature is controlled real-time using the air chamber temperature and a feedback loop to accurately simulate a shut-in.
    - Force sensors indicate if/when thermal lock begins to actuate, when it is fully actuated, and with how much force it pushes.
    - If valve does not actuate after a specified characteristic time then the experiment is over.
    - If valve actuates, then air is circulated through the air-chamber at a known temperature and rate until the force sensors indicate that the thermal lock has retracted.
    - Test is repeated for various injection air temperatures, static air chamber temperatures, flowing air chamber temperatures, and air flow rates.

3. Test valve seal

    - Air in the air chamber is heated to a known specified temperature.
    - Force sensors indicate when the thermal lock is actuated.
    - Hot water of known temperature and pressure is pumped into the GLV for a specified amount of time.
    - The volume of liquid passing through the GLV is measured at the outlet to determine a leak rate.

4. Test valve opening force

    - Cool air of known temperature is pumped through the GLV (this simulates injection gas).
    - The three-way valve is then switched and hot water of known temperature is pumped through the GLV until the thermal lock is actuated (this simulates check valve failure and oil passage through the GLV).
    - Force sensors detect and thermal lock opening forces.
    - Test is repeated for various injection air, water, and air chamber temperatures to determine opening forces.

5. Test cycling and recovery percentage: (test should be automated with Labview)

    - Using known transition temperature, pass enough current through wire to heat it up to the transition point. Measure length.
    - Allow wire to cool down. Repeat process.

7.2.2 Application to Blowout Preventers

As described in chapter 1, the thermally-actuated positive lock may have applications to other oil well safety equipment. The Deepwater Horizon drilling rig accident of April 20th, 2010 is thought to have been caused by a failed blowout preventer, a set of valves at the wellhead meant to seal off the well in the event of a blowout. Future work with the thermally-actuated positive lock could focus on applications to blowout preventers to increase reliability.

Bibliography

[1] M. Ashby and D. Jones. *Engineering Materials 1: An Introduction to Their Properties and Applications.* Butterworth Heineman, 1996.

[2] M.F. Ashby. *Materials Selection in Mechanical Design.* Pergamon Press Ltd, 1996.

[3] H. Asheim. SPE Annual Technical Conference and Exhibition, Houston, TX, USA. In *Verification of Transient, Multi-Phase Flow Simulation for Gas Lift Applications*, October 1999.

[4] K. Bendiksen, D. Maines, R. Moe, and S. Nuland. The Dynamic Two-Fluid Model OLGA: Theory and Application. *SPE Production Engineering*, 6(2):171–180, May 1991.

[5] D. Bertovic, D. Doty, R. Blais, and Z. Schmidt. Calculating Accurate Gas-Lift Flow Rate Incorporating Temperature Effects. In *SPE Production Operations Symposium, Oklahoma City, OK, USA*, March 1997.

[6] Harley Bible. Control system and improved pneumatically operated temperature controlled valve construction therefore or the like. In *US Patent Number 4016853*, 1977.

[7] Kermit Brown. *The Technology of Artificial Lift Methods, vol 2A.* The Petroleum Publishing Company, 1980.

[8] W. F. Cloud. *Petroleum Production.* Norman, OK: University of Oklahoma Press, 1937.

[9] S. Crandall, C. Dahl, and T. Lardner. *An Introduction to the Mechanics of Solids.* McGraw Hill, 1999.

[10] DK Das, S Nerella, and D Kulkarni. Thermal properties of petroleum and gas-to-liquid products. *Petroleum Science and Technology*, 25(4):415–425, April 2007.

[11] Melton KN Stockel D Wayman CM Deurig, TW. *Engineering Aspects of Shape Memory Alloys.* Reed Books Services Ltd: Rushden, UK, 1990.

[12] Dynalloy. Dynalloy Inc. Makers of Dynamic Alloys. http://www.dynalloy.com, 2010.

[13] Y Ermolin. Mathematical modeling for optimized control of moscow sewer network. *Applied Mathematical Modeling*, 23(7):543–556, July 1999.

[14] J. Faustinelli and D. Doty. Dynamic Flow Performance Modeling of a Gas-Lift Valve. In *SPE Latin American and Caribbean Petroleum Engineering Conference, Buenos Aires, Argentina*, March 2001.

[15] Ford and White. Thermomechanical behavior of 55ni45ti nitinol. *Acta Materialia*, 44(6):2295–2307, 1993.

[16] H Fountain. With spill, focus turns to well-blocking system. *The New York Times*, May 2010.

[17] I.B. Fridleifsson, R. Bertani, E. Huenges, J.W. Lund, A. Ragnarsson, and L. Ryback. The possible role and contribution of geothermal energy to the mitigation of climate change, Luebck, Germany. In *IPCC SCoping Meeting on Renewable Energy Sources*, January 2008.

[18] C. Gott. Successful rod pumping at 14,500 feet. *SPE Production Engineering*, 1(6):485–493, 1986.

[19] Boyun Guo. *Petroleum Production Engineering: A Computer-Assisted Approach.* Gulf Professional Pub, 2007.

[20] William Hart. Temperature-responsive valve. In *US Patent Number 4227646*, 1980.

[21] A. Hasan, C. Kabir, and M. Sayarpour. A Basic Approach to Wellbore Two-Phase Flow Modeling. In *SPE Annual Technical Conference and Exhibition, Anaheim, CA, USA*, May 2007.

[22] Gad Hetsroni. *Handbook of multiphase systems.* Hemisphere Publishing Corporation, 1982.

[23] C Hoffman. Oil rig explosion was likely a blowout. *Popular Mechanics.*

[24] Dai Homma. Valve driven by shape memory alloy. In *US Patent Number 4973024*, 1990.

[25] G. Hopguler, Z. Schmidt, R. Blais, and D. Doty. Dynamic model of gas-lift valve performance. *Journal of Petroleum Technology*, 45(6):576–583, June 1993.

[26] W. Huang. On the selection of shape memory alloys for actuators. *Materials and Design*, 23(1):11–19, 2002.

[27] Frank Incropera. *Fundamentals of Heat and Mass Transfer.* Hoboken, NJ: John Wiley, 2007.

[28] J. A. Veil and M. G. Puder and D. Elcock and R. J. Redweik Jr. A white Paper Describing Produced Water from Production of Crude Oil, Natural Gas, and Coal Bed Methane. Technical report, US Department of Engergy, 2004.

[29] J. Wood G. Long D. Morehouse. Long-Term World Oil Supply Scenarious: The Future is Neither as Bleak or Rosy as Some Assert. http://www.eia.doe.gov/pub/oilgas/petroleum/featurearticles/2004/worldoilsupply/oilsupply04.html, Aug 2004.

[30] G. Kauffman and I. Mayo. Memory metal. *Chem Matters*, October 1993.

[31] Kelly. Fire safety valve. In *US Patent Number 3659624*, 1972.

[32] J. Kennedy and A. Neville. *Basic Statistical Methods for Engineers and Scientists.*

[33] W. R. King. Time and volume control for gas intermitters. In *US Patent Number 2339487*, 1944.

[34] A.E.H. Love. *A Treatise on the Mathematical Theory of Elasticity.* Cambridge University Press, 1927.

[35] D. Lynch. Deepwater oilfields are a final frontier. *USA Today*, June 2008.

[36] K. Aleklett M. Hook, R. Hirsch. Giant oilfield decline rates and their influence on world oil production. *Energy Policy*, 37(6):2262–2272, June 2009.

[37] John Mayfield. Temperature controlled valve mechanism and method. In *US Patent Number 4356833*, 1982.

[38] John McDonald. Thermal actuator. In *US Patent Number 4841730*, 1989.

[39] CJN Mckie, E Rojas, N Quintero, C Fonseca, and N Perozo. Economic Benefits From Automated Optimization of High Pressure Gas Usage in an Oil Production System. In *SPE Productions and Operations Symposium, Oklahoma City, Oklahoma*, March 2001.

[40] R morris, C Sulfredge, R Sanders, and H Stanford Rydell. Using the visac program to calculate the vulnerability of nuclear power plants to terrorism. *International Journal of Nuclear Governance, Economy, and Ecology*, 1(2):193–211, 2006.

[41] S. Munkejord, M. Molnvik, J. Melheim, I. Gran, and R. Olsen. Prediction of Two-Phase Pipe Flows Using Simple Closure Relations in a 2D Two-Fluid Model. In *International Conference on CFD in the Oil and Gas, Metallurgical and Process Industries SINTEF/NTNU, Trondheim, Norway*, June 2005.

[42] A. Oppenheim. *Discrete-Time Signal Processing.* Englewood Cliffs, NJ: Prentice-Hall, 1989.

[43] Benjamin Osto. *Design, Planning, and Development Methodology.* Prentice Hall, 1977.

[44] M. Elisabeth Pate-Cornell. Learning from the Piper Alpha Accident: A Post-mortem Analysis of Technical and Organizational Factors. *Risk Analysis*, 13(2):215–232, 1993.

[45] Richard Perl. Thermal valve. In *US Patent Number 4102496*, 1978.

[46] Petroleum Experts Ltd. PROSPER. http://www.petex.com/products/?ssi=3, December 2009.

[47] Fred Pirkle. Temperature-responsive valve. In *US Patent Number 4883082*, 1989.

[48] Donald Place. Temperature responsive valve. In *US Patent Number 4133478*, 1979.

[49] James Pymm. Temperature controlled valve. In *US Patent Number 2004636*, 1935.

[50] Roy Fleshman and Harryson Lekic. Artificial Lift for High-Volume Production. http://www.slb.com/media/Files/resources/oilfieldreview/ors99/spr99/lift.ashx, 2010.

[51] Schlumberger. XLift Brochure. http://www.slb.com/media/Files/artificiallift/brochures/xlift.ashx, July 2006.

[52] Schlumberger. Rod Pump. http://www.glossary.oilfield.slb.com/Display.cfm?Term=rodpump, 2010.

[53] F. Sczerzenie. Consideration of the ASTM Standards for NiTi Alloys. In *Proceedings of the International Conference on Shape Memory and Superelastic Technologies, Baden-Baden Germany* , October 2004.

[54] S. F. Shaw. *Gas Lift Principles and Practices.* Houston, TX: Gulf Publishing Co., 1939.

[55] James Siddall. *Probabilistic Engineering Design: Principles and Applications.* New York: M. Dekkler, 1983.

[56] Alex Slocum. *Precision Machine Design.* Society of Manufacturing Engineers, 1992.

[57] Peter Smith and R. W. Zappe. *Valve Selection Handbook, 5th edition: Engineering Fundamentals for Selecting the Right Valve Design for Every Industrial Flow Application.* Gulf Professional Publishing, 2004.

[58] James G. Speight. *The Chemistry and Technology of Petroleum.* New York ; Basel : M. Dekker, 2007.

[59] SPT Group. OLGA. http://www.sptgroup.com/en/Products/olga/, December 2009.

[60] Nam Suh. *Axiomatic Design: Advances and Applications.* New York: Oxford University Press, 2001, 2001.

[61] Gabor Takacs. *Gas Lift Manual.* Pennwell Corporation, 2005.

[62] Tanju. Shape memory alloy actuation. In *US Patent Number US2009/0139727*, 2009.

[63] Robert Tarvis. Temperature controlled valve. In *US Patent Number 4454983*, 1984.

[64] S. Timoshenko. Analysis of bi-metal thermostats. *Journal of the Optical Society of America*, 11:233–243, 1925.

[65] US Central Intelligence Agency. The World Factbook 2009, Country Comparison: Oil - Proved.

[66] US Energy Information Administration. International Total Primary Energy Consumption and Energy Intensity. http://www.eia.doe.gov/emeu/international/energyconsumption.html, May 2009.

[67] R. Sagar Z. Schmidt D. Doty K. Weston. A Mechanistic Model of a Nitrogen-Charged, Pressure-Operated Gas Lift Valve. In *SPE Annual Technical Conference and Exhibition, Washington D. C., USA*, October 1992.

[68] Frank White. *Fluid Mechanics, Third Edition.* McGraw Hill, 1994.

[69] Willson. Temperature-responsive valve operators. In *US Patent Number 3613732*, 1971.

[70] H. Winkler and G. Camp. Dynamic Performance Testing of Single-Element Unbalanced Gas-Lift Valves. *SPE Production Engineering*, 2(3):183–190, August 1987.

[71] Y. Xuan and Q Li. Investigation on Convective Heat Transfer and Flow Features of Nanofluids. *Journal of Heat Transfer*, 125(1):151–156, 2003.